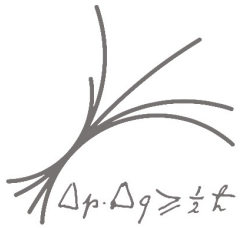

Measurement of Higgs Boson Properties in the Final State with Four Leptons at the ATLAS Experiment

Verena Maria Walbrecht

on behalf of the ATLAS Collaboration

Phenomenology 2020 Symposium, University of Pittsburgh

5th May 2020

Introduction

- Results with full Run 2 data set ($\mathcal{L} = 139$ fb^{-1}):
  - Higgs boson mass
    ATLAS-CONF-2020-005
  - Inclusive fiducial, (double) differential fiducial cross-section and interpretations (pseudo-observables)
    arXiv:2004.03969v2
  - (Simplified template) production cross-sections and interpretations (kappa-framework, EFT…)
    arXiv:2004.03447v1

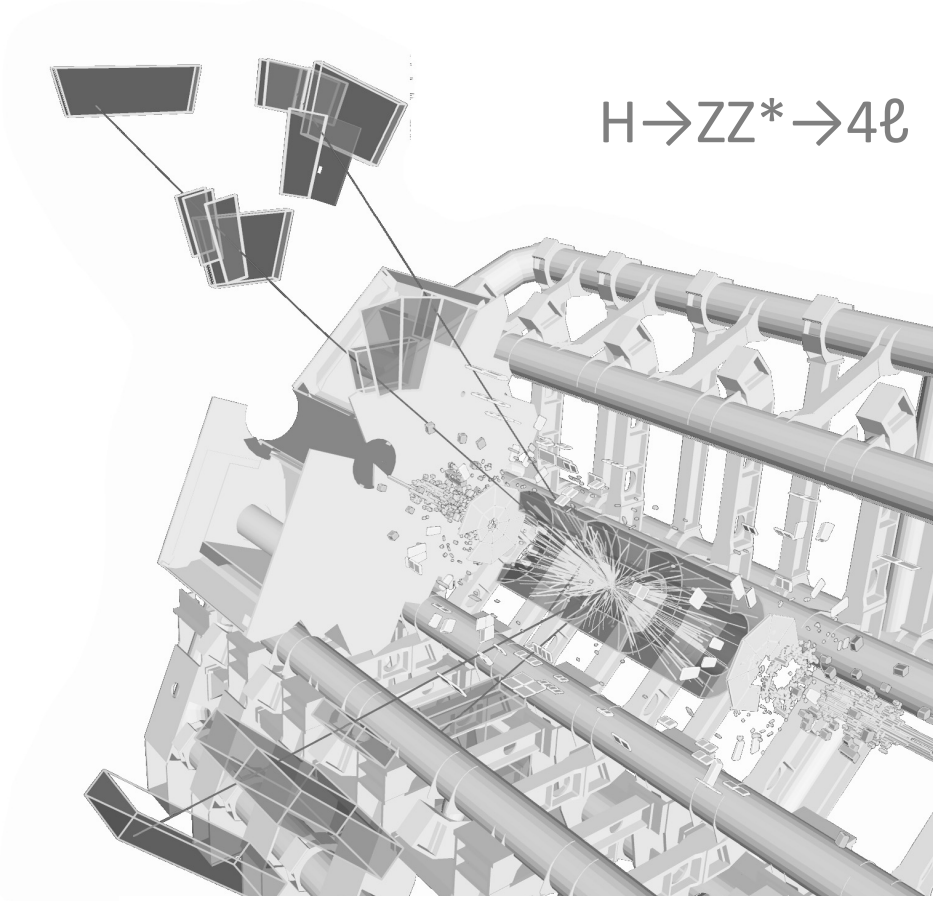

The H→ZZ*→4ℓ Decay Channel

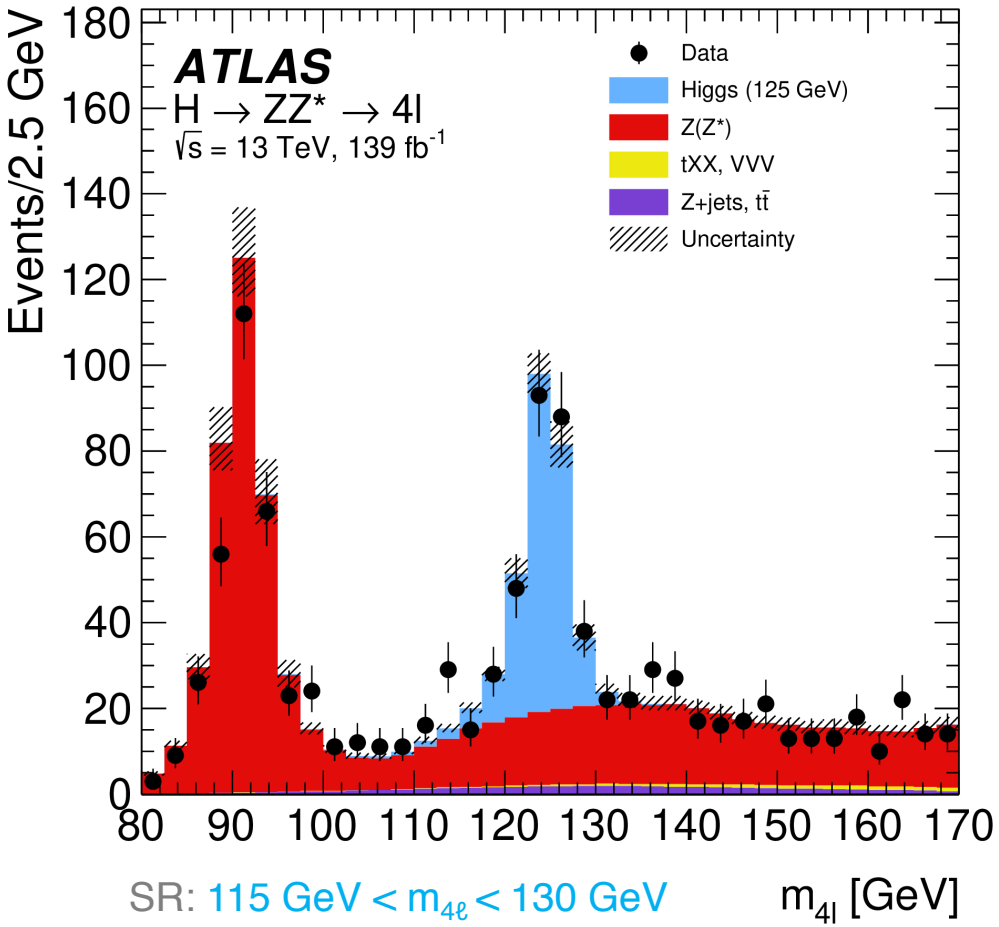

Signal:

BR=0.00125%

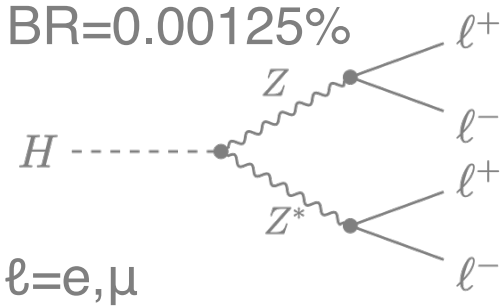

ℓ=e,μ

- Four prompt isolated leptons
- Two same-flavour and opposite-charged lepton pairs
- Leading lepton pair: On-shell Z boson (m_{12})
- Sub-leading lepton pair: Off-shell Z boson (m_{34})

Final state	Total expected	Observed
4μ	119 ± 5	115
2e2μ	82.0 ± 3.4	96
2μ2e	61.0 ± 3.2	57
4e	53.2 ± 3.1	42
Total	315 ± 14	310

The H→ZZ*→4ℓ Decay Channel

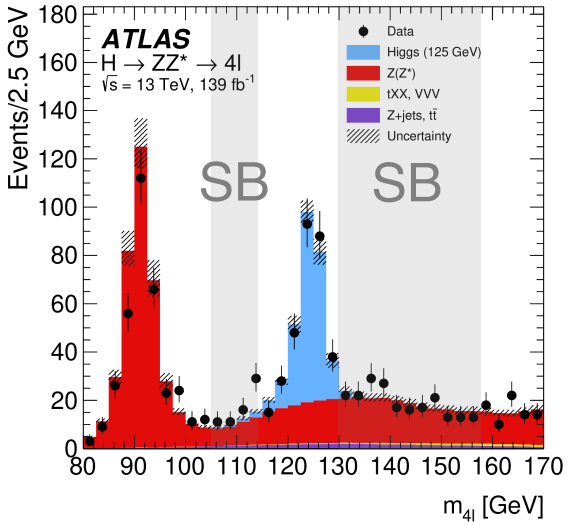

Processes with non-prompt leptons:

Z+jets, tt

Data-driven estimation from control regions (inverted/relaxed selections) separately for ℓℓ+μμ and ℓℓ+ee final states

Processes with prompt leptons:

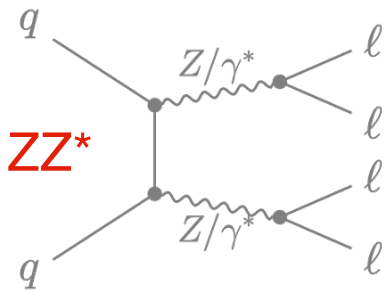

ZZ*

for the first time estimated from SB instead of simulation

Fit from upper/lower SB regions

tXX

Estimated from simulation or fit from extended upper/lower SB regions

VVV

Estimated from simulation

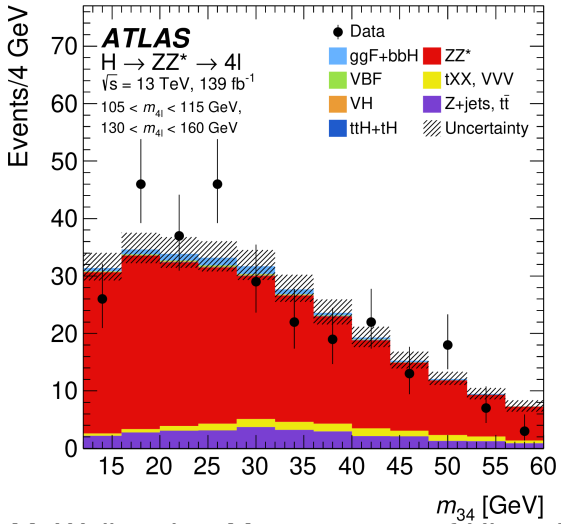

Control regions

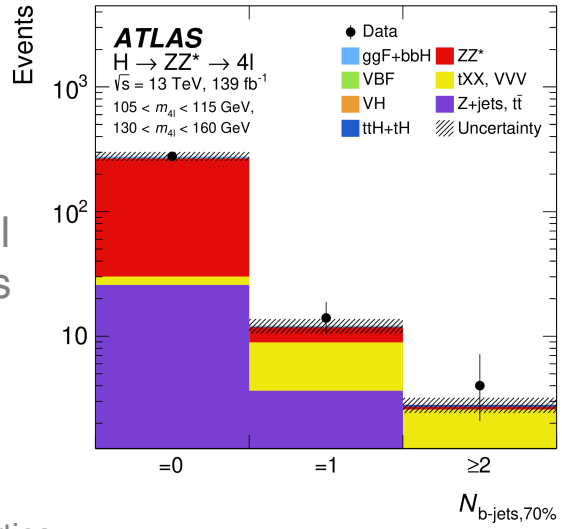

Mass Measurement

Mass Measurement: Method

- Measure m_H from $m_{4\ell}$ using a per-event resolution method
  - Improves the uncertainty by about 10 MeV
- Kinematic fit: constrain invariant mass of the leading lepton pair to the Z boson mass
  - Improves $m_{4\ell}$ resolution by 17%
- Boosted decision tree to discriminate signal from ZZ* background:
  - Improves precision by about 2%
- 16 signal regions:
  - Four BDT bins for each decay channel
- Simultaneous profile likelihood fit to $m_{4\ell}$

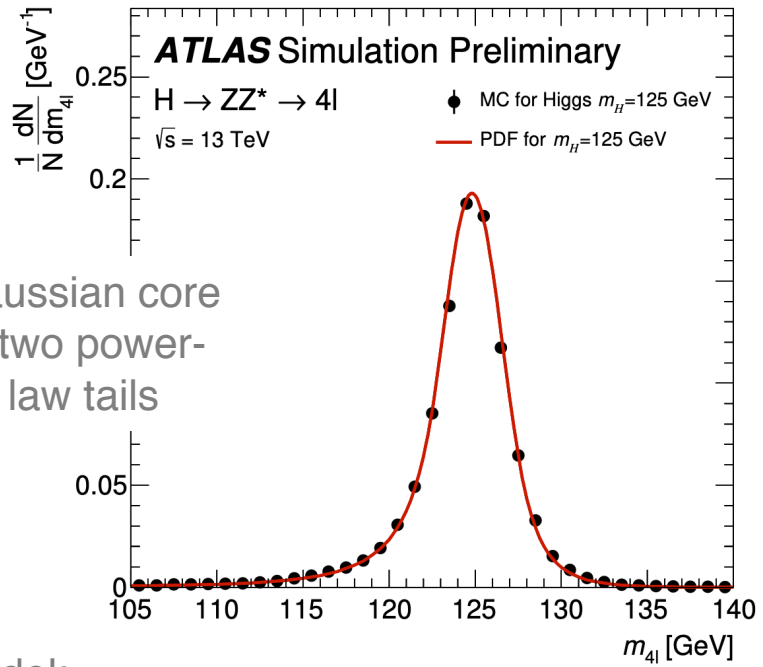

Gaussian core + two power-law tails

Signal model:

Double-sided Crystal Ball:

$\mathrm{DCB}(m_{4\ell}; \mu, \kappa\times\sigma_i, \alpha_1, n_1, \alpha_2, n_2|\sigma_i)$

σ_i: per event $m_{4\ell}$ resolution, estimate using a quantile regression NN

κ: calibration constant

μ , σ_i: mean and standard deviation of the Gaussian

α_i, n_i: parameters of power law tails

Mass Measurement: Results

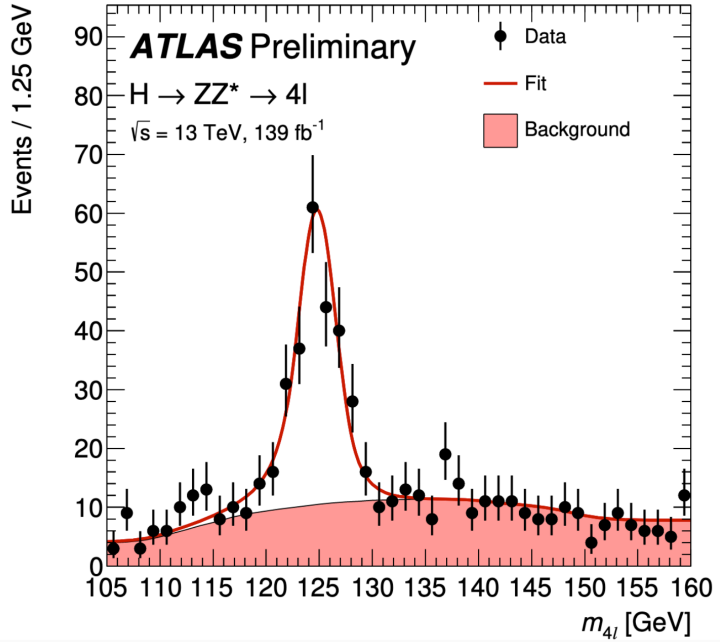

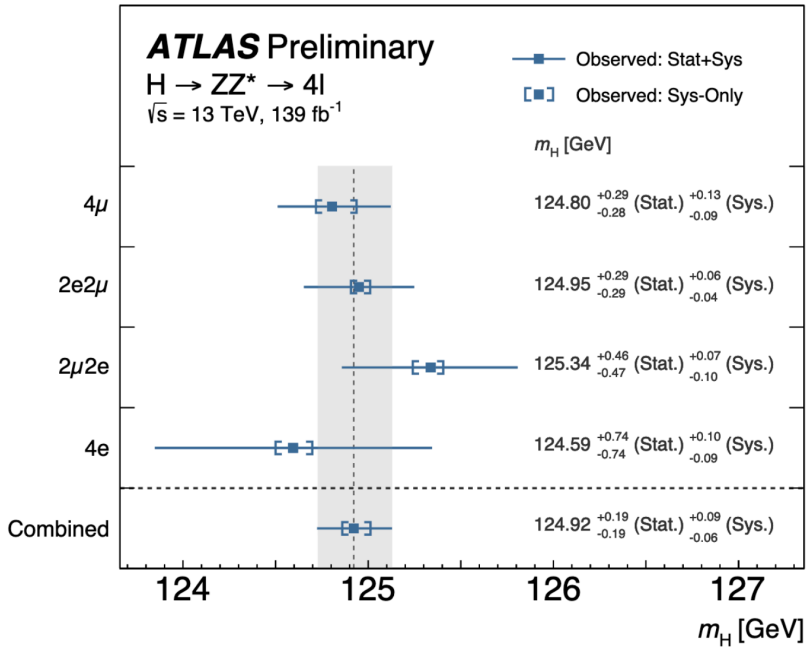

$$m_H^{ZZ^*} = 124.92 \pm 0.19\,(\text{stat})\,^{+0.09}_{-0.06}\,(\text{syst})\ \text{GeV} = 124.92^{+0.21}_{-0.20}\ \text{GeV}$$

- Uncertainty is dominated by statistical uncertainty
- Improved uncertainty compared to the previous combined Run 1 measurement performed by ATLAS and CMS

Recent CMS measurement (35.9 fb^{-1})

$H \to \gamma\gamma + H \to 4\ell$:
$m_H = 125.46 \pm 0.16\ \text{GeV}$
+ Run 1 measurement:
$m_H = 125.38 \pm 0.14\ \text{GeV}$

Measurements of Inclusive and Differential Fiducial Cross-Sections

Fiducial Cross-Sections: Method

- Cross-section measurement in fiducial phase space in a model independent way:

$$\sigma_i^{fid} = \sigma_i \times \mathcal{A}_i \times \mathcal{BR}$$

$\mathcal{A}_i$: fiducial phase space acceptance, σ_i: cross section in fiducial bin and $\mathcal{BR}$: branching ratio

- Measurements:
  - Total cross-section
  - Inclusive fiducial cross-sections:
    - Four decay channels / sum / combination
  - (Double) differential cross-sections:
    - 20 observables sensitive to Higgs boson production and decay e.g. $p_{T,4\ell}$
    - Eight two-dimensional combinations e.g. m_{12} vs m_{34}
- Strategy:
  - Fiducial selection close to analysis selection
  - Template fits of $m_{4\ell}$ spectra to data to extract the number of signal events for each bin
  - ZZ* normalisation obtained from $m_{4\ell}$-fit in the full 105-160 GeV mass region
  - Unfolding: detector response matrix

Detector response matrix $p_{T,4\ell}$:

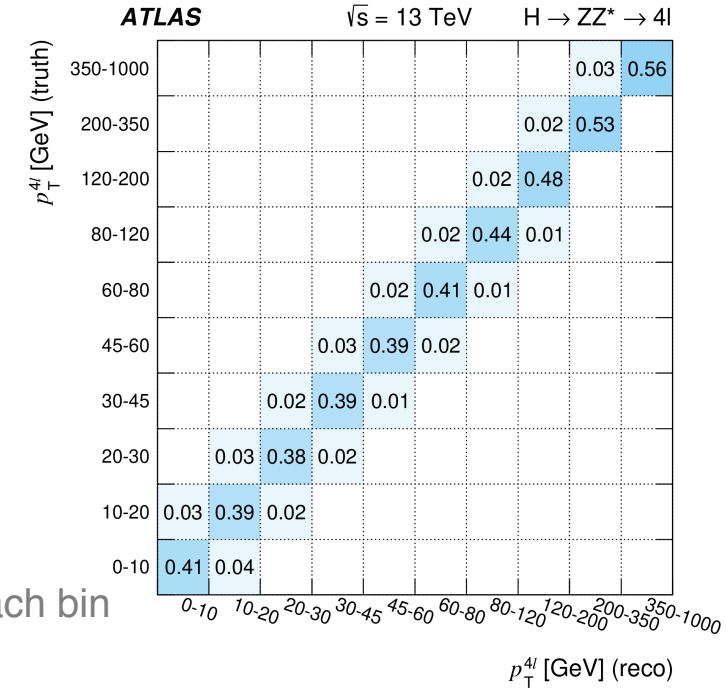

Fiducial Cross-Sections: Results

- Total and inclusive fiducial cross-section measurement
- Total cross-section:

$$\sigma_{tot} = 53.5 \pm 4.9\,(stat.) \pm 2.1\,(syst.)\ \text{pb}$$

- SM prediction:

$$\sigma_{tot} = 55.7 \pm 2.8\ \text{pb}$$

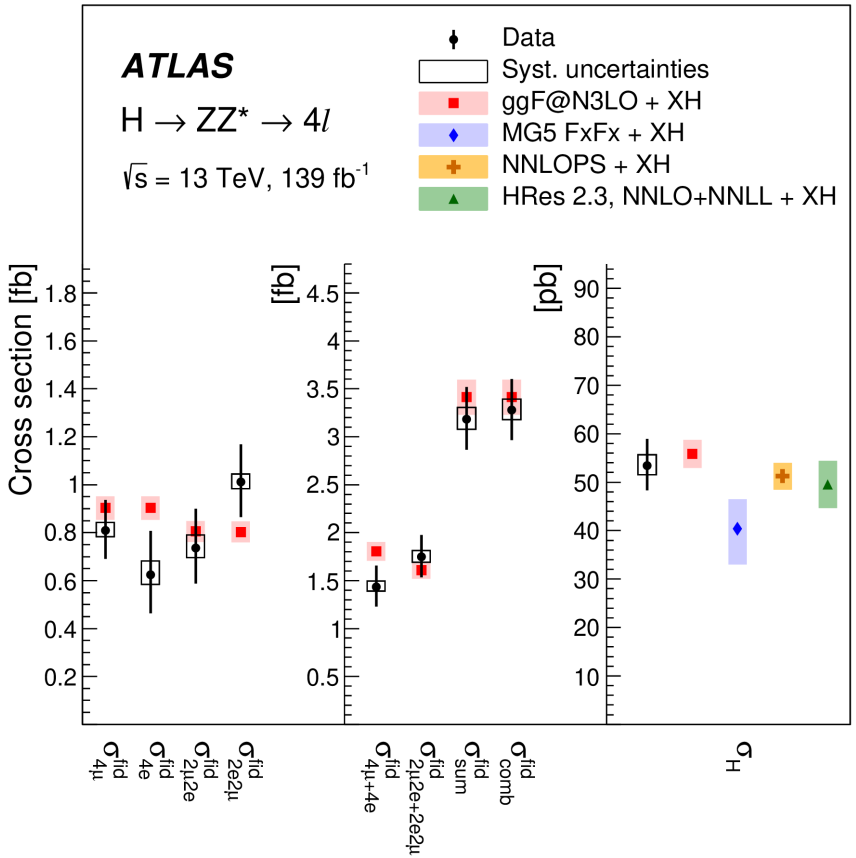

In good agreement with the SM prediction

Fiducial Cross-Sections: Results

→ Remaining Backup

- Observables:
  - Higgs boson kinematics e.g. $p_{T,4\ell}$, m_{12}…
  - Jets e.g. N_{jets}, m_{jj}…
  - Higgs boson and jets e.g. $p_{T,4\ell jj}$…

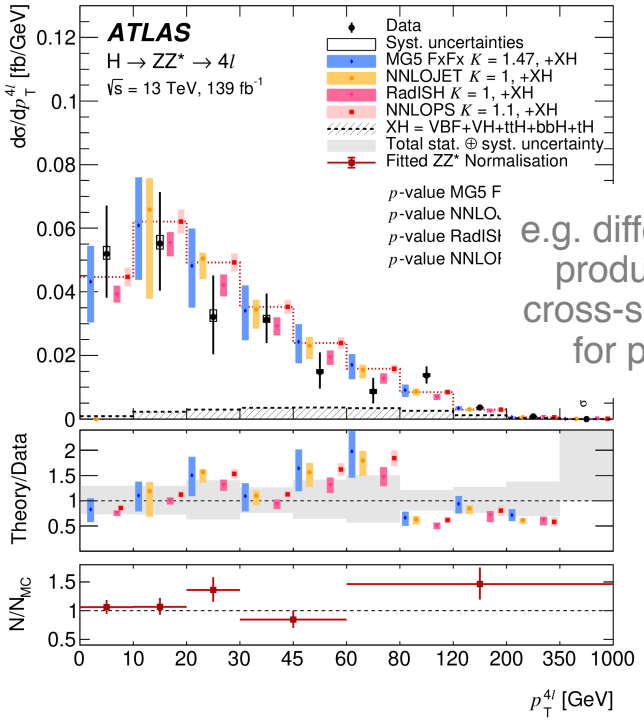

e.g. differential production cross-sections for $p_{T,4\ell}$:

- Constrain Yukawa couplings of the Higgs boson with c- and b-quarks
- Fiducial cross-section in each $p_{T,4\ell}$-bin parametrised as a function of coupling modifiers κ_c and κ_b

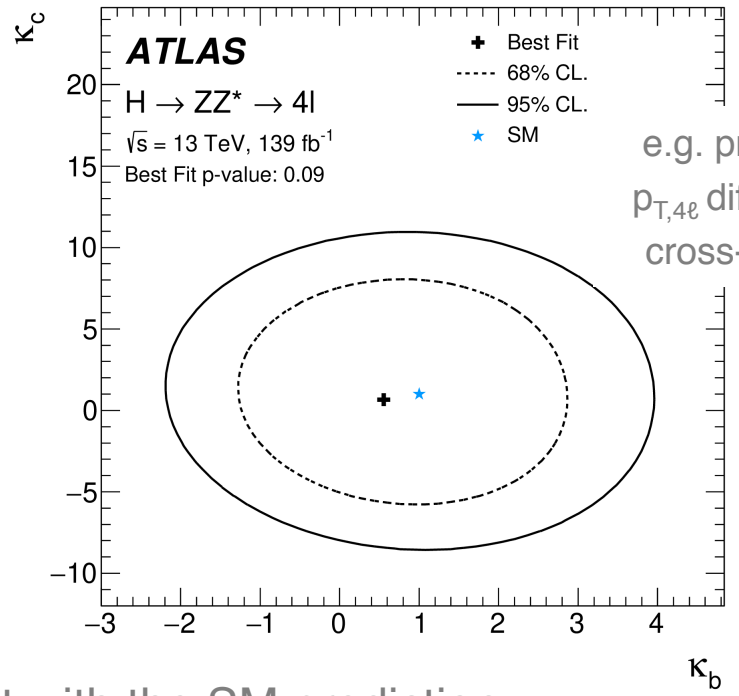

e.g. predicted $p_{T,4\ell}$ differential cross-section

1D results:

Best-fit value	95% CL
$\hat{\kappa}_c$ = 0.66	[-7.46,9.27]
$\hat{\kappa}_b$ = 0.55	[-1.82,3.34]

In good agreement with the SM prediction

Measurement of Exclusive Production Cross-Sections

Exclusive Production Cross-Sections: Method

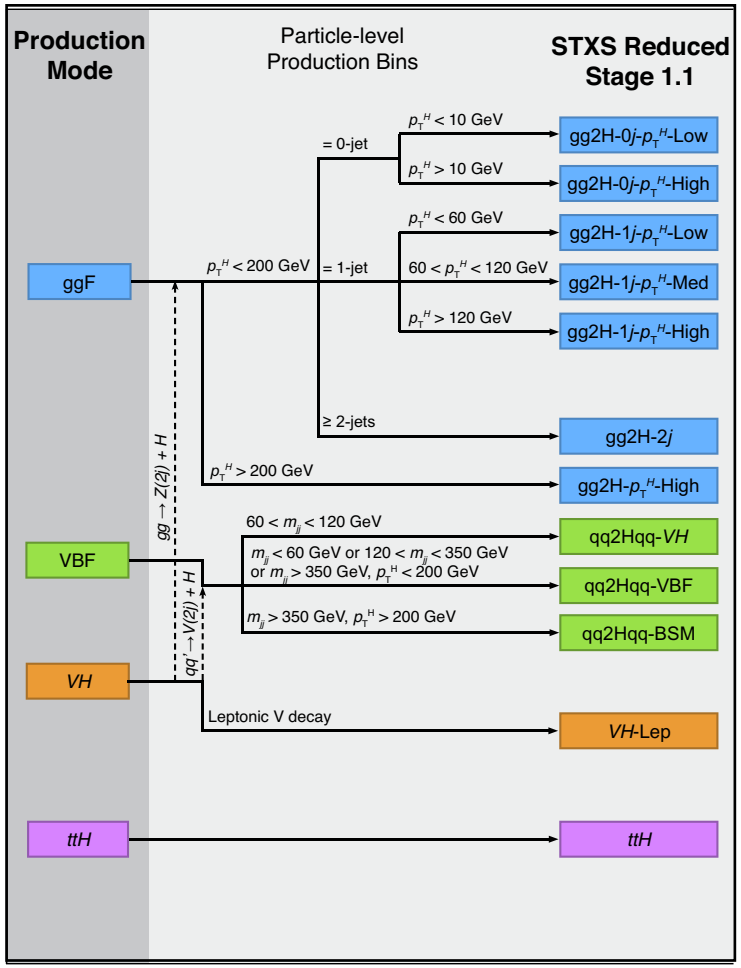

Gluon fusion (ggF)

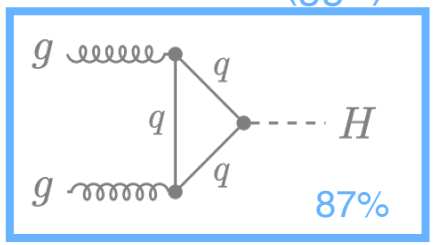

Vector boson fusion (VBF)

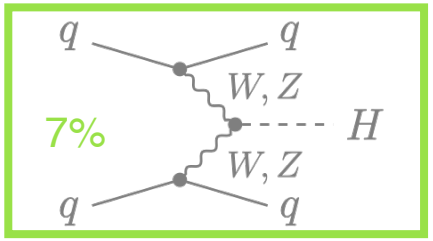

With a vector boson (VH)

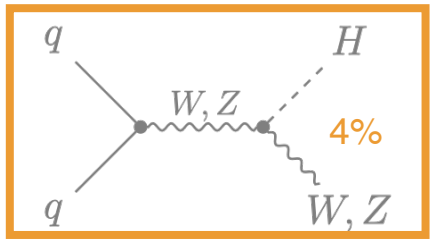

With heavy quarks (ttH/bbH)

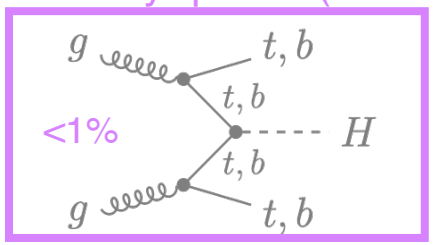

- Production cross-section measurement:
  - Simplified template cross-section (STXS) framework
- Production Mode Stage:
  - Four main production modes
- STXS Reduced Stage 1.1:
  - Several exclusive phase-space bins in dedicated fiducial regions
  - Particle-level production bins

Exclusive Production Cross-Sections: Method

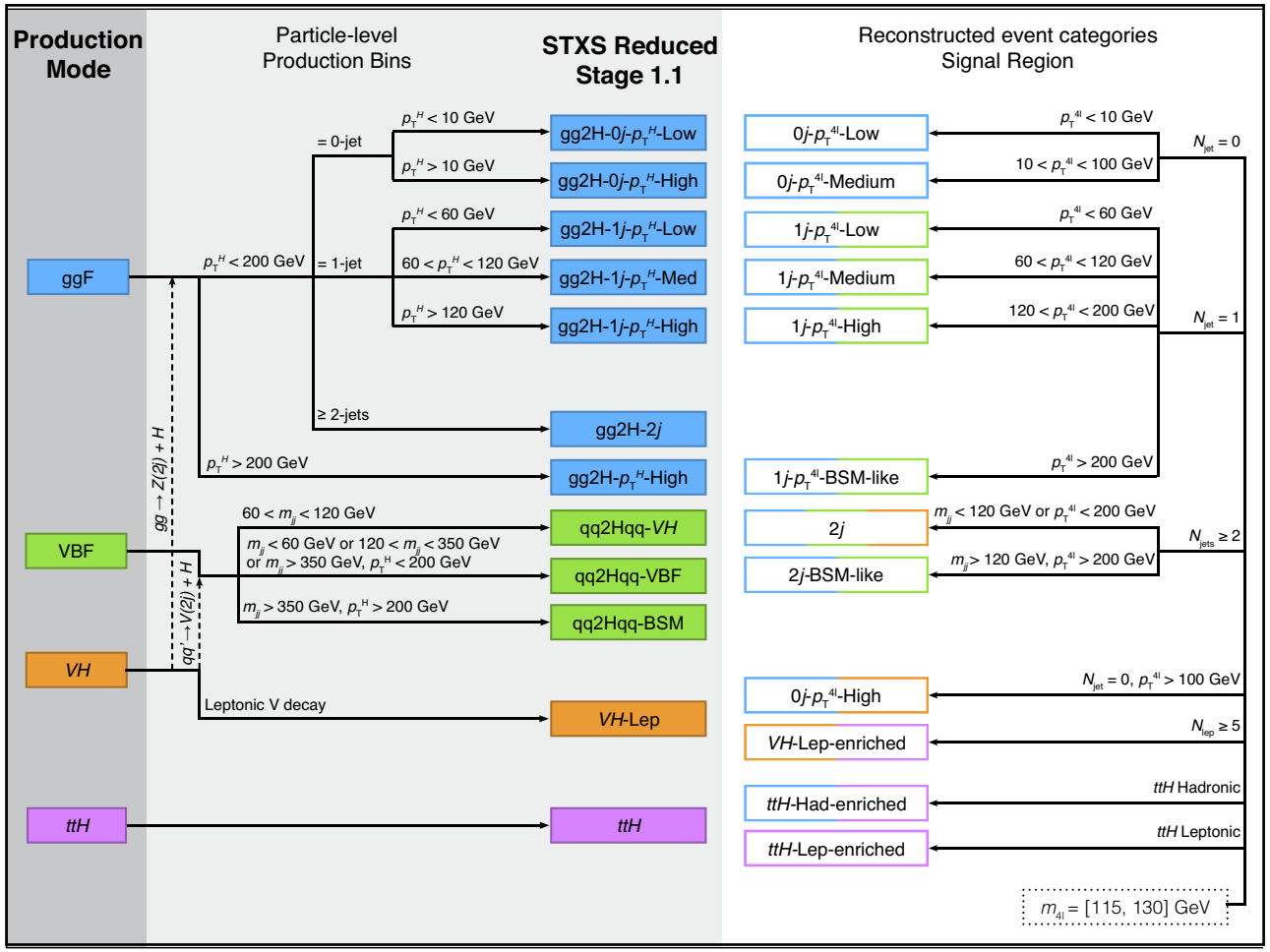

- Selected Higgs boson candidates:
  - Classified according to the production mode
  - Reconstructed event categories
    - ”mostly” match the production bins
  - Neural Networks (NNs):
    - Improve the separation of different signal components and background processes

Exclusive Production: Results

Production Mode Stage

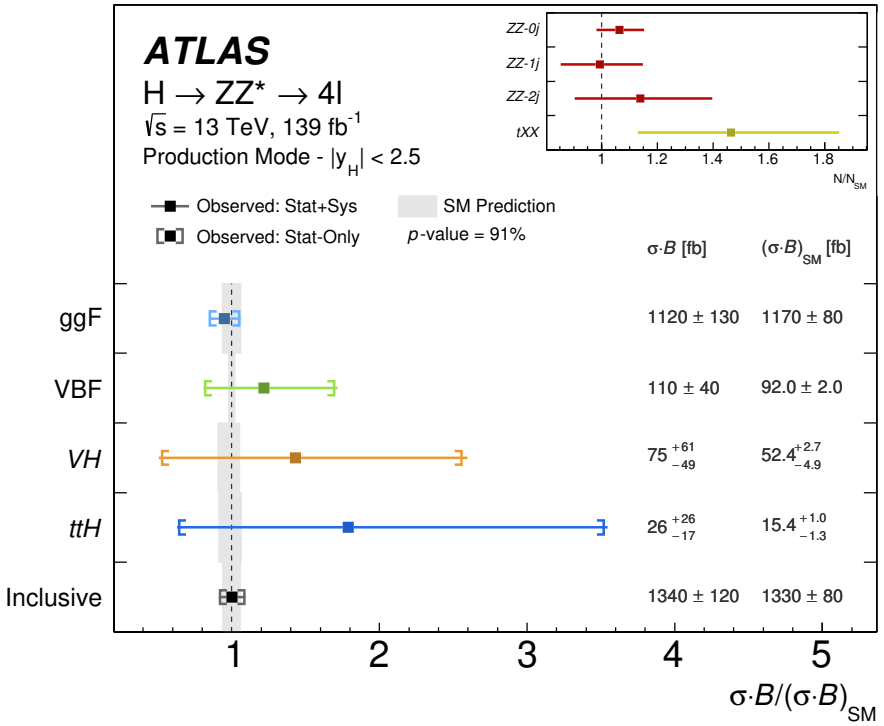

- Constraints on Higgs boson coupling-strength modifiers (κ-Framework)

- Parametrise deviations from the SM predictions of the Higgs boson couplings to SM bosons (κ_V) and fermions (κ_F) assuming the SM tensor coupling structure

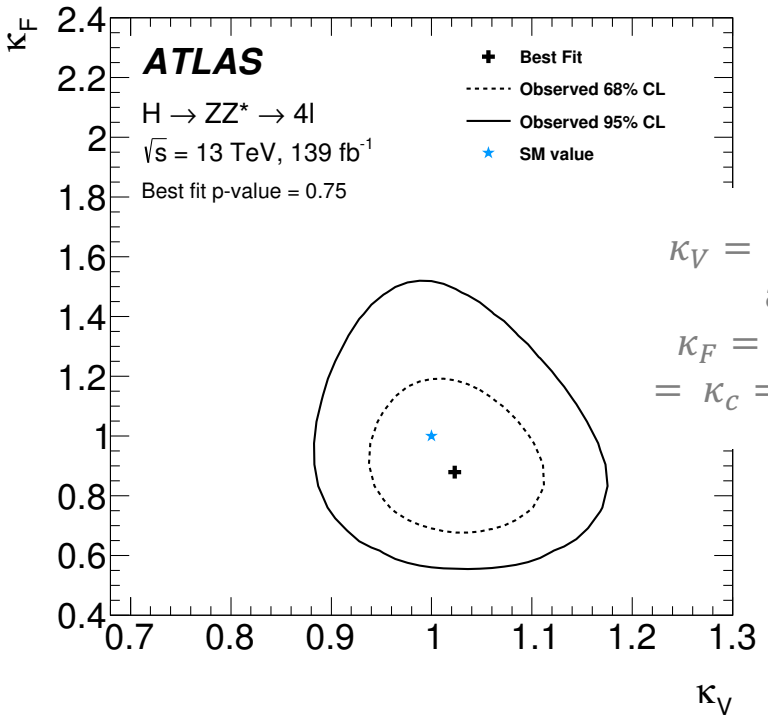

$\kappa_V = \kappa_W = \kappa_Z$
and
$\kappa_F = \kappa_t = \kappa_b = \kappa_c = \kappa_\tau = \kappa_\mu$

In good agreement with the SM prediction

Exclusive Production: Results

→ Remaining Backup

Reduced Stage 1.1

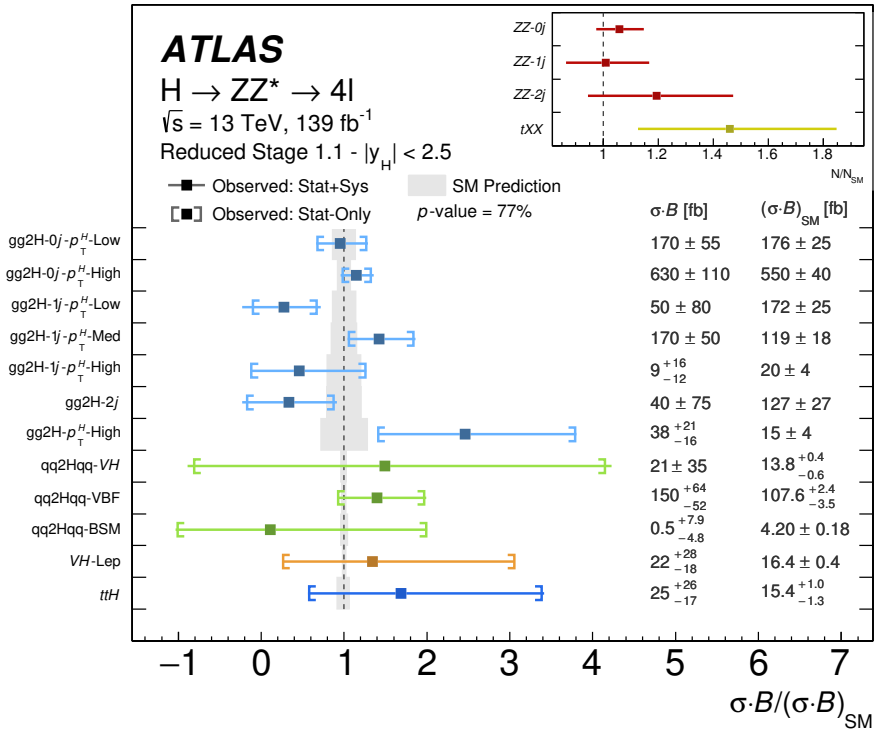

- Probing the tensor structure of Higgs boson couplings using an effective field theory approach

- Parametrisation in terms of BSM coupling parameters (i.e. Wilson coefficients of the Standard Model EFT with Warsaw basis)

$$\sigma^p(c_i) \cdot \mathcal{B}(c_i) \cdot \mathcal{A}^p(c_i) \cdot \prod_i^{N_{Cat}} \varepsilon_i^p$$

ε: reconstruction efficiency

$\mathcal{A}^p$: acceptance

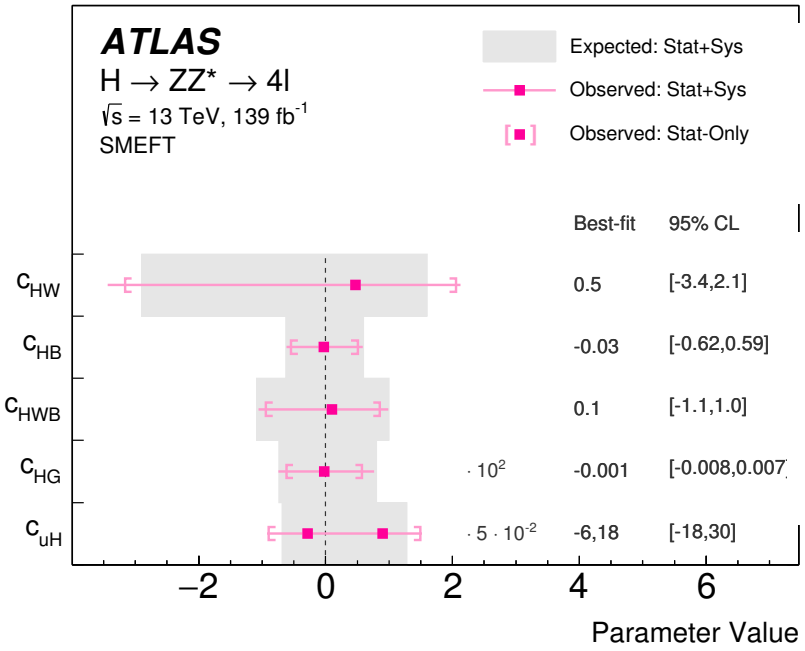

e.g. CP-even BSM couplings

Only one parameter fitted at a time, all others set to zero

2D fits also available

In good agreement with the SM prediction

Summary

- Measurement of Higgs boson properties using the full Run 2 data set:
  - Mass measurement:
    - Improved resolution compared to the combined ATLAS and CMS Run 1 measurement
  - Inclusive and differential fiducial cross-section measurements:
    - Large number of observables
    - Sensitive to BSM physics
  - Measurement of exclusive production cross-sections:
    - Can be combined with other Higgs decay channels in a straight forward manner
    - Allowing also for a combined EFT-interpretation
- Data are consistent with the SM hypothesis

BACKUP

Event Selection

Trigger	
Combination of single-lepton, dilepton and trilepton triggers	
Leptons and Jets	
Electrons	$E_T > 7$ GeV and $\|\eta\| < 2.47$
Muons	$p_T > 5$ GeV and $\|\eta\| < 2.7$, calorimeter-tagged: $p_T > 15$ GeV
Jets	$p_T > 30$ GeV and $\|\eta\| < 4.5$
Quadruplets	
All combinations of two same-flavour and opposite-charge lepton pairs - Leading lepton pair: lepton pair with invariant mass m_{12} closest to the Z boson mass m_Z - Subleading lepton pair: lepton pair with invariant mass m_{34} second closest to the Z boson mass m_Z Classification according to the decay final state: 4μ, $2e2\mu$, $2\mu2e$, $4e$	
Requirements on each quadruplet	
Lepton reconstruction	- Three highest-p_T leptons must have p_T greater than 20, 15 and 10 GeV - At most one calorimeter-tagged or stand-alone muon
Lepton pairs	- Leading lepton pair: $50 < m_{12} < 106$ GeV - Subleading lepton pair: $m_{min} < m_{34} < 115$ GeV - Alternative same-flavour opposite-charge lepton pair: $m_{\ell\ell} > 5$ GeV - $\Delta R(\ell,\ell') > 0.10$ for all lepton pairs
Lepton isolation	- The amount of isolation E_T after summing the track-based and 40% of the calorimeter-based contribution must be smaller than 16% of the lepton p_T
Impact parameter significance	- Electrons: $\|d_0\|/\sigma(d_0) < 5$ - Muons: $\|d_0\|/\sigma(d_0) < 3$
Common vertex	- χ^2-requirement on the fit of the four lepton tracks to their common vertex

Event Selection

Selection of the best quadruplet
- Select quadruplet with m_{12} closest to m_Z from one decay final state in decreasing order of priority: 4μ, $2e2\mu$, $2\mu2e$ and $4e$ - If at least one additional (fifth) lepton with $p_T > 12$ GeV meets the isolation, impact parameter and angular separation criteria, select the quadruplet with the highest matrix-element value
Higgs boson mass window
- Correction of the four-lepton invariant mass due to the FSR photons in Z boson decays - Four-lepton invariant mass window in the signal region: $115 < m_{4\ell} < 130$ GeV - Four-lepton invariant mass window in the sideband region: $105 < m_{4\ell} < 115$ GeV or $130 < m_{4\ell} < 160$ (350) GeV

The H→ZZ*→4ℓ Decay Channel

Processes with non-prompt leptons:

Z+jets

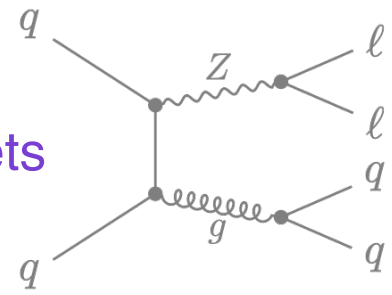

tt

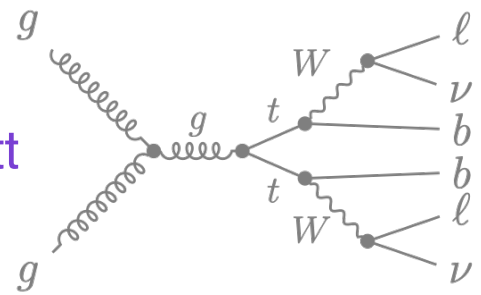

- Estimated separately for ℓℓ+μμ and ℓℓ+ee final states

- Data-driven estimation from control regions (inverted/relaxed selections)
- Estimated through simultaneous fit in control regions

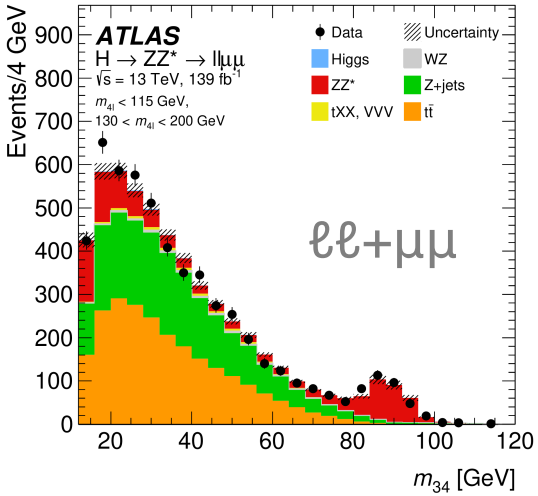

Control regions

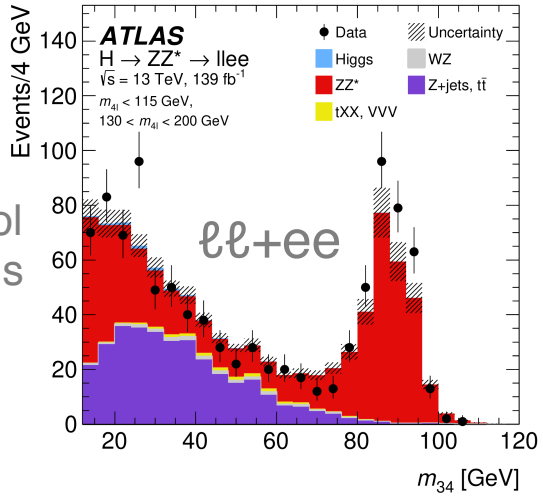

Reducible Background

- Fake lepton background:
  - Estimated in ℓℓμμ and ℓℓee final states
  - Dedicated fits in control regions for each reconstructed categories
  - Shape of the observable also extrapolated from a control region

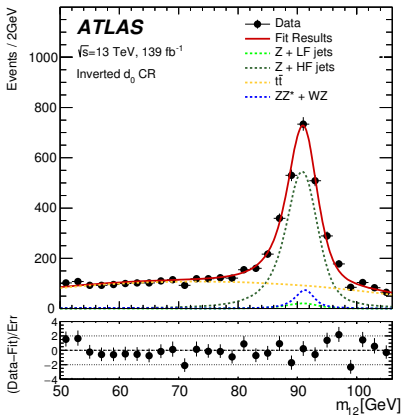

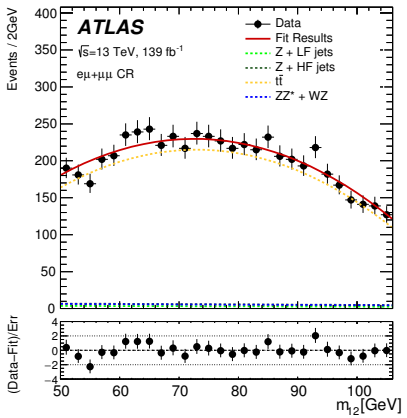

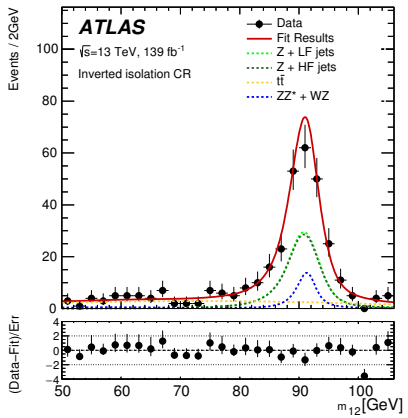

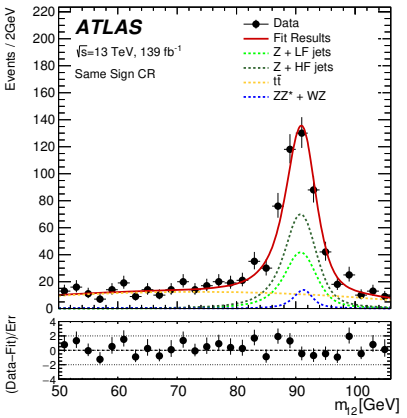

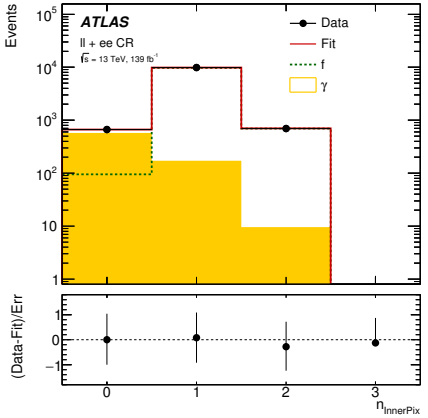

Reducible Background

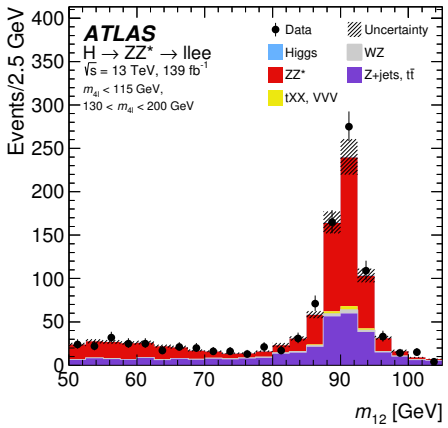

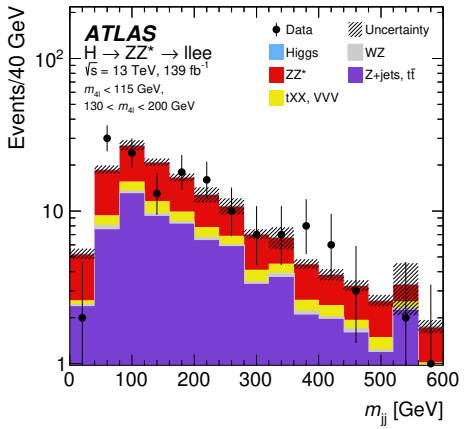

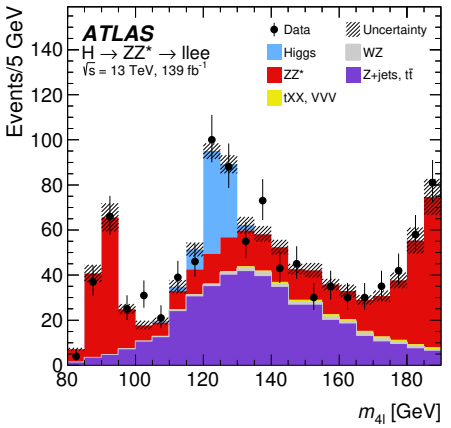

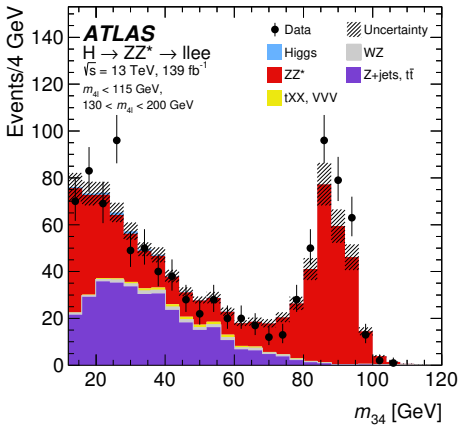

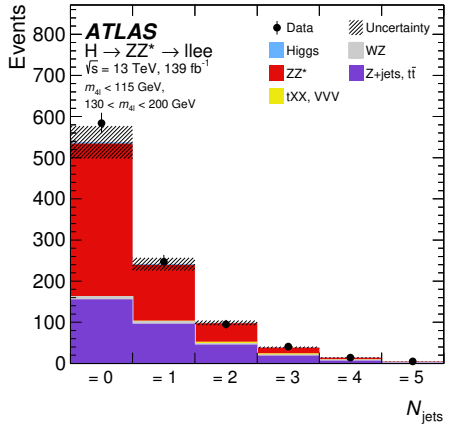

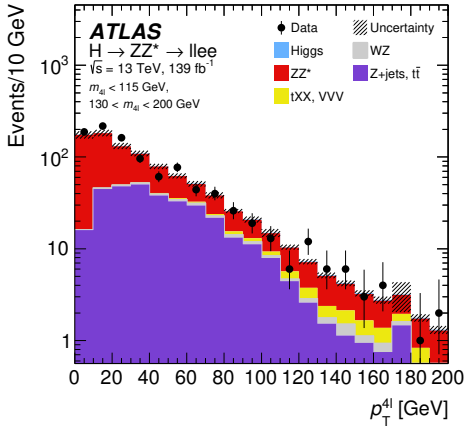

Reducible Background

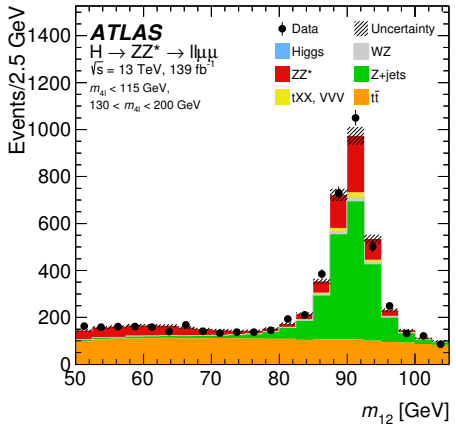

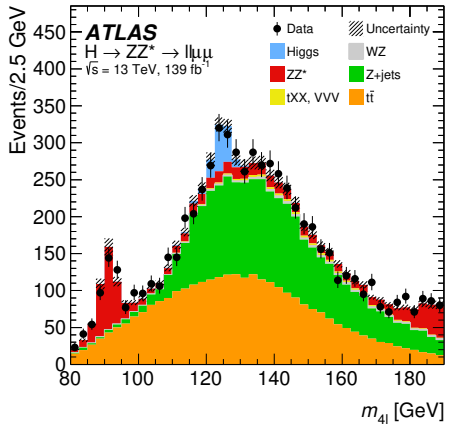

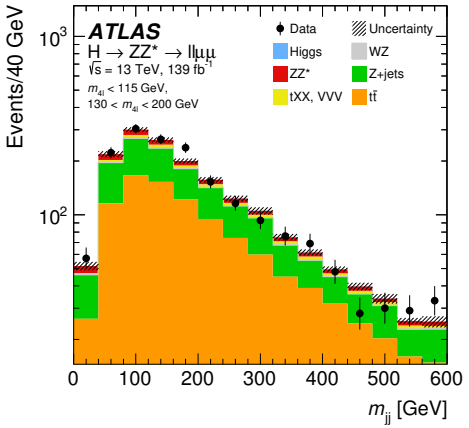

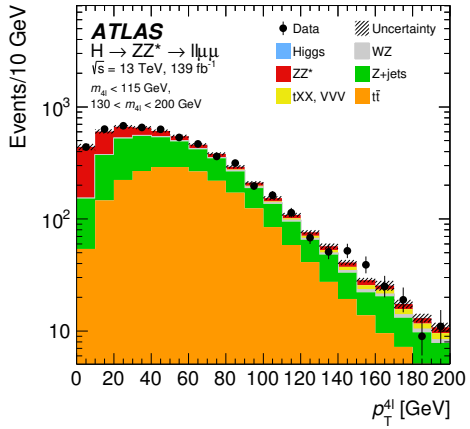

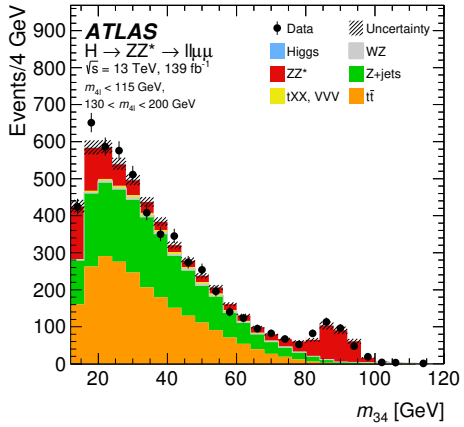

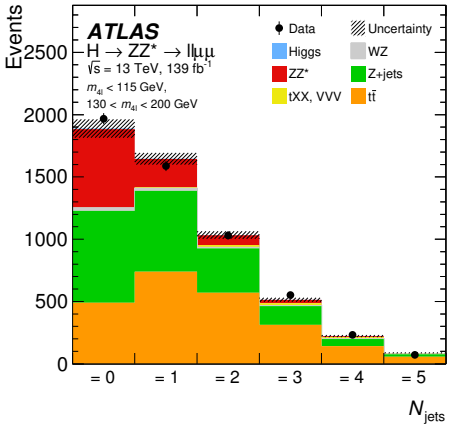

Mass Measurement – ZZ Bkg

Input observables:

- p_T^{4l}
- η_{4l}
- ME based: $\ln\left(|\mathcal{M}_{HZZ^*}|^2/|\mathcal{M}_{ZZ^*}|^2\right)$

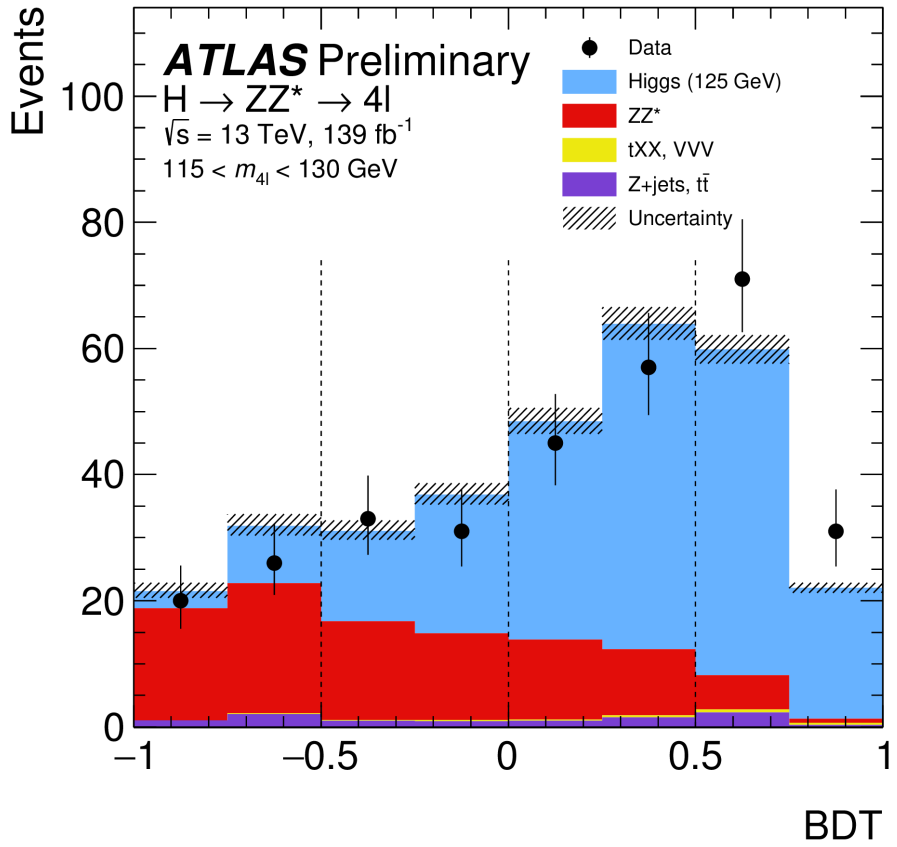

Per Event Resolution

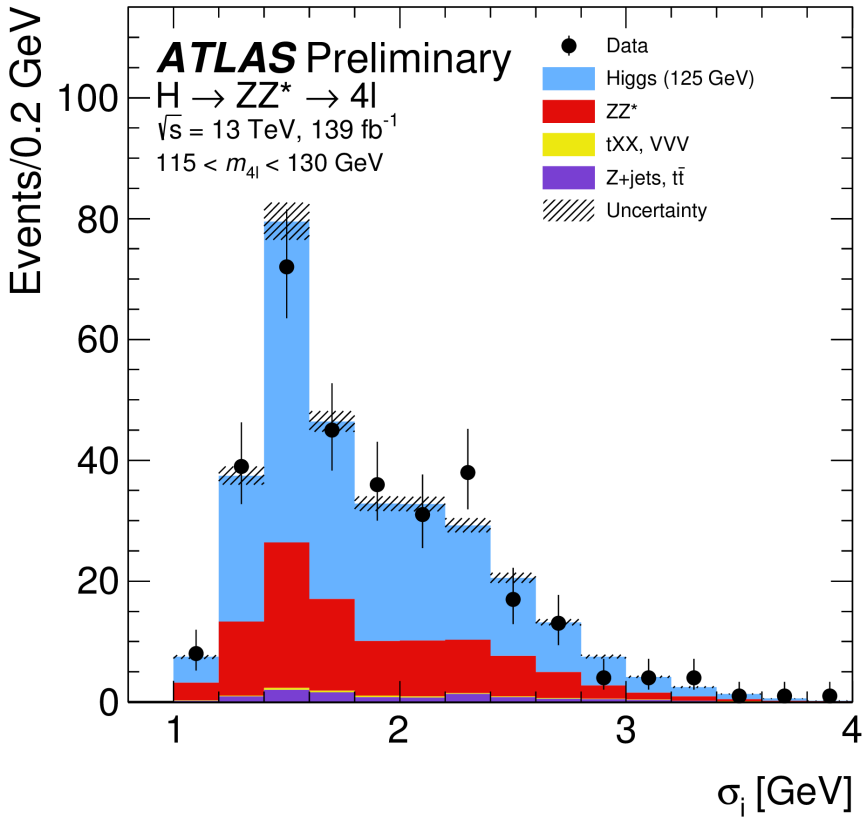

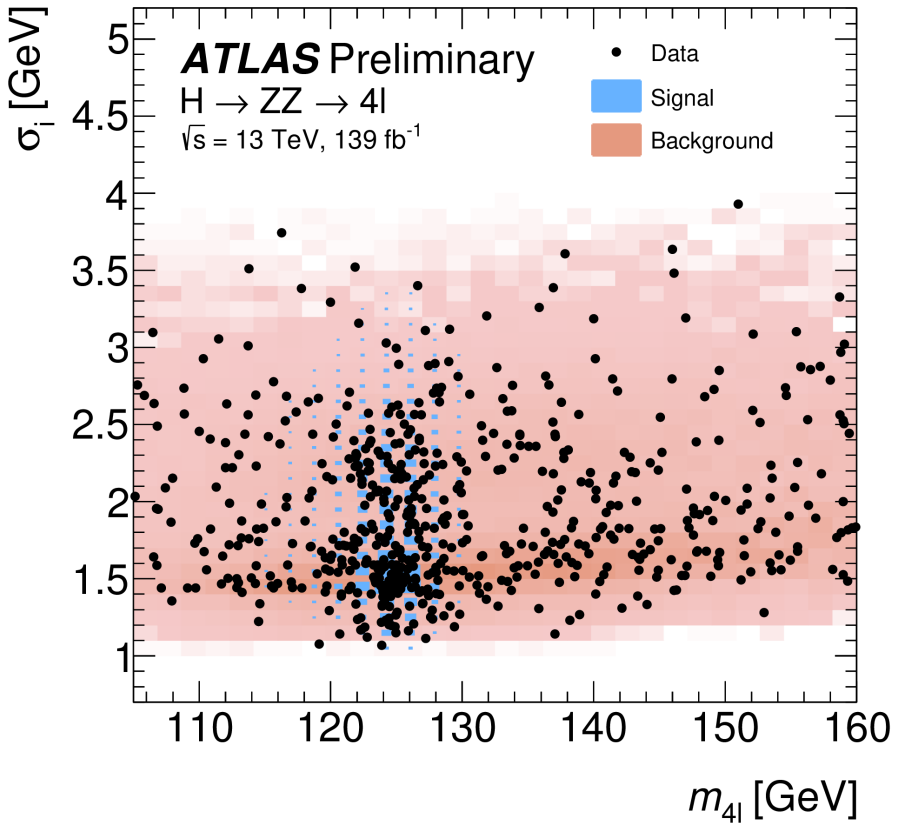

Mass Fit

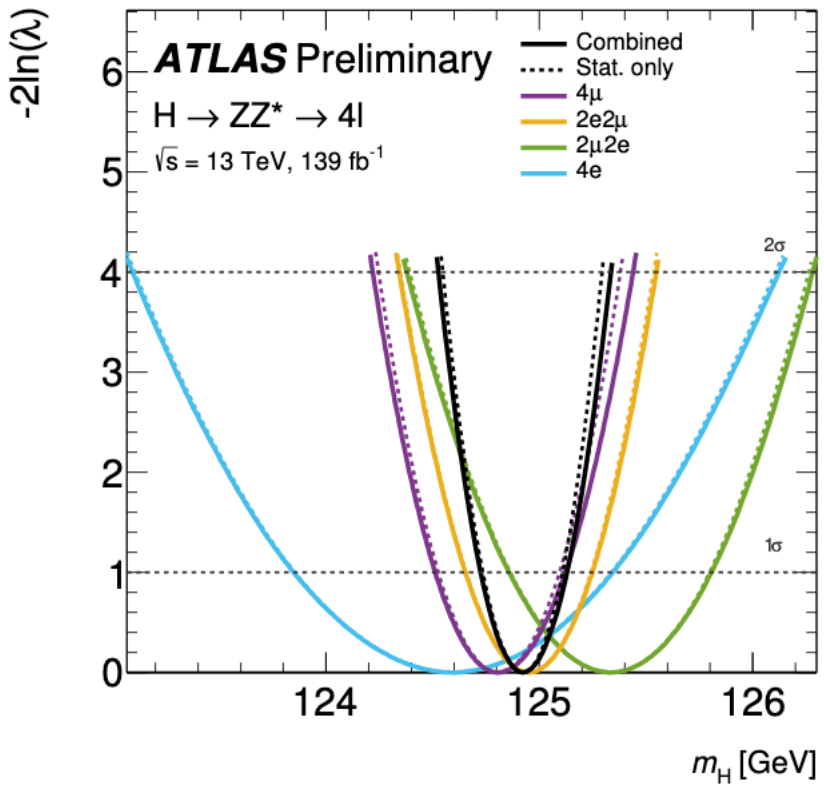

Table 4: Impact of the leading systematic uncertainties on m_H.

Systematic Uncertainty	Impact (GeV)
Muon momentum scale	+0.08,−0.06
Electron energy scale	±0.02
Muon momentum resolution	±0.01
Muon sagitta bias correction	±0.01

$$\mu = a^{\mu}(m_H - 125\ \text{GeV}) + b^{\mu} + 125\ \text{GeV}.$$

$$DCB\,(m_{4\ell};\mu,\sigma,\alpha_1,n_1,\alpha_2,n_2) = C\begin{cases}\left(\frac{n_1}{\alpha_1}\right)^{n_1}\cdot e^{-\frac{\alpha_1^2}{2}}\cdot\left(\frac{n_1}{\alpha_1}-\alpha_1-\frac{m_{4\ell}-\mu}{\sigma}\right)^{-n_1}, & \left(\frac{m_{4\ell}-\mu}{\sigma}\right) < -\alpha_1 \\ e^{-0.5\frac{(m_{4\ell}-\mu)^2}{\sigma^2}}, & -\alpha_1 \le \left(\frac{m_{4\ell}-\mu}{\sigma}\right) \le \alpha_2 \\ \left(\frac{n_2}{\alpha_2}\right)^{n_2}\cdot e^{-\frac{\alpha_2^2}{2}}\cdot\left(\frac{n_2}{\alpha_2}-\alpha_2+\frac{m_{4\ell}-\mu}{\sigma}\right)^{-n_2}, & \alpha_2 < \left(\frac{m_{4\ell}-\mu}{\sigma}\right)\end{cases}$$

Fiducial Cross-Sections

Higgs boson kinematic-related variables	
$p_{\mathrm{T}}^{4\ell}$, $\lvert y_{4\ell}\rvert$	Transverse momentum and rapidity of the four-lepton system
m_{12}, m_{34}	Invariant mass of the leading and subleading lepton pair
$\lvert\cos\theta^{*}\rvert$	Magnitude of the cosine of the decay angle of the leading lepton pair in the four-lepton rest frame relative to the beam axis
$\cos\theta_1$, $\cos\theta_2$	Production angles of the anti-leptons from the two Z bosons, where the angle is relative to the Z vector.
ϕ, ϕ_1	Two azimuthal angles between the three planes constructed from the Z bosons and leptons in the Higgs boson rest frame.
Jet-related variables	
N_{jets}, $N_{b\text{-jets}}$	Jet and b-jet multiplicity
$p_{\mathrm{T}}^{\text{lead. jet}}$, $p_{\mathrm{T}}^{\text{sublead. jet}}$	Transverse momentum of the leading and subleading jet, for events with at least one and two jets, respectively. Here, the leading jet refers to the jet with the highest p_{T} in the event, while subleading refers to the jet with the second-highest p_{T}.
m_{jj}, $\lvert\Delta\eta_{jj}\rvert$, $\Delta\phi_{jj}$	Invariant mass, difference in pseudorapidity, and signed difference in ϕ of the leading and subleading jets for events with at least two jets
Higgs boson and jet-related variables	
$p_{\mathrm{T}}^{4\ell\mathrm{j}}$, $m_{4\ell j}$	Transverse momentum and invariant mass of the four-lepton system and leading jet, for events with at least one jet
$p_{\mathrm{T}}^{4\ell\mathrm{jj}}$, $m_{4\ell jj}$	Transverse momentum and invariant mass of the four-lepton system and leading and subleading jets, for events with at least two jets

Fiducial Cross-Sections

Observable	Stat.	Syst.	Dominant systematic components [%]						
	unc. [%]	unc. [%]	Lumi.	e/μ	Jets	Other Bkg.	ZZ^* Th.	Sig. Th.	Comp.
σ_{comb}	9	3	1.7	2	< 0.5	< 0.5	1.0	1.5	< 0.5
$\sigma_{4\mu}$	15	4	1.7	3	< 0.5	< 0.5	1.5	1.0	< 0.5
$\sigma_{4\text{e}}$	26	8	1.7	7	< 0.5	< 0.5	1.5	1.5	< 0.5
$\sigma_{2\mu 2\text{e}}$	20	7	1.7	5	< 0.5	< 0.5	2	1.5	< 0.5
$\sigma_{2\text{e}2\mu}$	15	3	1.7	2	< 0.5	< 0.5	1	1.5	< 0.5
$\mathrm{d}\sigma \,/\, \mathrm{d}p_{\mathrm{T}}^{4\ell}$	20–46	2–8	1.7	1–3	1–2	< 0.5	1–6	1–2	< 1
$\mathrm{d}\sigma \,/\, \mathrm{d}m_{12}$	12–42	3–6	1.7	2–3	< 1	< 0.5	1–2	1–2	< 1
$\mathrm{d}\sigma \,/\, \mathrm{d}m_{34}$	20–82	3–12	1.7	2–3	< 1	1–2	1–8	1–3	< 1
$\mathrm{d}\sigma \,/\, \mathrm{d}\lvert y_{4\ell}\rvert$	22–81	3–6	1.7	2–3	< 1	< 0.5	1–5	1–3	< 1
$\mathrm{d}\sigma \,/\, \mathrm{d}\lvert\cos\theta^*\rvert$	23–113	3–6	1.7	2–3	< 1	1–2	1–7	1–3	< 0.5
$\mathrm{d}\sigma \,/\, \mathrm{d}\cos\theta_1$	23–44	3–6	1.7	2–3	< 1	< 0.5	1–3	1–2	< 1
$\mathrm{d}\sigma \,/\, \mathrm{d}\cos\theta_2$	22–39	3–6	1.7	2–3	< 1	< 0.5	1–3	1–3	< 1
$\mathrm{d}\sigma \,/\, \mathrm{d}\phi$	20–29	2–5	1.7	2–3	< 1	< 0.5	1–3	1–2	< 0.5
$\mathrm{d}\sigma \,/\, \mathrm{d}\phi_1$	22–33	3–6	1.7	2–3	< 1	< 0.5	1–2	1–3	< 0.5
$\mathrm{d}\sigma \,/\, \mathrm{d}N_{\text{jets}}$	15–37	6–14	1.7	1–3	4–10	< 0.5	1–4	3–7	1–4
$\mathrm{d}\sigma \,/\, \mathrm{d}N_{b-\text{jets}}$	15–67	6–15	1.7	1–3	4–5	1–3	1–2	3–9	1–4
$\mathrm{d}\sigma \,/\, \mathrm{d}p_{\mathrm{T}}^{\text{lead. jet}}$	15–34	3–13	1.7	1–3	4–10	< 0.5	1–2	1–5	< 0.5
$\mathrm{d}\sigma \,/\, \mathrm{d}p_{\mathrm{T}}^{\text{sublead. jet}}$	11–67	5–22	1.7	1–3	2–12	< 1	1–3	2–15	1–5
$\mathrm{d}\sigma \,/\, \mathrm{d}m_{\text{jj}}$	11–50	5–18	1.7	1–3	1–11	< 0.5	1–3	2–15	1–2
$\mathrm{d}\sigma \,/\, \mathrm{d}\eta_{jj}$	11–57	5–17	1.7	1–3	2–10	< 0.5	1–2	2–14	1–4
$\mathrm{d}\sigma \,/\, \mathrm{d}\phi_{jj}$	11–50	4–18	1.7	1–3	2–9	< 0.5	1–3	2–14	1–6
$\mathrm{d}\sigma \,/\, \mathrm{d}m_{4\ell\text{j}}$	15–66	4–19	1.7	1–3	3–9	< 0.5	1–6	3–14	1–8
$\mathrm{d}\sigma \,/\, \mathrm{d}m_{4\ell\text{jj}}$	11–182	5–67	1.7	1–3	4–24	< 0.5	1–5	2–35	1–9
$\mathrm{d}\sigma \,/\, \mathrm{d}p_{\mathrm{T}}^{4\ell\text{j}}$	15–76	6–13	1.7	1–3	2–8	< 1	1–5	3–9	1–3
$\mathrm{d}\sigma \,/\, \mathrm{d}p_{\mathrm{T}}^{4\ell\text{jj}}$	11–76	5–27	1.7	2–3	2–9	1–2	1–4	3–17	1–12
$\mathrm{d}^2\sigma \,/\, \mathrm{d}m_{12}\,\mathrm{d}m_{34}$	16–65	3–11	1.7	2–3	< 1	1–2	1–9	1–3	1–2
$\mathrm{d}^2\sigma \,/\, \mathrm{d}p_{\mathrm{T}}^{4\ell}\,\mathrm{d}\lvert y_{4\ell}\rvert$	23–63	2–13	1.7	1–3	1–2	< 1	1–6	1–5	1–2
$\mathrm{d}^2\sigma \,/\, \mathrm{d}p_{\mathrm{T}}^{4\ell}\,\mathrm{d}N_{\text{jets}}$	23–93	4–193	1.7	2–14	2–25	1–3	1–7	1–12	1–92
$\mathrm{d}^2\sigma \,/\, \mathrm{d}p_{\mathrm{T}}^{4\ell\text{j}}\,\mathrm{d}m_{4\ell\text{j}}$	15–41	4–12	1.7	1–3	2–8	< 0.5	1–5	2–9	< 1
$\mathrm{d}^2\sigma \,/\, \mathrm{d}p_{\mathrm{T}}^{4\ell}\,\mathrm{d}p_{\mathrm{T}}^{4\ell\text{j}}$	15–53	3–10	1.7	1–3	2–8	< 1	1–2	2–6	1–2
$\mathrm{d}^2\sigma \,/\, \mathrm{d}p_{\mathrm{T}}^{4\ell}\,\mathrm{d}p_{\mathrm{T}}^{\text{lead. jet}}$	15–84	3–21	1.7	1–3	2–18	1–10	1–3	2–9	1–3
$\mathrm{d}^2\sigma \,/\, \mathrm{d}p_{\mathrm{T}}^{\text{lead. jet}}\,\mathrm{d}\lvert y^{\text{lead. jet}}\rvert$	15–38	3–11	1.7	1–3	2–9	< 0.5	1–2	1–4	1–2
$\mathrm{d}^2\sigma \,/\, \mathrm{d}p_{\mathrm{T}}^{\text{lead. jet}}\,\mathrm{d}p_{\mathrm{T}}^{\text{sublead. jet}}$	15–63	5–22	1.7	1–3	4–15	< 0.5	1–4	3–11	1–7

Fiducial Cross-Sections: Results

Cross section [fb]	Data ($\pm$ (stat.)	$\pm$ (syst.))	Standard Model prediction	p-value [%]
$\sigma_{4\mu}$	0.81	± 0.12	± 0.03	0.90(5)	46
σ_{4e}	0.62	± 0.17	± 0.05	0.90(5)	14
$\sigma_{2\mu 2e}$	0.74	± 0.15	± 0.05	0.80(4)	67
$\sigma_{2e2\mu}$	1.01	± 0.15	± 0.03	0.80(4)	15
$\sigma_{4\mu+4e}$	1.43	± 0.21	± 0.05	1.81(10)	10
$\sigma_{2\mu 2e+2e2\mu}$	1.75	± 0.21	± 0.06	1.61(9)	51
σ_{sum}	3.18	± 0.31	± 0.11	3.41(18)	49
σ_{comb}	3.28	± 0.30	± 0.11	3.41(18)	67
σ_{tot} [pb]	53.5	± 4.9	± 2.1	55.7(28)	66

Fiducial Cross-Sections: Results

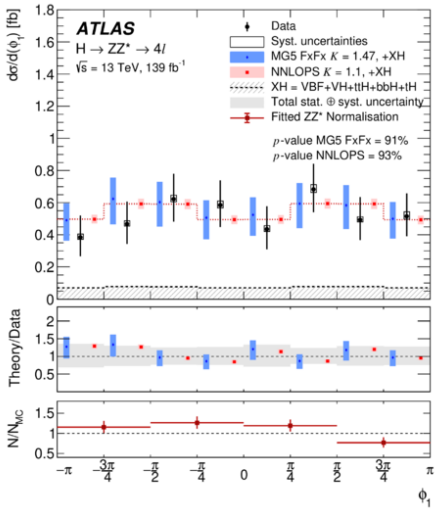

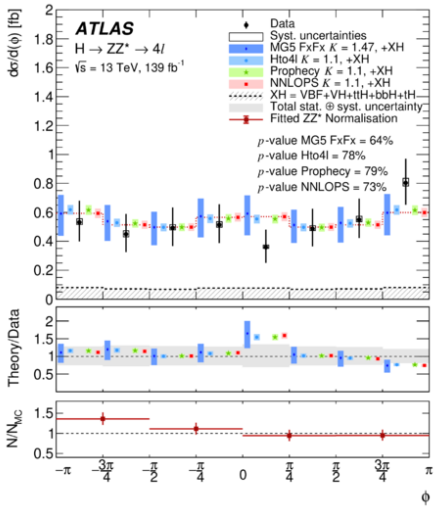

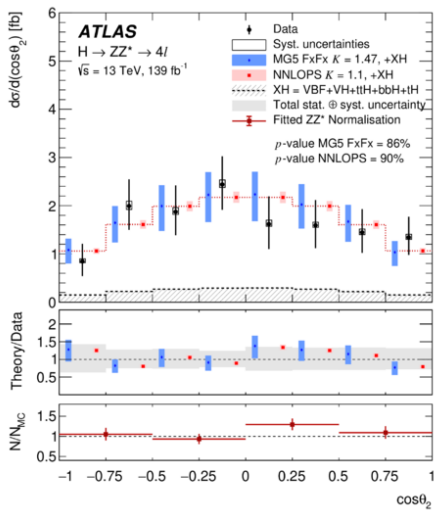

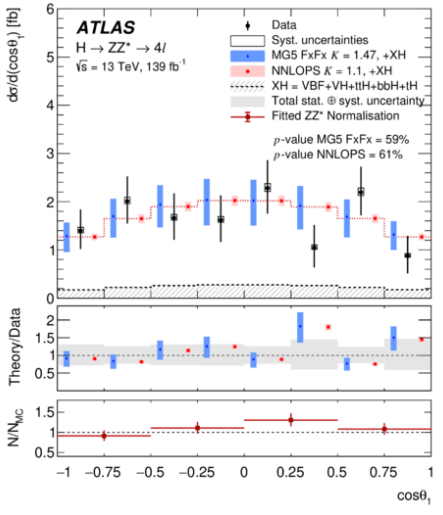

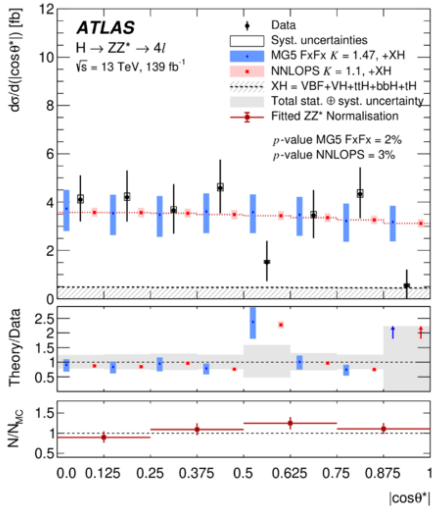

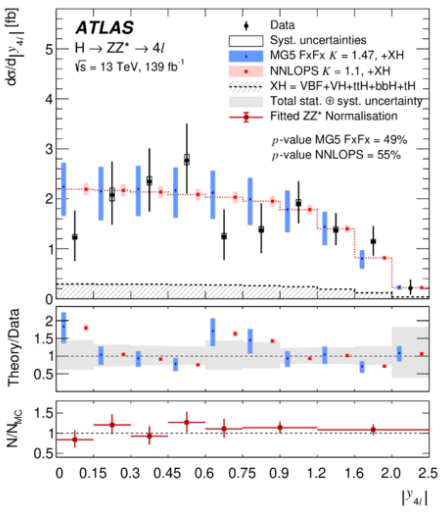

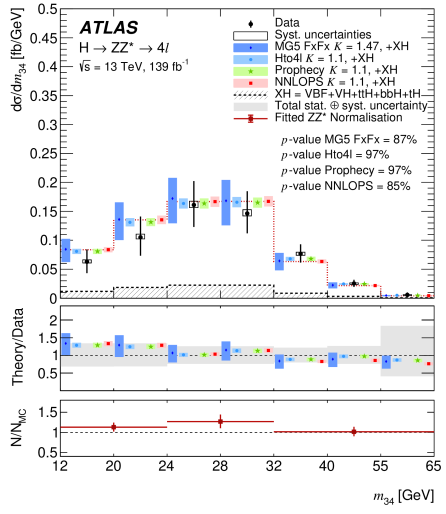

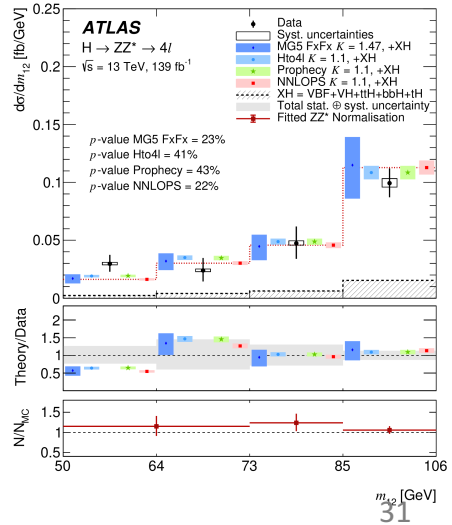

rement of

Fiducial Cross-Sections: Results

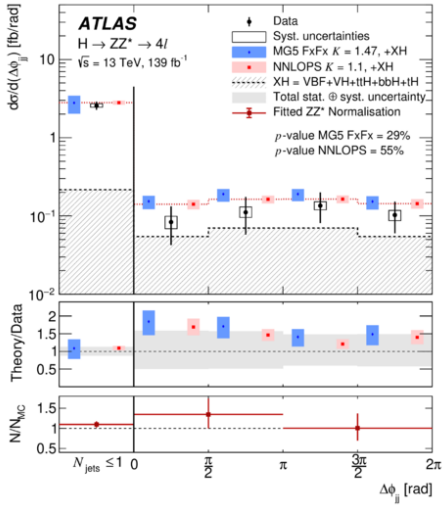

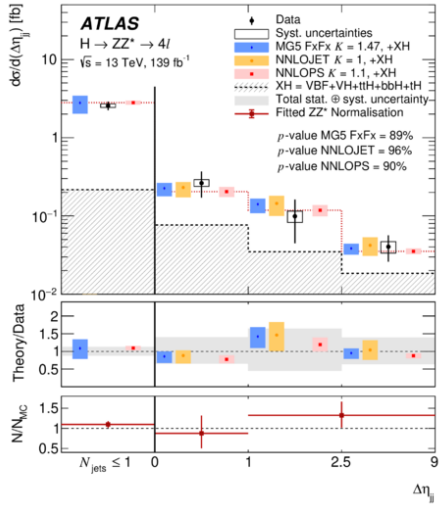

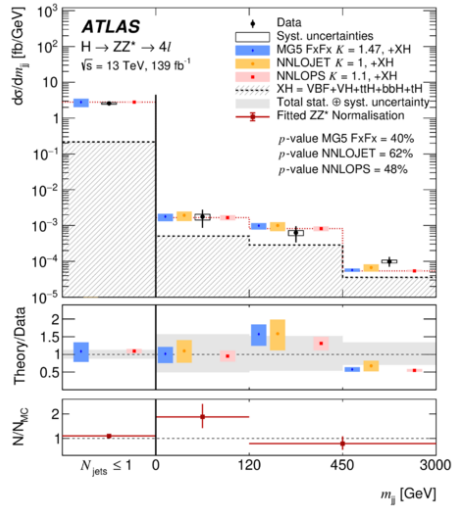

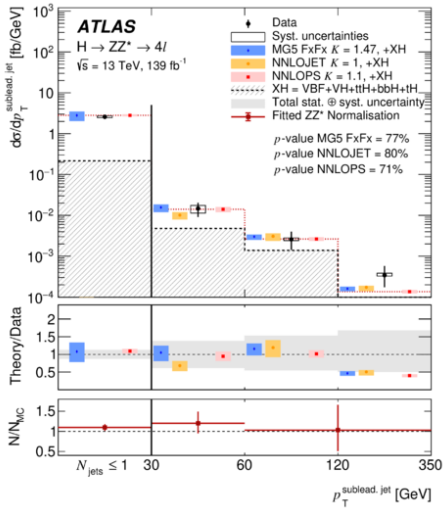

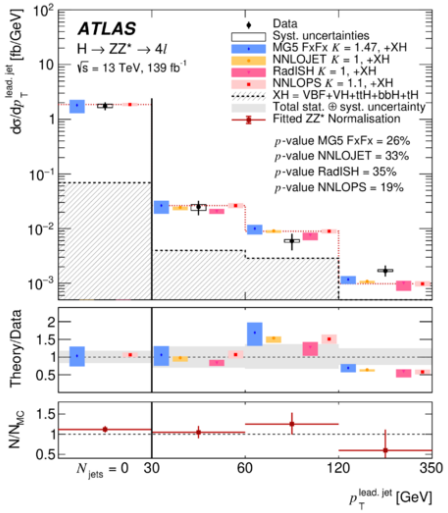

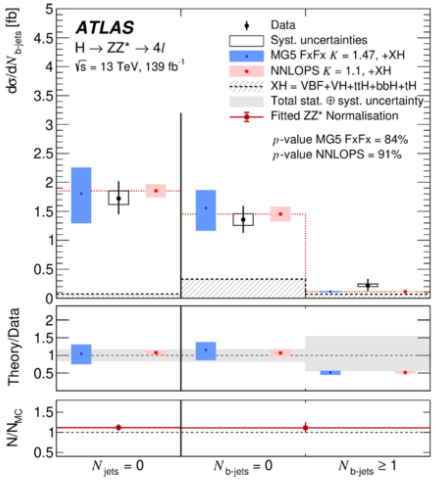

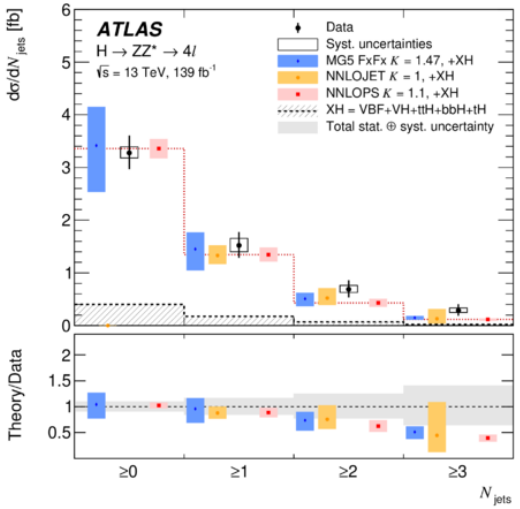

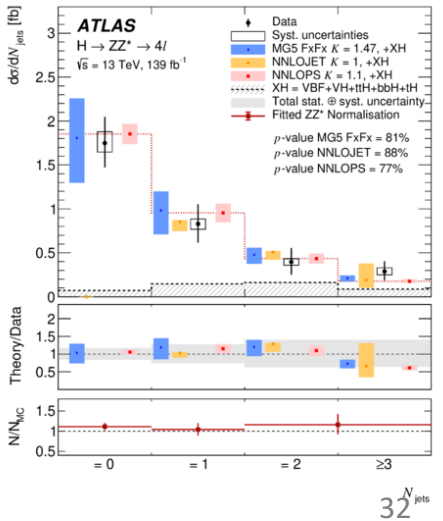

Fiducial Cross-Sections: Results

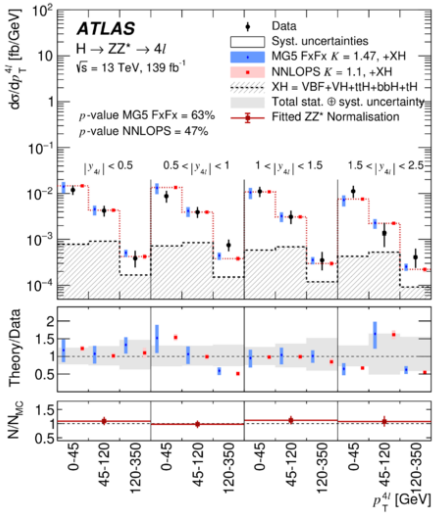

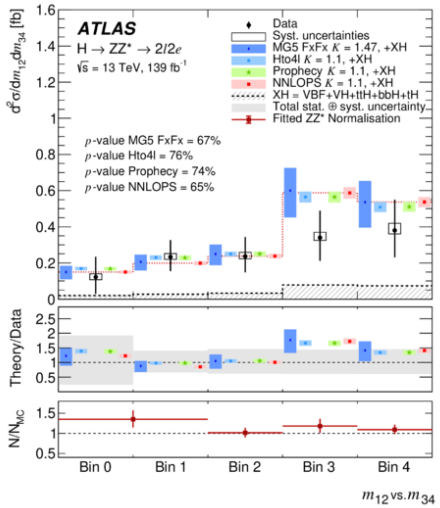

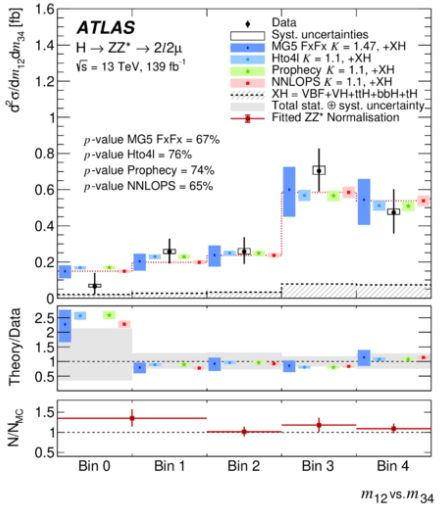

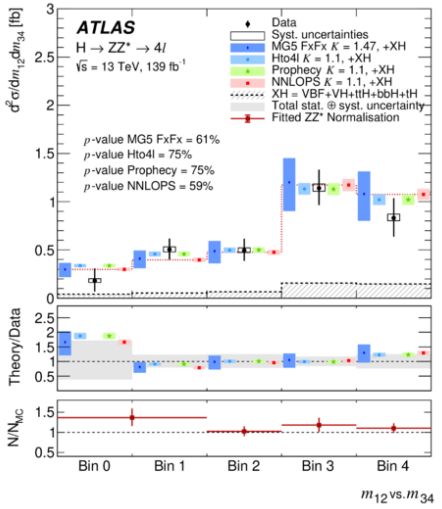

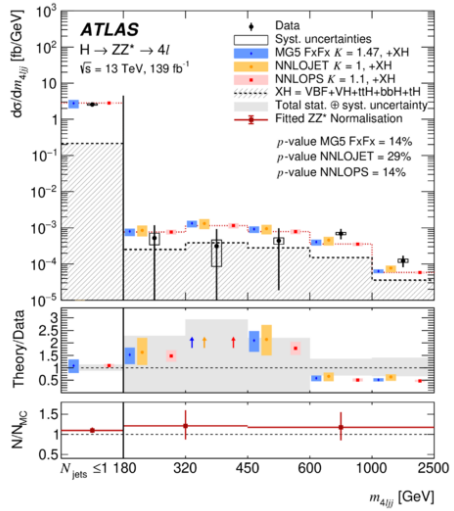

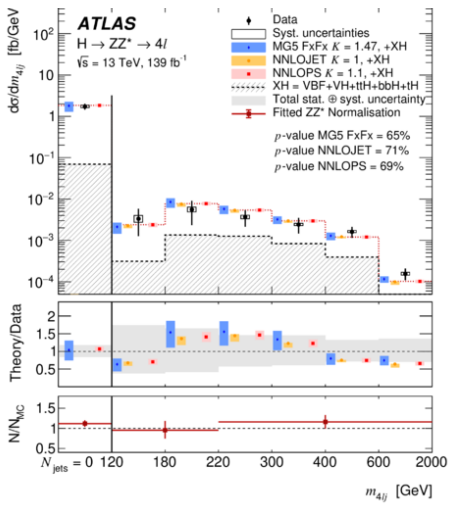

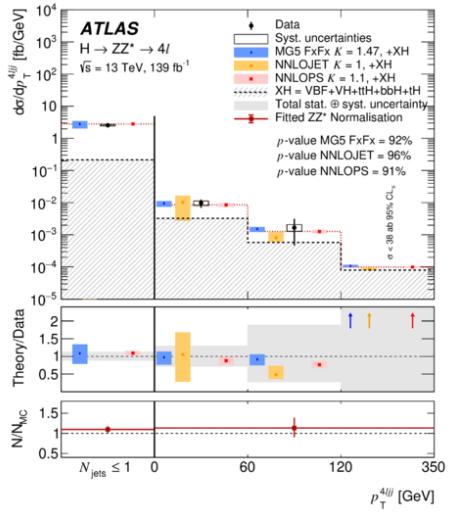

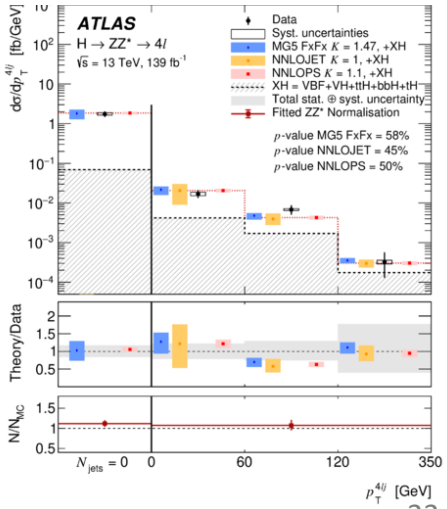

Fiducial Cross-Sections: Results

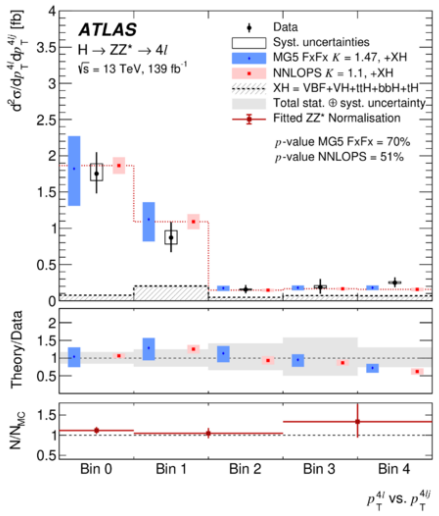

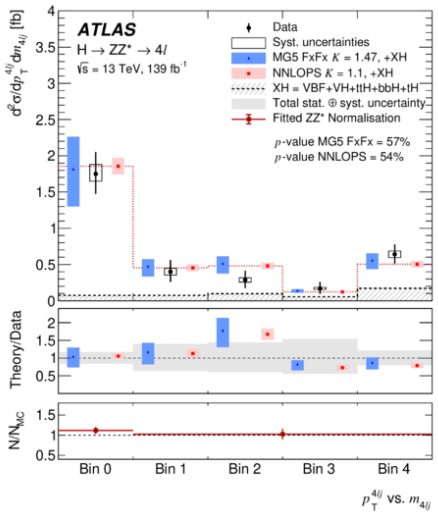

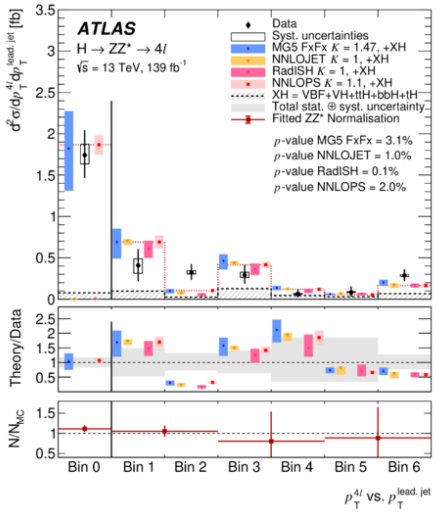

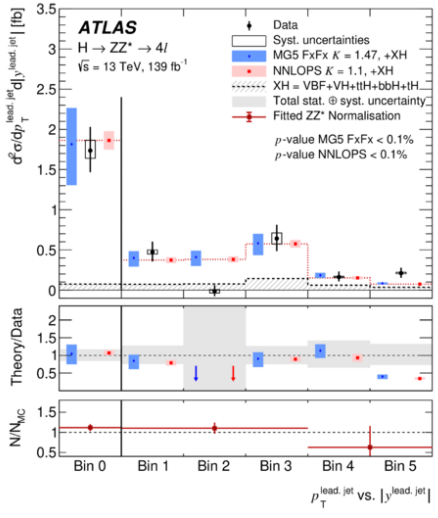

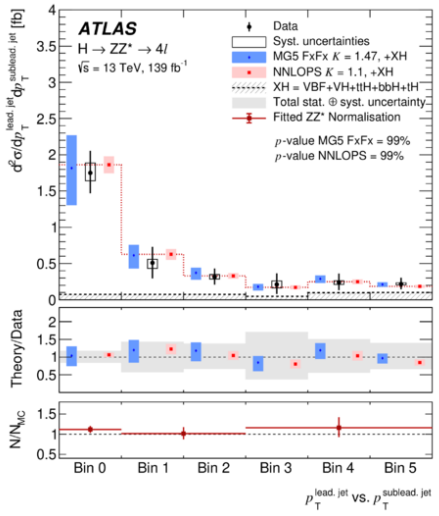

Fiducial Cross-Sections: Interpretations

- Transverse momentum distribution:
  - A test of perturbative QCD
  - Sensitive to the structure of Higgs boson interactions
  - Sensitive to charm and bottom Yukawa couplings
- Invariant masses:
  - Sensitive to higher-order EW corrections to the Higgs boson decay
  - Sensitive to BSM contributions
- Jet related variables:
  - Probe QCD radiation effects
  - Higgs boson production

Fiducial Cross-Sections: Results

→ Remaining Backup

Double differential e.g. m_{12} vs. m_{34}:

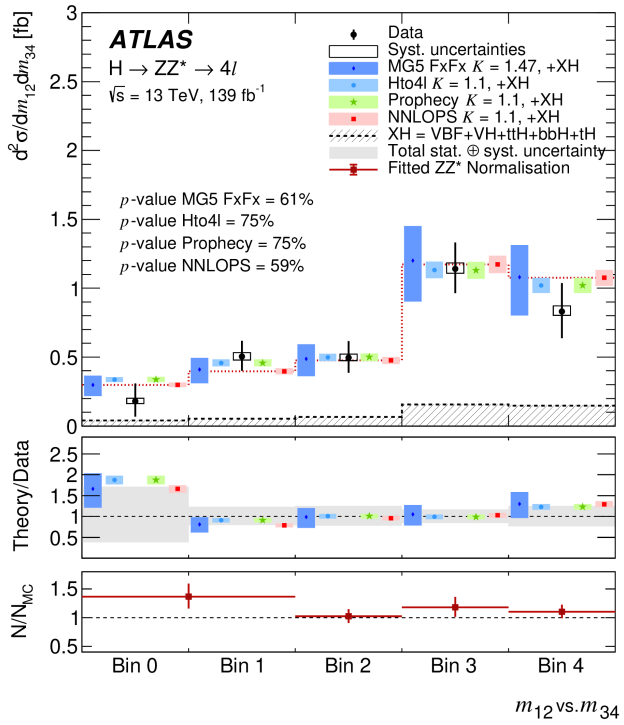

- Constraints on BSM effects within the pseudo-observables framework

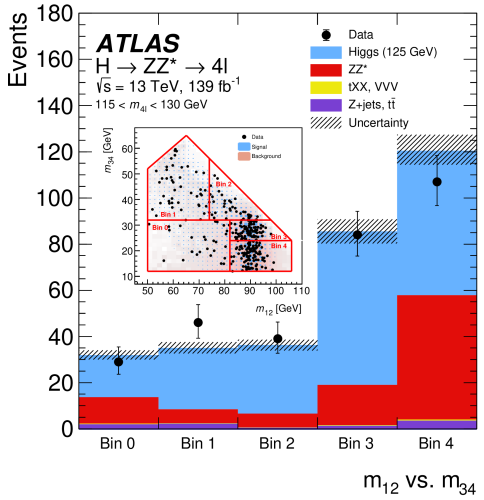

- Introduction of modified contact terms between Higgs boson, Z boson and left- or right-handed leptons e.g. κ_{ZZ} and ϵ_L ($\epsilon_R = 0.48\ \epsilon_L$)
- Parametrise fiducial cross-section in each m_{12} vs. m_{34} bin as a function of BSM couplings

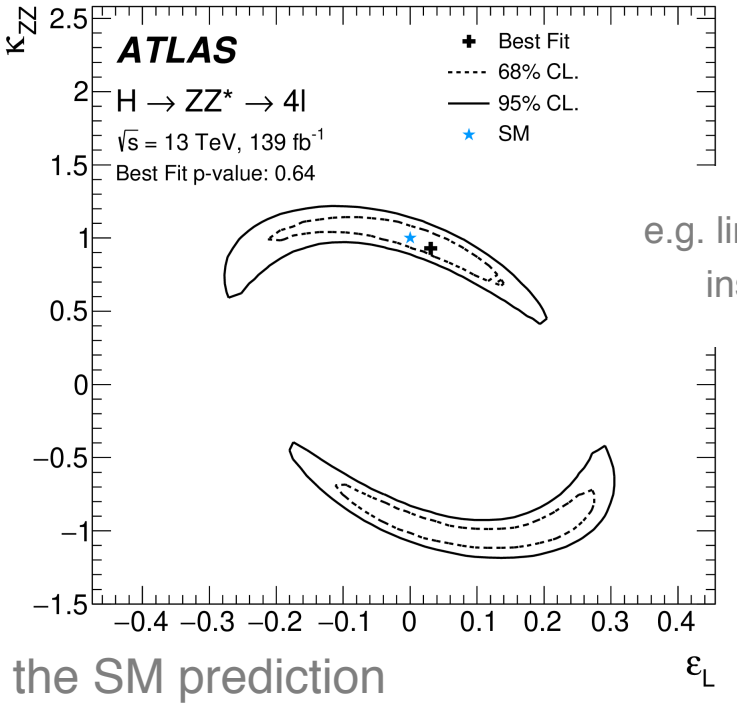

e.g. linear EFT-inspired

In good agreement with the SM prediction

Interpretations within Pseudo-Observables

flavour universal contact terms

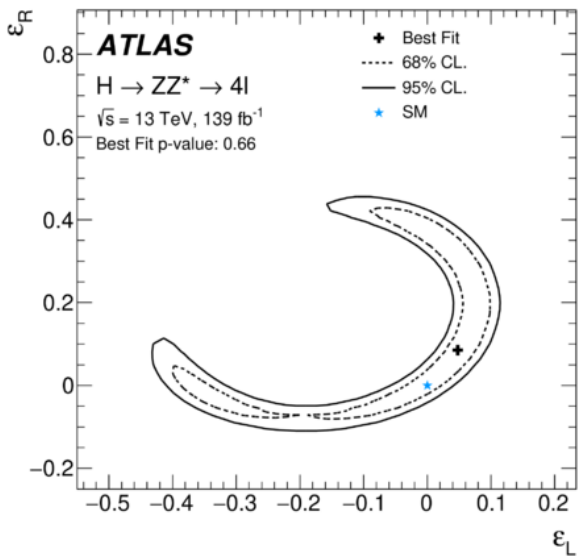

flavour non-universal vector contact terms

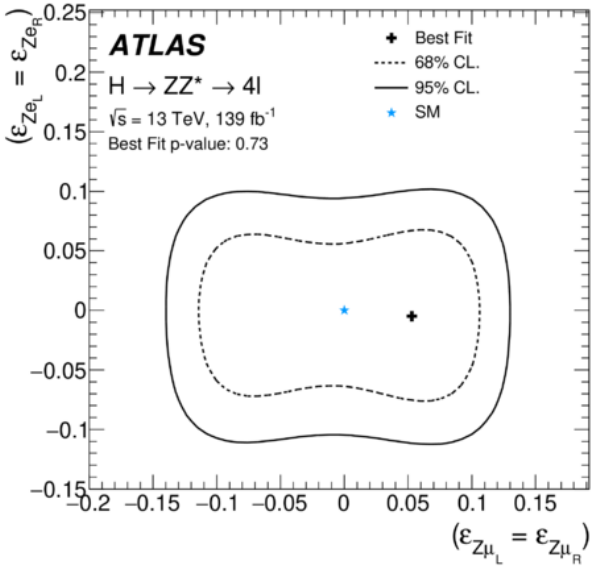

flavour non-universal axial-vector contact terms

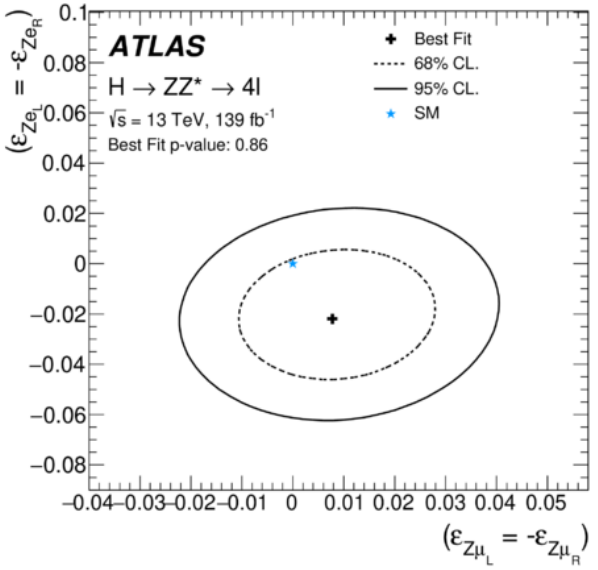

Interpretation	Parameter best-fit value	95% confidence interval
EFT-inspired	ϵ_L = 0.03	$[-0.25, 0.17]$
	κ_{ZZ} = 0.93	$[0.51, 1.16]$
Flavour non-universal vector	ϵ_{Ze} = -0.005	$[-0.097, 0.082]$
	$\epsilon_{Z\mu}$ = 0.054	$[-0.131, 0.114]$
Flavour non-universal axial-vector	ϵ_{Ze} = -0.022	$[-0.056, 0.012]$
	$\epsilon_{Z\mu}$ = 0.008	$[-0.016, 0.033]$

Interpretations: Yukawa Couplings

only the $p_T^{4\ell}$ shape

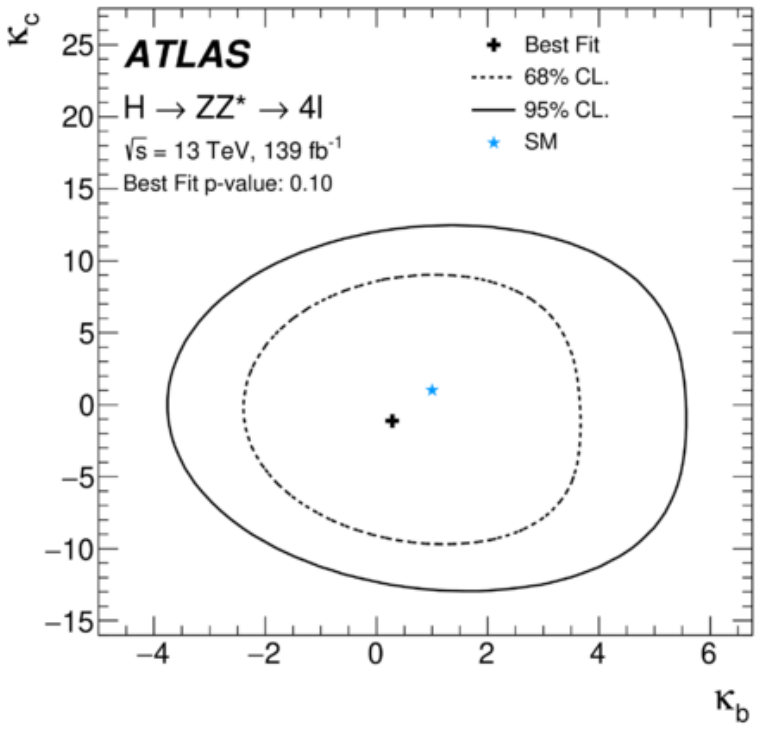

both the prediction of the $p_T^{4\ell}$ differential cross section and the modification to the branching ratio

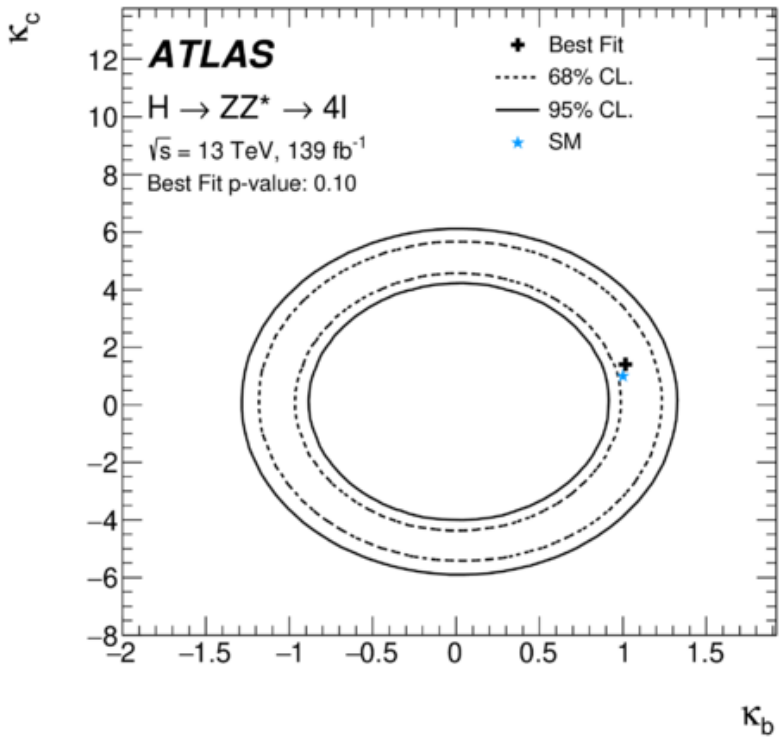

Exclusive Production Cross-Sections

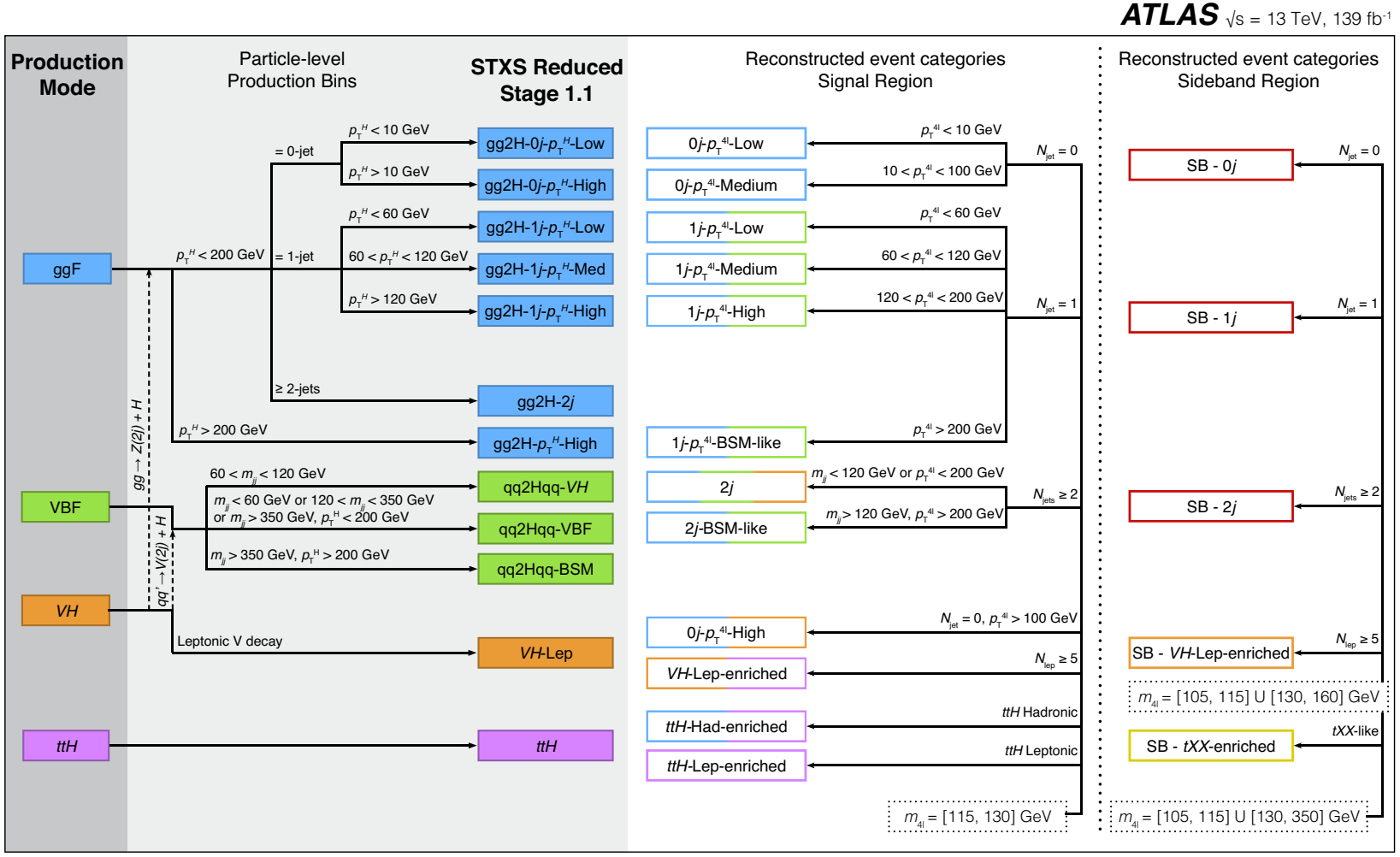

NN Input Variables

Category	Processes	MLP	Lepton RNN	Jet RNN	Discriminant
$0j$-$p_{\mathrm{T}}^{4\ell}$-Low $0j$-$p_{\mathrm{T}}^{4\ell}$-Med	ggF, ZZ^*	$p_{\mathrm{T}}^{4\ell}$, D_{ZZ^*}, m_{12}, m_{34}, $\lvert\cos\theta^*\rvert$, $\cos\theta_1$, ϕ_{ZZ}	p_{T}^{ℓ}, η_{ℓ}	-	$\mathrm{NN}_{\mathrm{ggF}}$
$1j$-$p_{\mathrm{T}}^{4\ell}$-Low	ggF, VBF, ZZ^*	$p_{\mathrm{T}}^{4\ell}$, p_{T}^{j}, η_j, $\Delta R_{4\ell j}$, D_{ZZ^*}	p_{T}^{ℓ}, η_{ℓ}	-	$\mathrm{NN}_{\mathrm{VBF}}$ for $\mathrm{NN}_{ZZ} < 0.25$ NN_{ZZ} for $\mathrm{NN}_{ZZ} > 0.25$
$1j$-$p_{\mathrm{T}}^{4\ell}$-Med	ggF, VBF, ZZ^*	$p_{\mathrm{T}}^{4\ell}$, p_{T}^{j}, η_j, $E_{\mathrm{T}}^{\mathrm{miss}}$, $\Delta R_{4\ell j}$, D_{ZZ^*}, $\eta_{4\ell}$	p_{T}^{ℓ}, η_{ℓ}	-	$\mathrm{NN}_{\mathrm{VBF}}$ for $\mathrm{NN}_{ZZ} < 0.25$ NN_{ZZ} for $\mathrm{NN}_{ZZ} > 0.25$
$1j$-$p_{\mathrm{T}}^{4\ell}$-High	ggF, VBF	$p_{\mathrm{T}}^{4\ell}$, p_{T}^{j}, η_j, $E_{\mathrm{T}}^{\mathrm{miss}}$, $\Delta R_{4\ell j}$, $\eta_{4\ell}$	p_{T}^{ℓ}, η_{ℓ}	-	$\mathrm{NN}_{\mathrm{VBF}}$
$2j$	ggF, VBF, VH	m_{jj}, $p_{\mathrm{T}}^{4\ell jj}$	p_{T}^{ℓ}, η_{ℓ}	p_{T}^{j}, η_j	$\mathrm{NN}_{\mathrm{VBF}}$ for $\mathrm{NN}_{VH} < 0.2$ NN_{VH} for $\mathrm{NN}_{VH} > 0.2$
$2j$-BSM-like	ggF, VBF	$\eta_{ZZ}^{\mathrm{Zepp}}$, $p_{\mathrm{T}}^{4\ell jj}$	p_{T}^{ℓ}, η_{ℓ}	p_{T}^{j}, η_j	$\mathrm{NN}_{\mathrm{VBF}}$
VH-Lep-enriched	VH, ttH	N_{jets}, $N_{b\text{-jets},70\%}$, $E_{\mathrm{T}}^{\mathrm{miss}}$, H_{T}	p_{T}^{ℓ}	-	NN_{ttH}
ttH-Had-enriched	ggF, ttH, tXX	$p_{\mathrm{T}}^{4\ell}$, m_{jj}, $\Delta R_{4\ell j}$, $N_{b\text{-jets},70\%}$,	p_{T}^{ℓ}, η_{ℓ}	p_{T}^{j}, η_j	NN_{ttH} for $\mathrm{NN}_{tXX} < 0.4$ NN_{tXX} for $\mathrm{NN}_{tXX} > 0.4$

Results: Observed Data

- Several kinematic properties used for the categorisation of reconstructed events:

N_{jets}:

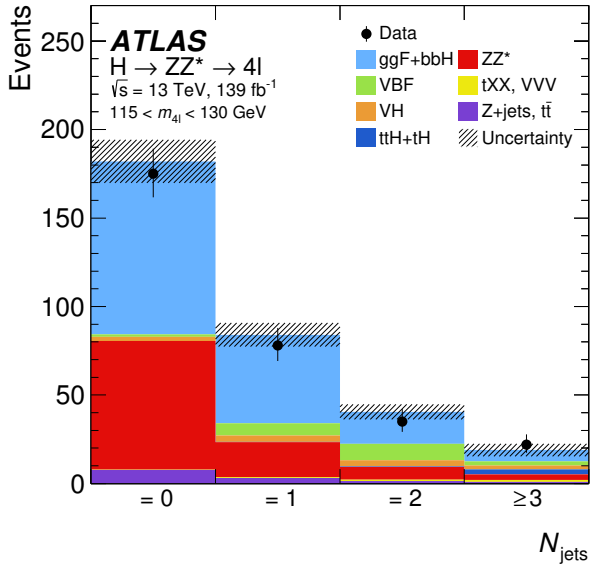

$p_{T,4l}$ for $N_{jets} = 0$:

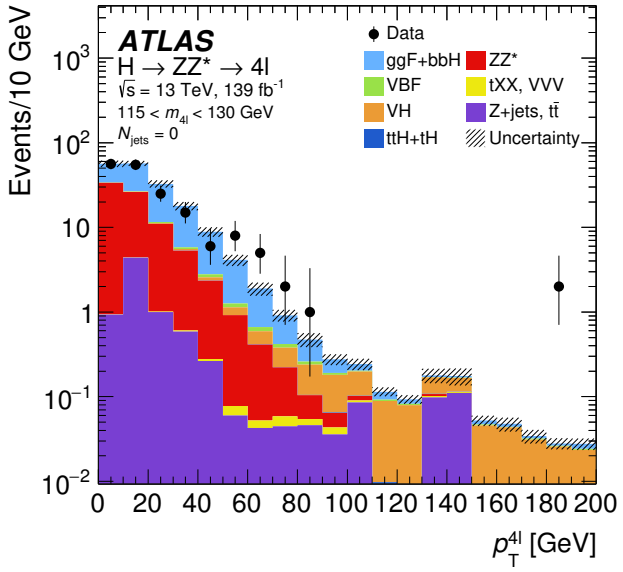

$p_{T,4l}$ for $N_{jets} = 1$:

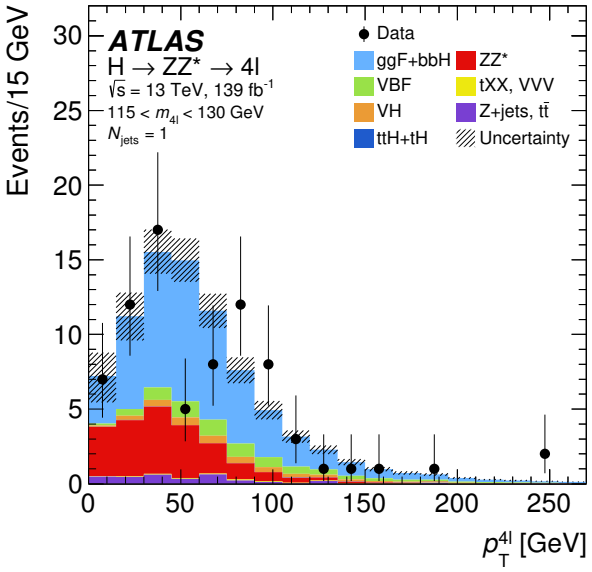

- All distributions are in good agreement with the data

Results: Observed Data

- Several kinematic properties used for the categorisation of reconstructed events:

$p_{T,4l}$ for $N_{jets} \geqq 2$:

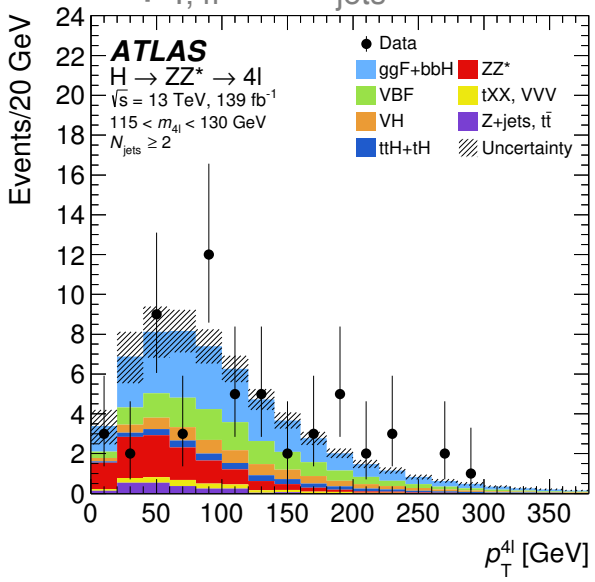

m_{jj} for $N_{jets} \geqq 2$:

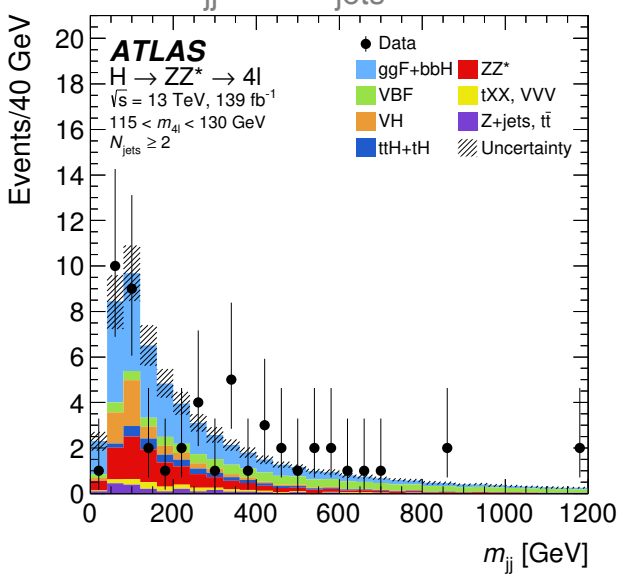

- All distributions are in good agreement with the data

Exclusive Production: Multivariate Discriminants

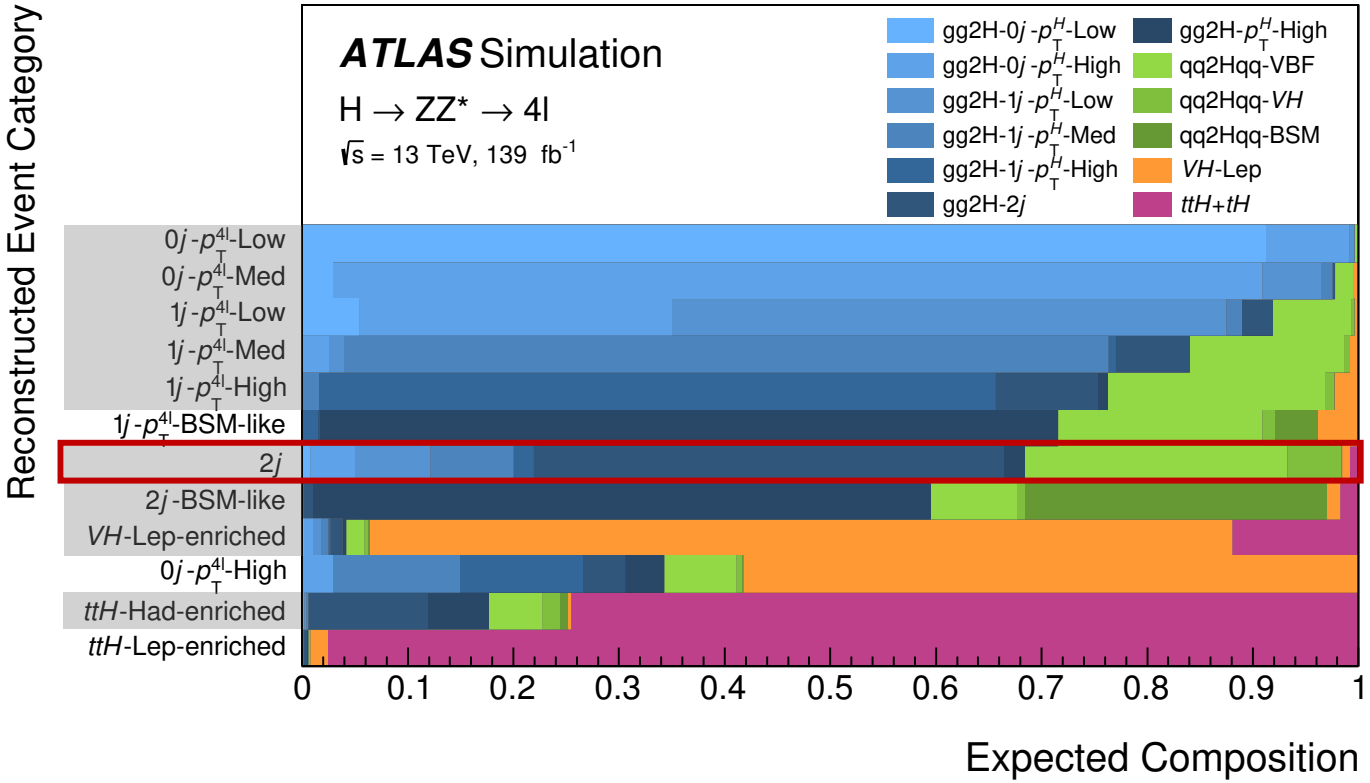

- Purity in some of the reconstructed categories low
- Neural Networks (NNs):
  - Improve the separation of different signal components and background processes

e.g. 2j category:

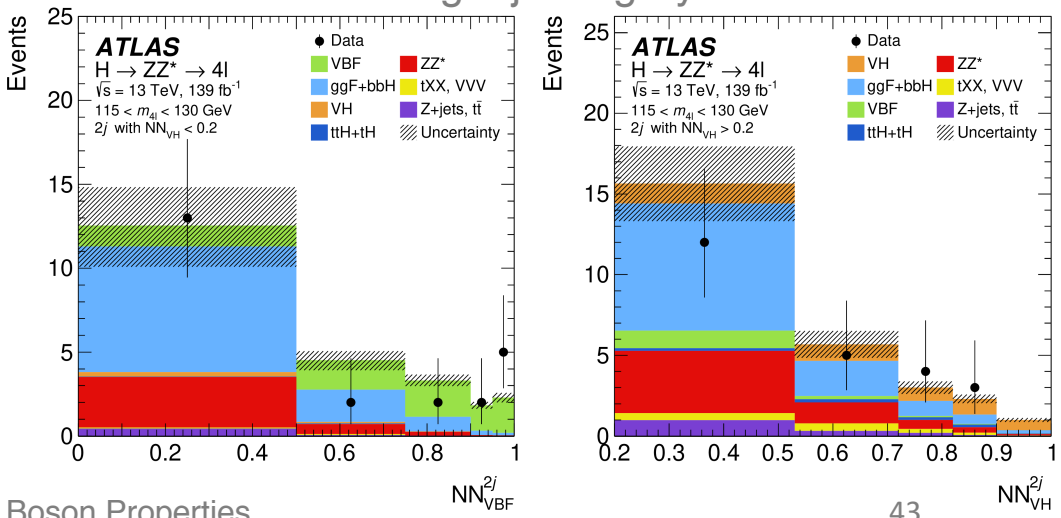

Results: Observed Data

- Observed and expected distributions of the NN discriminants in reconstructed event categories:

0j – $p_{T,4l}$ – Med:

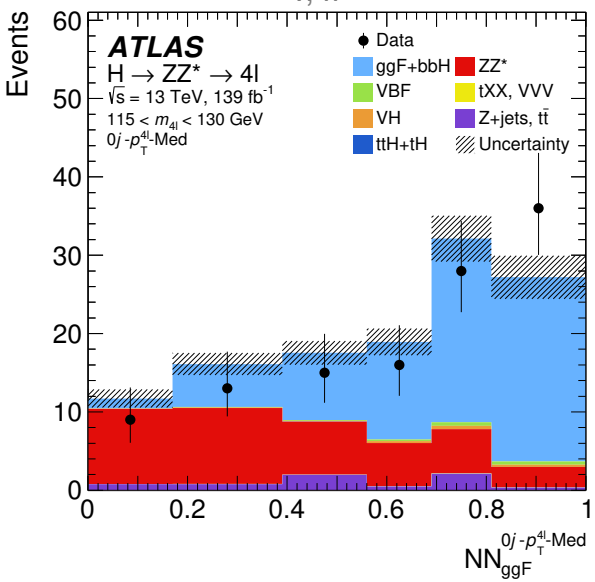

2j:

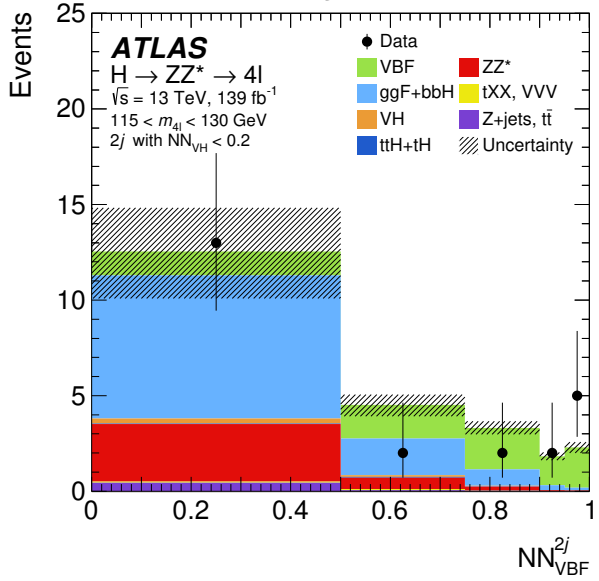

2j:

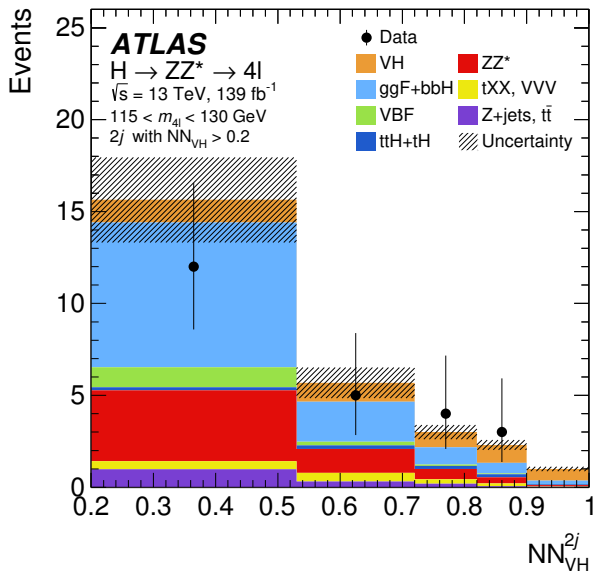

No NN:

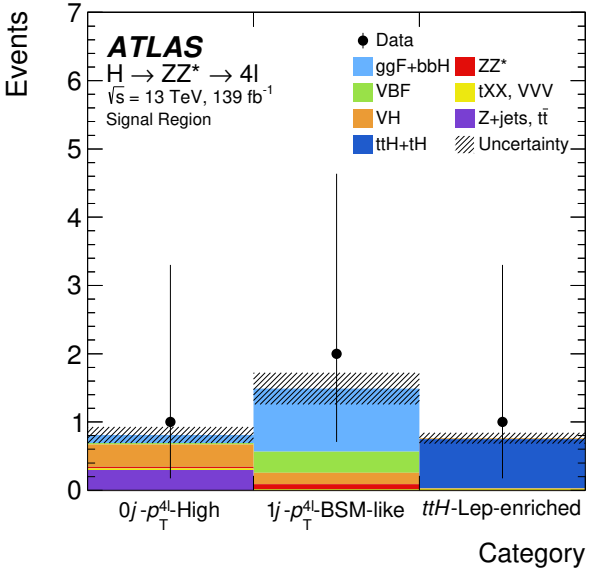

- All distributions are in good agreement with the data

Remaining → BACKUP

NN Discriminants

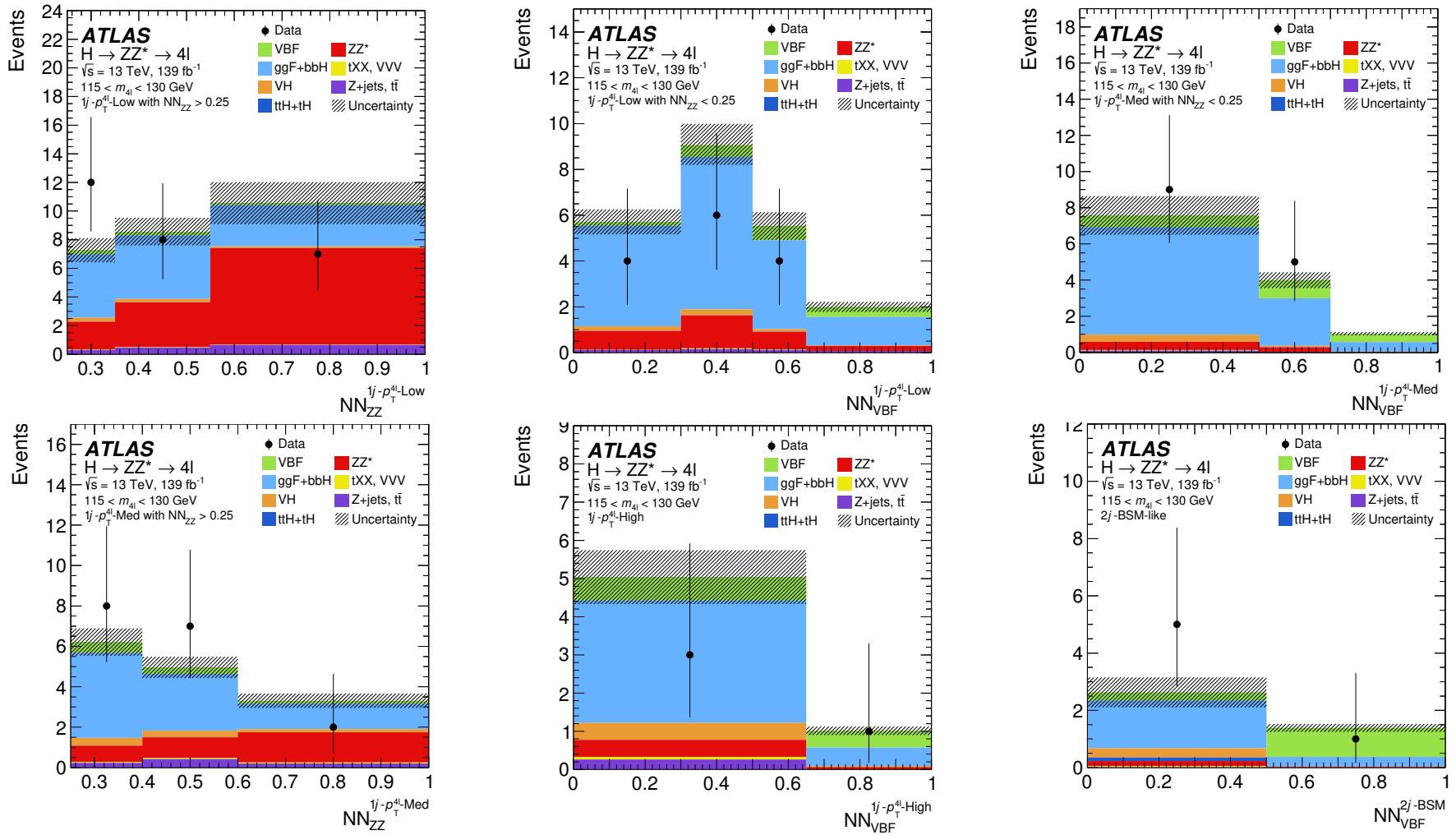

NN Discriminants

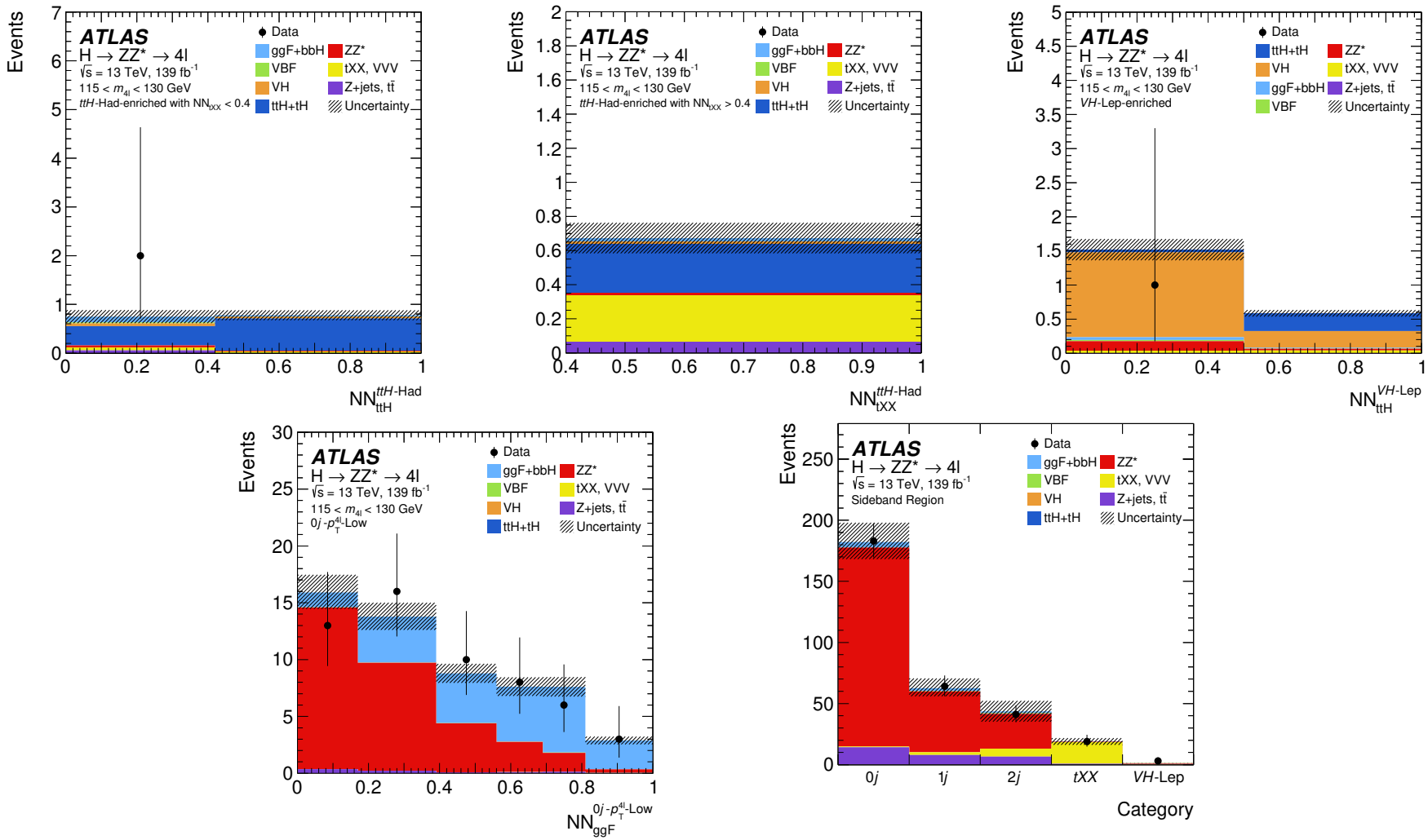

Systematics

Measurement	Experimental uncertainties [%]				Theory uncertainties [%]				
	Lumi.	e, μ, pile-up	Jets, flav. tag	Reducible bkg	Background ZZ^*	Background tXX	Signal PDF	Signal QCD	Signal Shower
Inclusive cross-section									
	1.7	2.5	0.5	< 0.5	1	< 0.5	< 0.5	1	2
Production mode cross-sections									
ggF	1.7	2.5	1	< 0.5	1.5	< 0.5	0.5	1	2
VBF	1.7	2	4	< 0.5	1.5	< 0.5	1	5	7
VH	1.9	2	4	1	6	< 0.5	2	13.5	7.5
ttH	1.7	2	6	< 0.5	1	0.5	0.5	12.5	4
Reduced Stage-1.1 production bin cross-sections									
gg2H-0j-p_{T}^{H}-Low	1.7	3	1.5	0.5	6.5	< 0.5	< 0.5	1	1.5
gg2H-0j-p_{T}^{H}-High	1.7	3	5	< 0.5	3	< 0.5	< 0.5	0.5	5.5
gg2H-1j-p_{T}^{H}-Low	1.7	2.5	12	0.5	7	< 0.5	< 0.5	1	6
gg2H-1j-p_{T}^{H}-Med	1.7	3	7.5	< 0.5	1	< 0.5	< 0.5	1.5	5.5
gg2H-1j-p_{T}^{H}-High	1.7	3	11	0.5	2	< 0.5	< 0.5	2	7.5
gg2H-2j	1.7	2.5	16.5	1	12.5	0.5	< 0.5	2.5	10.5
gg2H-p_{T}^{H}-High	1.7	1.5	3	0.5	3.5	< 0.5	< 0.5	2	3.5
qq2Hqq-VH	1.8	4	17	1	4	1	0.5	5.5	8
qq2Hqq-VBF	1.7	2	3.5	< 0.5	5	< 0.5	< 0.5	6	10.5
qq2Hqq-BSM	1.7	2	4	< 0.5	2.5	< 0.5	< 0.5	3	8
VH-Lep	1.8	2.5	2	1	2	0.5	< 0.5	1.5	3
ttH	1.7	2.5	5	0.5	1	0.5	< 0.5	11	3

Observed and Expected Yields

Reconstructed event category	Signal	ZZ^* background	tXX background	Other backgrounds	Total expected	Observed
Signal			$115 < m_{4\ell} < 130$ GeV			
$0j$-$p_{\mathrm{T}}^{4\ell}$-Low	24.2 ± 3.5	30 ± 4	–	0.93 ± 0.13	55 ± 5	56
$0j$-$p_{\mathrm{T}}^{4\ell}$-Med	76 ± 8	37 ± 4	–	6.5 ± 0.6	120 ± 9	117
$0j$-$p_{\mathrm{T}}^{4\ell}$-High	0.355 ± 0.031	0.020 ± 0.012	0.0094 ± 0.0027	0.30 ± 0.05	0.69 ± 0.06	1
$1j$-$p_{\mathrm{T}}^{4\ell}$-Low	34 ± 4	15.5 ± 2.7	–	1.91 ± 0.29	52 ± 5	41
$1j$-$p_{\mathrm{T}}^{4\ell}$-Med	20.8 ± 2.8	4.0 ± 0.7	0.114 ± 0.013	1.02 ± 0.19	26.0 ± 2.9	31
$1j$-$p_{\mathrm{T}}^{4\ell}$-High	4.7 ± 0.8	0.48 ± 0.10	0.043 ± 0.008	0.27 ± 0.04	5.5 ± 0.8	4
$1j$-$p_{\mathrm{T}}^{4\ell}$-BSM-like	1.23 ± 0.23	0.069 ± 0.031	0.0067 ± 0.0031	0.062 ± 0.012	1.37 ± 0.23	2
$2j$	38 ± 5	9.1 ± 2.7	0.95 ± 0.08	2.13 ± 0.31	50 ± 6	48
$2j$-BSM-like	3.3 ± 0.6	0.18 ± 0.06	0.032 ± 0.005	0.091 ± 0.017	3.6 ± 0.6	6
VH-Lep-enriched	1.29 ± 0.07	0.156 ± 0.025	0.039 ± 0.009	0.0194 ± 0.0032	1.50 ± 0.08	1
ttH-Had-enriched	1.02 ± 0.18	0.058 ± 0.025	0.252 ± 0.032	0.119 ± 0.033	1.45 ± 0.18	2
ttH-Lep-enriched	0.42 ± 0.04	0.002 ± 0.005	0.0157 ± 0.0023	0.0028 ± 0.0029	0.44 ± 0.04	1
Sideband			$105 < m_{4\ell} < 115$ GeV or $130 < m_{4\ell} < 160$ GeV			
SB-$0j$	4.5 ± 0.5	150 ± 13	–	16.2 ± 2.2	171 ± 13	183
SB-$1j$	2.80 ± 0.30	51 ± 7	1.29 ± 0.16	8.4 ± 1.2	63 ± 7	64
SB-$2j$	2.02 ± 0.27	25 ± 7	4.4 ± 0.5	6.0 ± 0.9	38 ± 7	41
SB-VH-Lep-enriched	0.273 ± 0.015	0.48 ± 0.06	0.125 ± 0.018	0.126 ± 0.019	1.00 ± 0.07	3
			$105 < m_{4\ell} < 115$ GeV or $130 < m_{4\ell} < 350$ GeV			
SB-tXX-enriched	0.071 ± 0.012	0.32 ± 0.12	12.1 ± 1.3	0.84 ± 0.33	13.3 ± 1.4	19

Fit

$$\mathcal{L}(\vec{\sigma},\vec{\theta}) = \prod_{j}^{N_{\text{categories}}} \prod_{i}^{N_{\text{bins}}} P\left(N_{i,j} \mid L\cdot\vec{\sigma}\cdot\mathcal{B}\cdot\vec{A}_{i,j}(\vec{\theta}) + B_{i,j}(\vec{\theta})\right) \times \prod_{m}^{N_{\text{nuisance}}} C_m(\vec{\theta}),$$

$$q(\vec{\sigma}) = -2\ln\frac{\mathcal{L}(\vec{\sigma},\hat{\hat{\vec{\theta}}}(\vec{\sigma}))}{\mathcal{L}(\hat{\vec{\sigma}},\hat{\vec{\theta}})} = -2\ln\lambda(\vec{\sigma}),$$

$$\mu^p(\vec{c}) = \frac{\sigma^p(\vec{c})}{\sigma_{\text{SM}}}\cdot\frac{\mathcal{B}^{4\ell}(\vec{c})}{\mathcal{B}^{4\ell}_{\text{SM}}}\cdot\frac{A(\vec{c})}{A_{\text{SM}}}.$$

Results: Inclusive

- Inclusive H → ZZ* production cross-section for $|y_H| < 2.5$:

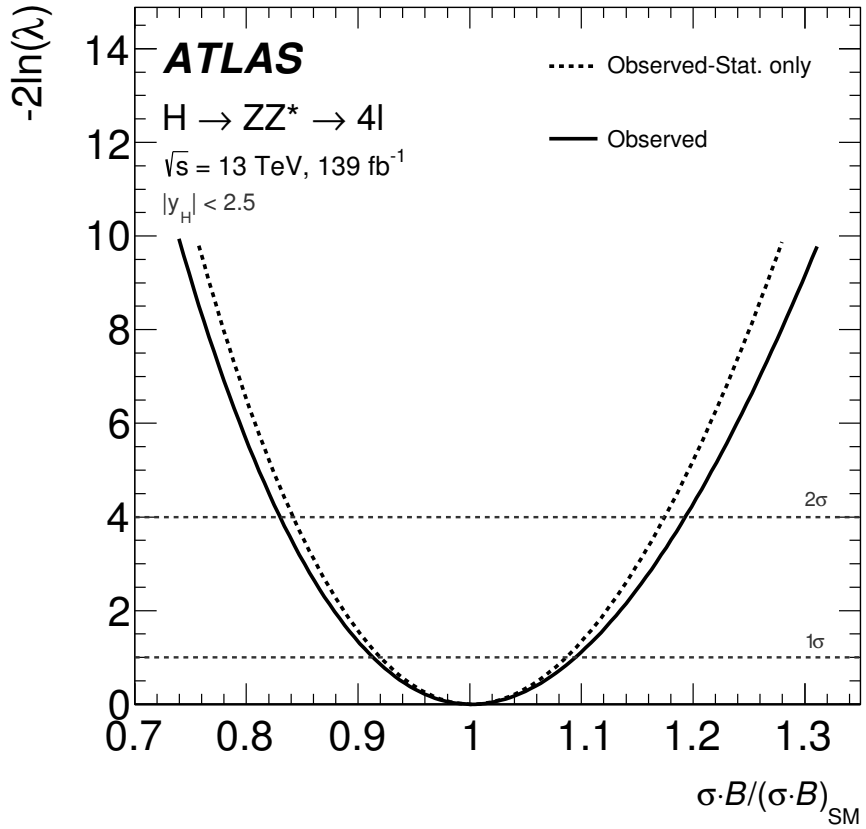

- Observed:

$$\sigma \cdot \mathcal{B}(H \to ZZ^*) = 1.34 \pm 0.12\ \text{pb}$$
$$= 1.34 \pm 0.11\ (stat.) \pm 0.04\ (exp.) \pm 0.04\ (theo.)\ \text{pb}$$

- SM prediction:

$$\sigma \cdot \mathcal{B}(H \to ZZ^*) = 1.33 \pm 0.08\ \text{pb}$$

- In good agreement with the SM prediction
- Precision improved by a factor of about four (two) w.r.t. to the Run 1 (Run 2 36.1 fb^{-1}) measurement

STXS: Correlation Matrices

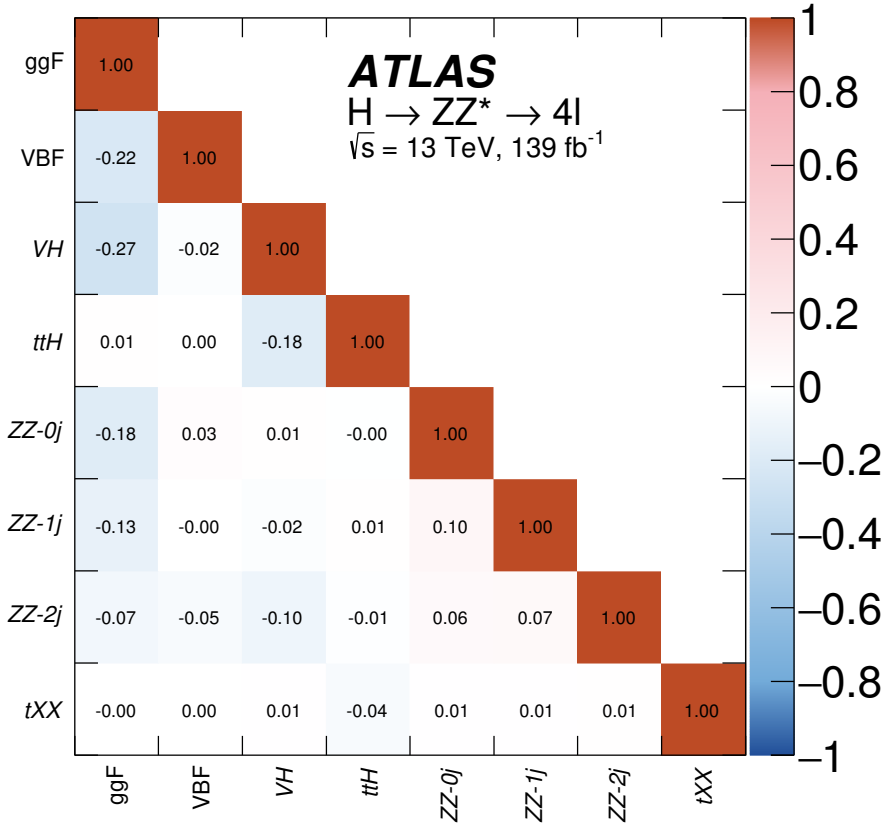

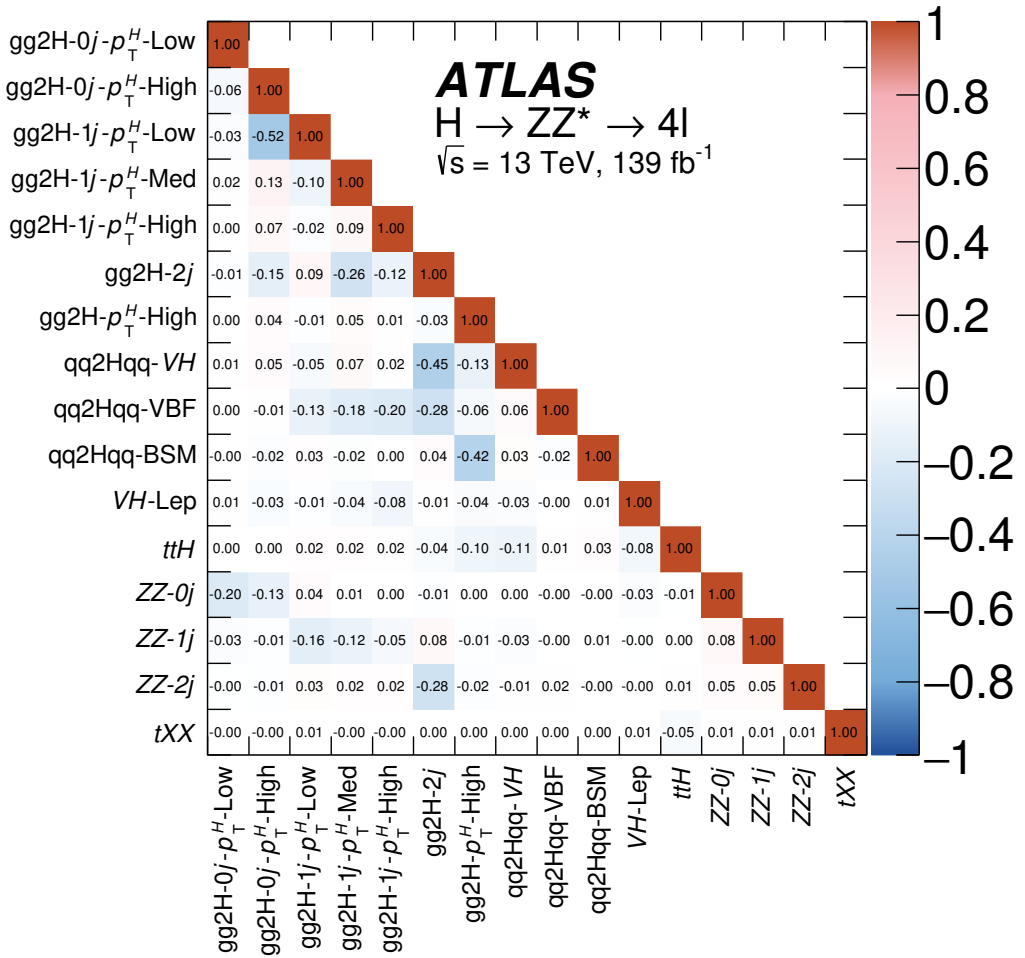

Results: STXS 2D

ggF vs. VBF

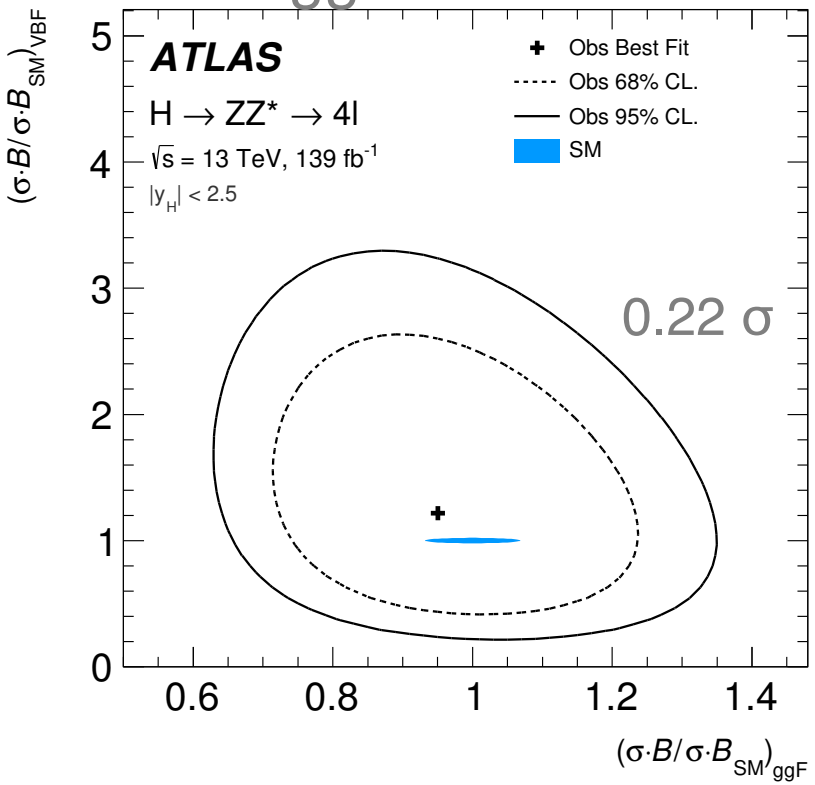

ggF vs. VH

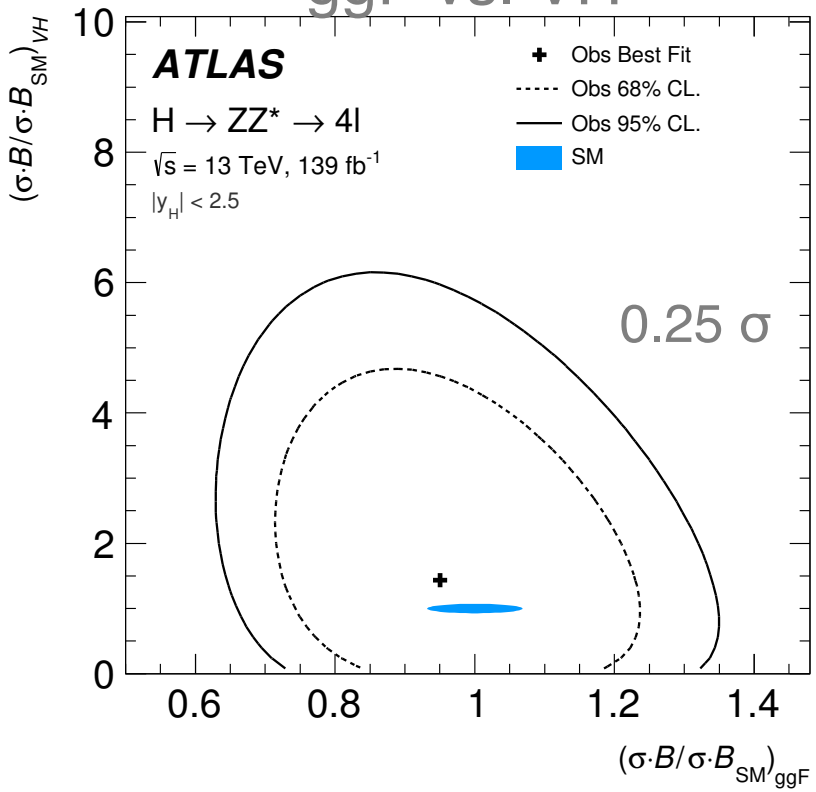

In agreement with the SM prediction

Remaining → BACKUP

Results: STXS 2D

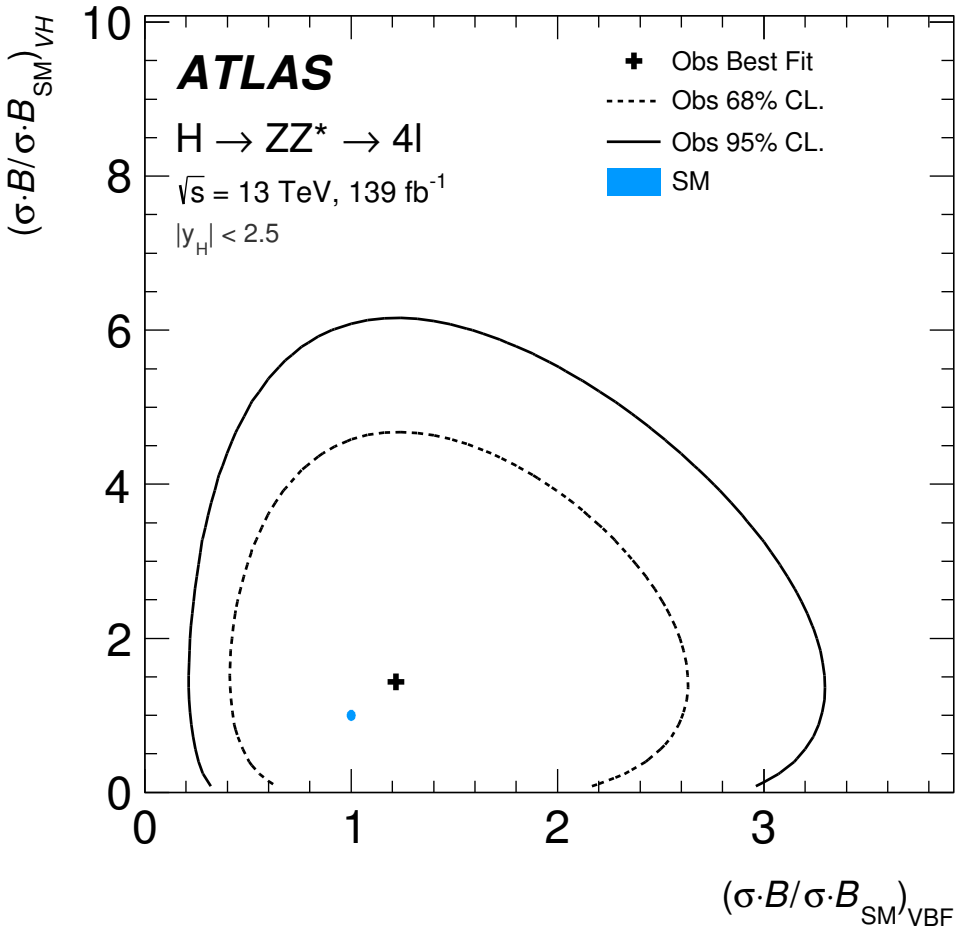

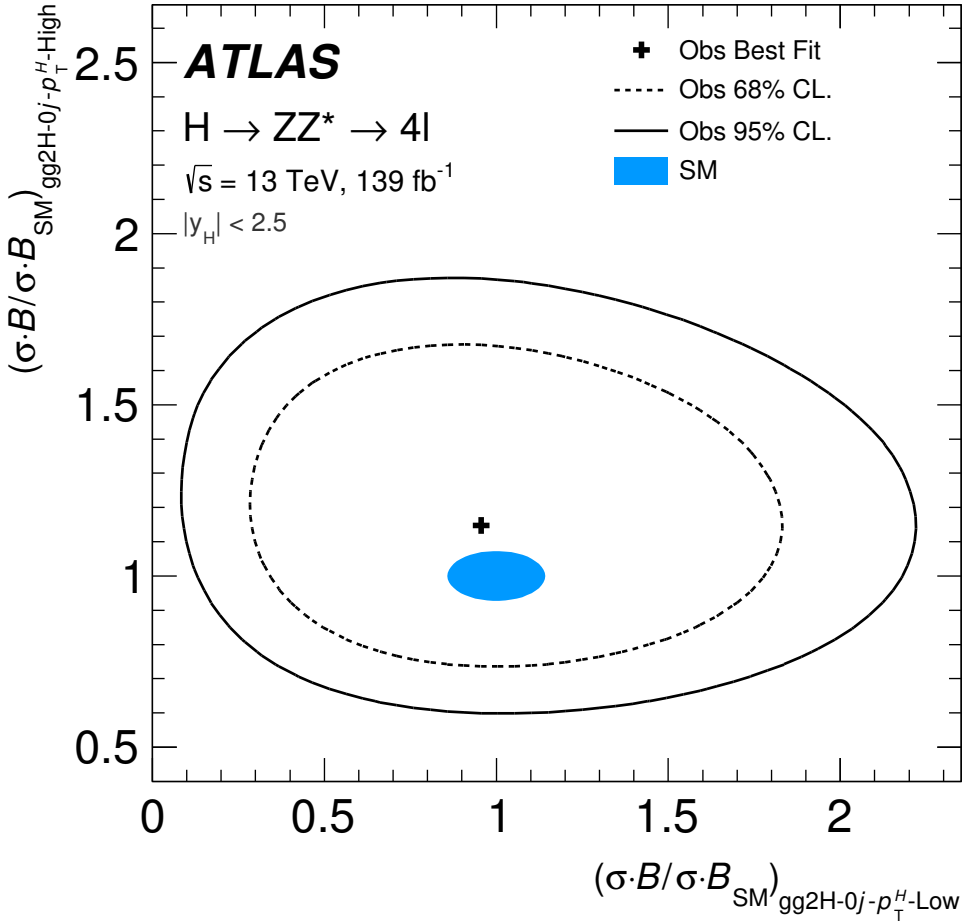

EFT

$$\sigma \propto |\mathcal{M}_{\mathrm{SMEFT}}|^2 = \left|\mathcal{M}_{\mathrm{SM}} + \sum_i \frac{C_i}{\Lambda^2}\mathcal{M}_i\right|^2 = |\mathcal{M}_{\mathrm{SM}}|^2 + \sum_i 2Re\left(\mathcal{M}^*_{\mathrm{SM}}\mathcal{M}_i\right)\frac{C_i}{\Lambda^2} + \sum_{ij} 2Re\left(\mathcal{M}^*_i\mathcal{M}_j\right)\frac{C_iC_j}{\Lambda^4},$$

$$\frac{\sigma^p(\vec{c})}{\sigma^p_{\mathrm{SM}}} = 1 + \sum_i A^p_i c_i + \sum_{ij} B^p_{ij} c_i c_j,$$

$$\mathcal{B}^{4\ell}(\vec{c}) = \frac{\Gamma^{4\ell}(\vec{c})}{\Gamma^{\mathrm{tot}}(\vec{c})} = \mathcal{B}^{4\ell}_{\mathrm{SM}} \cdot \frac{1 + \sum_i A^{4\ell}_i c_i + \sum_{ij} B^{4\ell}_{ij} c_i c_j}{1 + \sum_f \left(\sum_i A^f_i c_i + \sum_{ij} B^f_{ij} c_i c_j\right)},$$

κ-Framework

- Parametrise deviations from the SM predictions of the Higgs boson couplings to SM bosons and fermions

- Assumptions:
  - Single CP-even Higgs boson state
  - Tensor coupling structure same as in the SM

- Parametrisation:

$$\sigma \cdot \mathcal{B}(i \to H \to f) = \kappa_i^2 \cdot \kappa_f^2 \cdot \sigma_i^{SM} \cdot \frac{\Gamma_f^{SM}}{\Gamma_H\left(\kappa_i^2, \kappa_f^2\right)}$$

$$\kappa_i^2 = \frac{\sigma_i}{\sigma_i^{SM}} \text{ and } \kappa_f^2 = \frac{\Gamma_f}{\Gamma_f^{SM}}$$

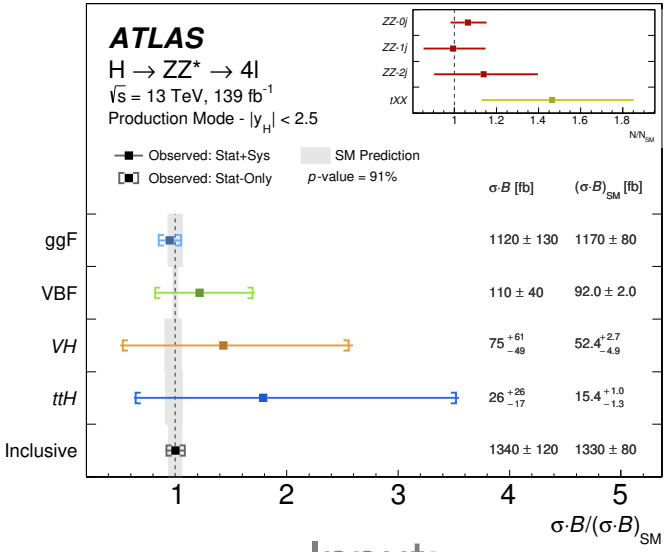

Input:
Production Mode Stage measurement

Results: κ-Framework

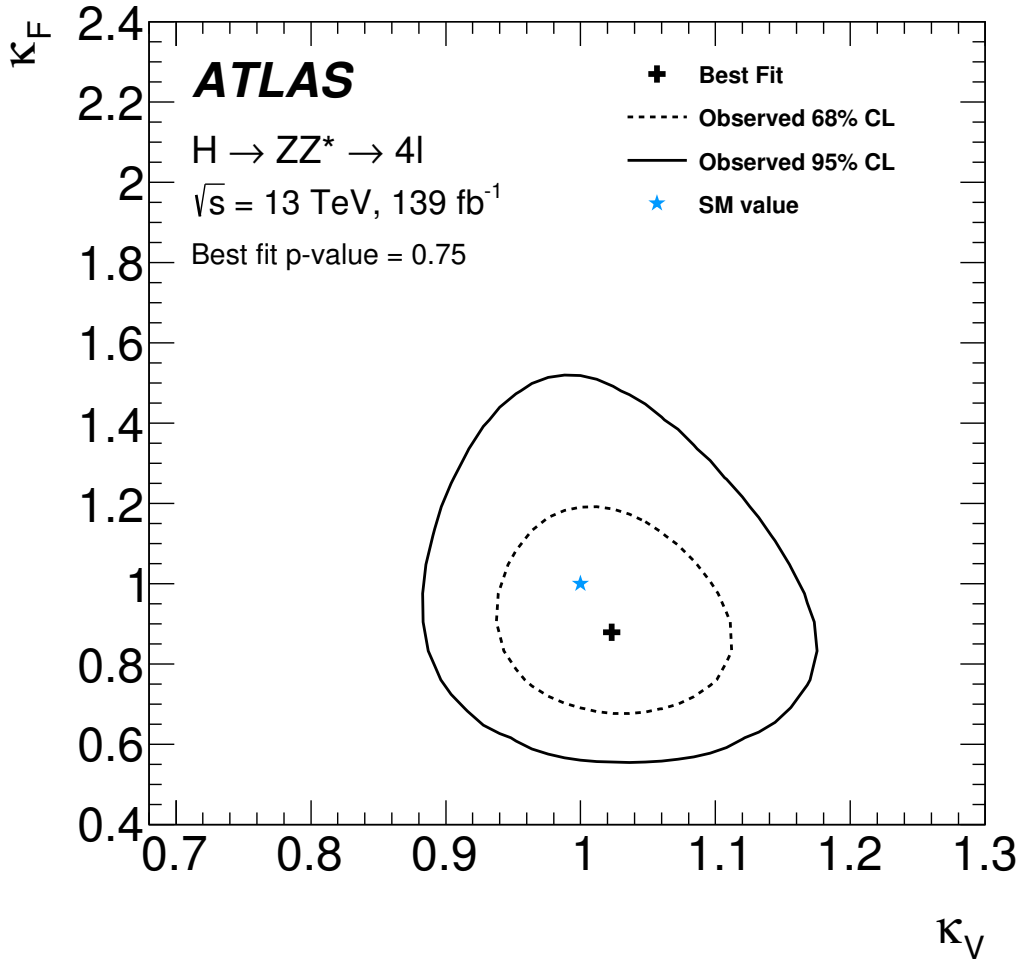

- Assumption:

$$\kappa_V = \kappa_W = \kappa_Z$$

and

$$\kappa_F = \kappa_t = \kappa_b = \kappa_c = \kappa_\tau = \kappa_\mu$$

- Best fit values:

$$\hat{\kappa}_V = 1.02 \pm 0.06 \text{ and } \hat{\kappa}_F = 0.88 \pm 0.16$$

- Good compatibility with the SM expectation: at the level of 75%

Standard Model Effective Field Theory

- Lagrangian is constructed out of $\mathcal{SU}_C(3)\times\mathcal{SU}_L(2)\times\mathcal{U}_Y(1)$ invariant higher dimensional operators built out of SM fields:

$$\mathcal{L}_{SMEFT} = \mathcal{L}_{SM} + c_{HG}H^\dagger H G^a_{\mu\nu}G^{a,\mu\nu} + c_{H\tilde{G}}H^\dagger H G^a_{\mu\nu}\tilde{G}^{a,\mu\nu} + c_{uH}H^\dagger H\overline{Q}_p u_r\tilde{H} + c_{\tilde{u}H}H^\dagger H\overline{Q}_p u_r\tilde{H}$$
$$+ c_{HW}H^\dagger H W^I_{\mu\nu}W^{I\mu\nu} + c_{H\tilde{W}}H^\dagger H\tilde{W}^I_{\mu\nu}W^{I\mu\nu} + c_{HB}H^\dagger H B_{\mu\nu}B^{\mu\nu} + c_{H\tilde{B}}H^\dagger H\tilde{B}_{\mu\nu}B^{\mu\nu}$$
$$+ c_{HWB}H^\dagger\tau^I H W^I_{\mu\nu}B^{I\mu\nu} + c_{H\tilde{W}B}H^\dagger\tau^I H\tilde{W}^I_{\mu\nu}B^{I\mu\nu}$$

BSM CP-even
BSM CP-odd

Non-SM coupling to gluons

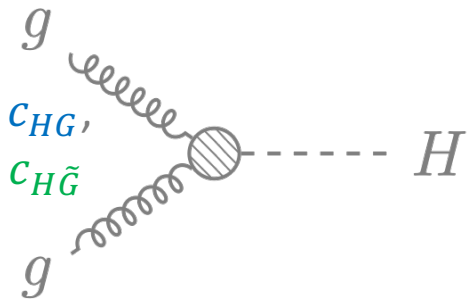

Non-SM coupling to vector bosons

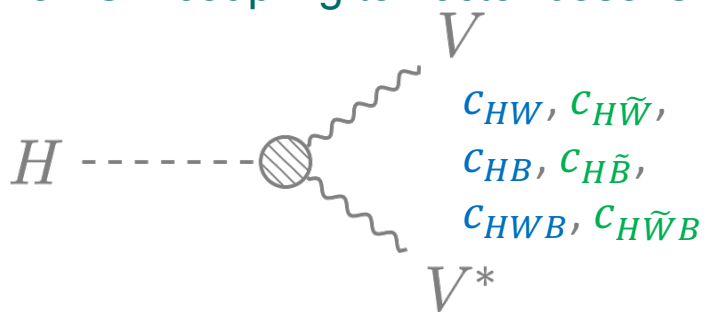

Non-SM coupling to top quarks

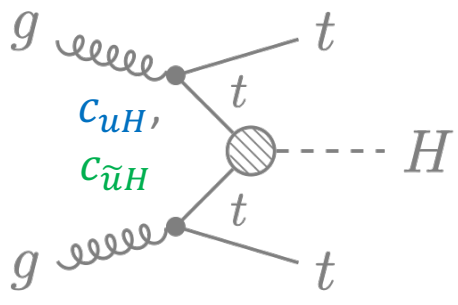

Approach

- Based on the Reduced Stage 1.1 measurement:

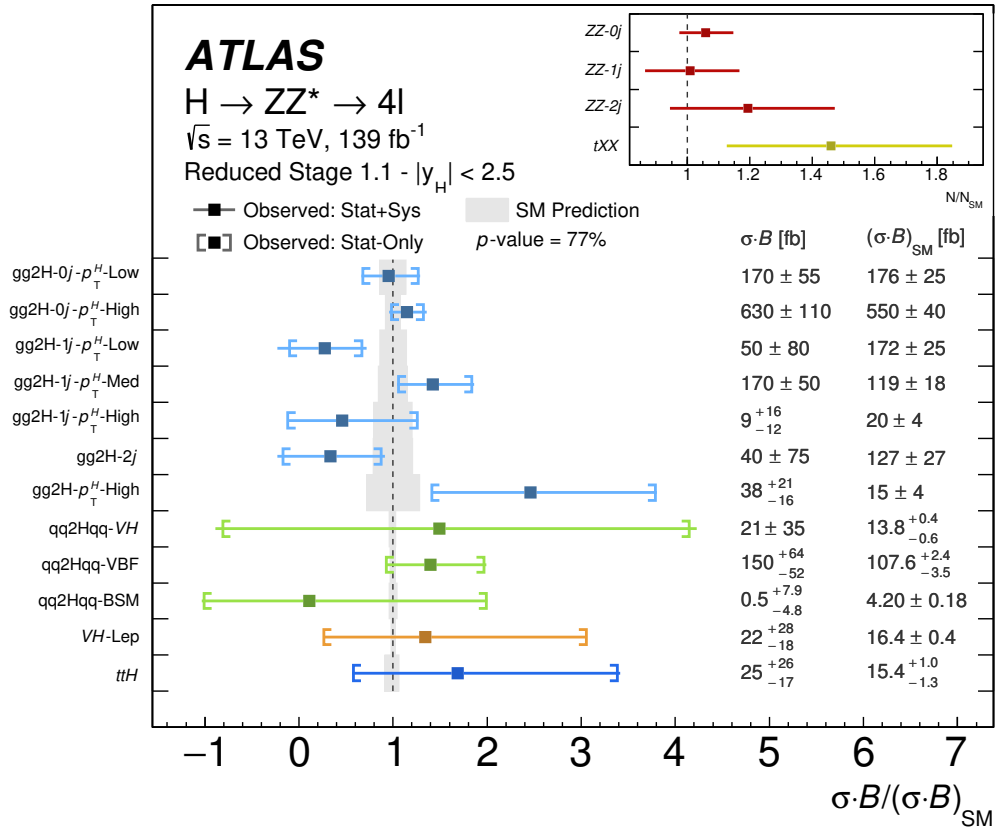

- Parametrise each of the production bins as a function of BSM couplings
- In each production bin p:

$$\sigma^p(c_i) \cdot \mathcal{B}(c_i) \cdot \mathcal{A}^p(c_i) \cdot \prod_i^{N_{Cat}} \varepsilon_i^p$$

BSM dependent

$\mathcal{A}^p$: acceptance ε: reconstruction efficiency

BSM Parametrisation of the Acceptance

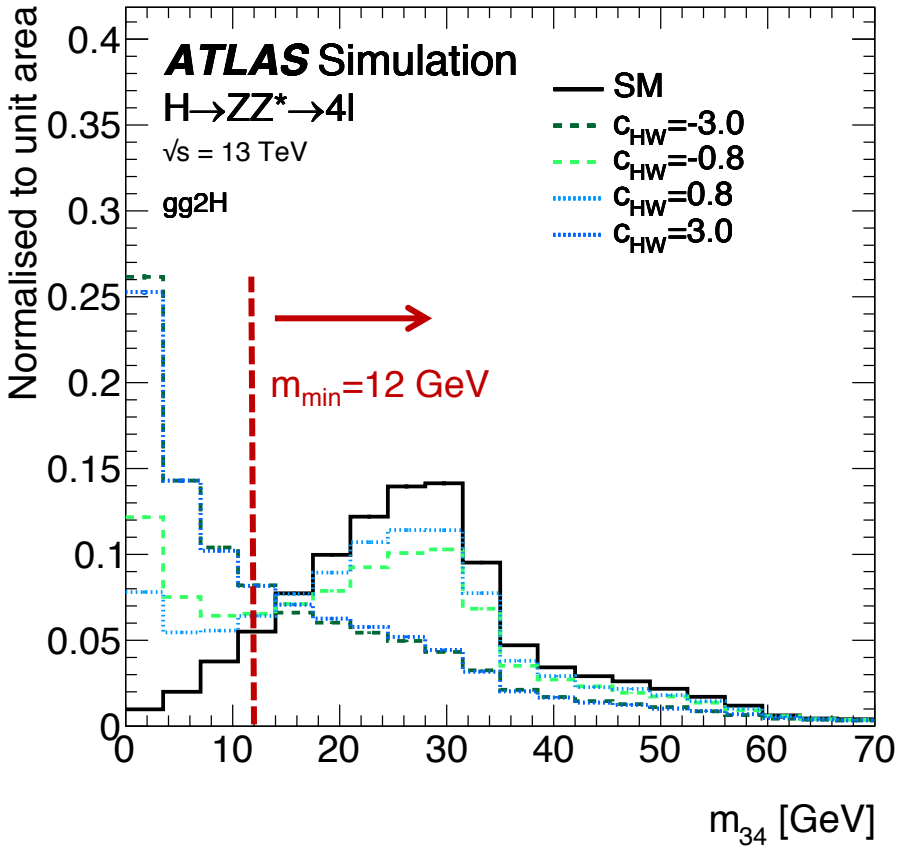

- For the first time: take into account the signal acceptance
- Selection criteria of the 4ℓ event selection introduce an additional BSM dependence
- m_{34} has a strong BSM dependence
- Separate parametrisation for CP-even and CP-odd BSM couplings

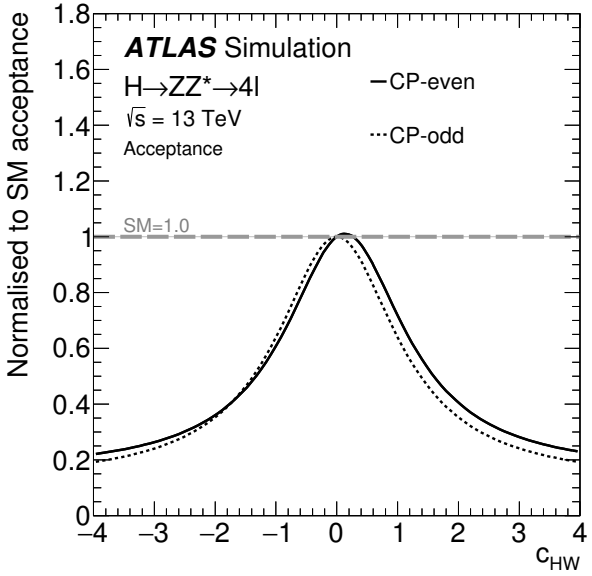

BSM Parametrisation

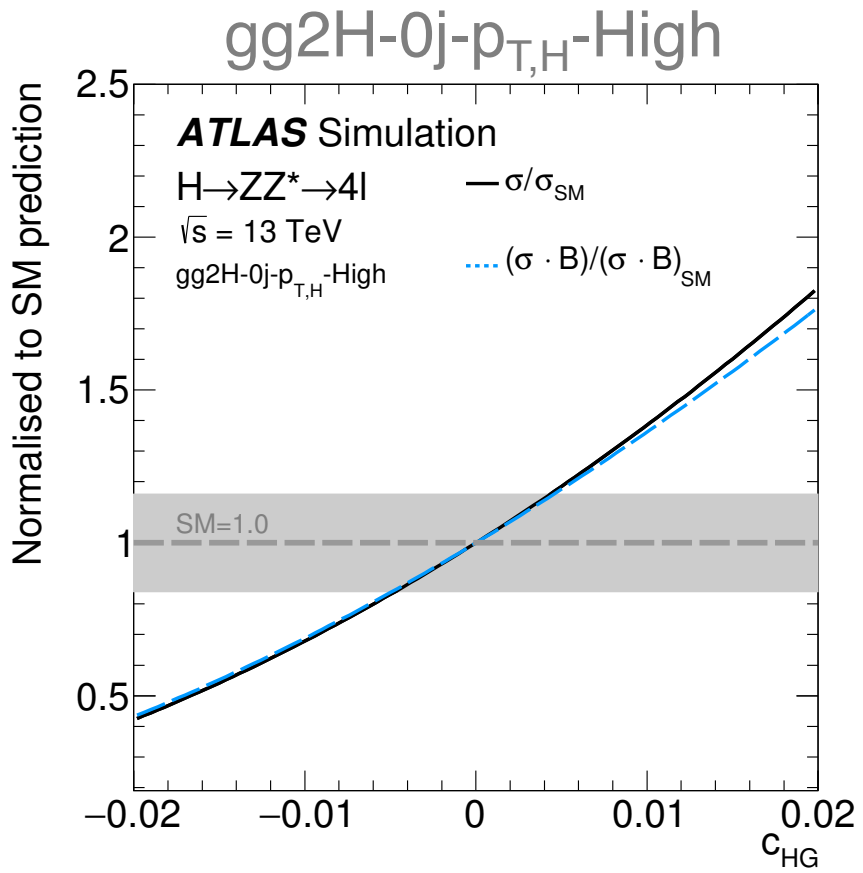

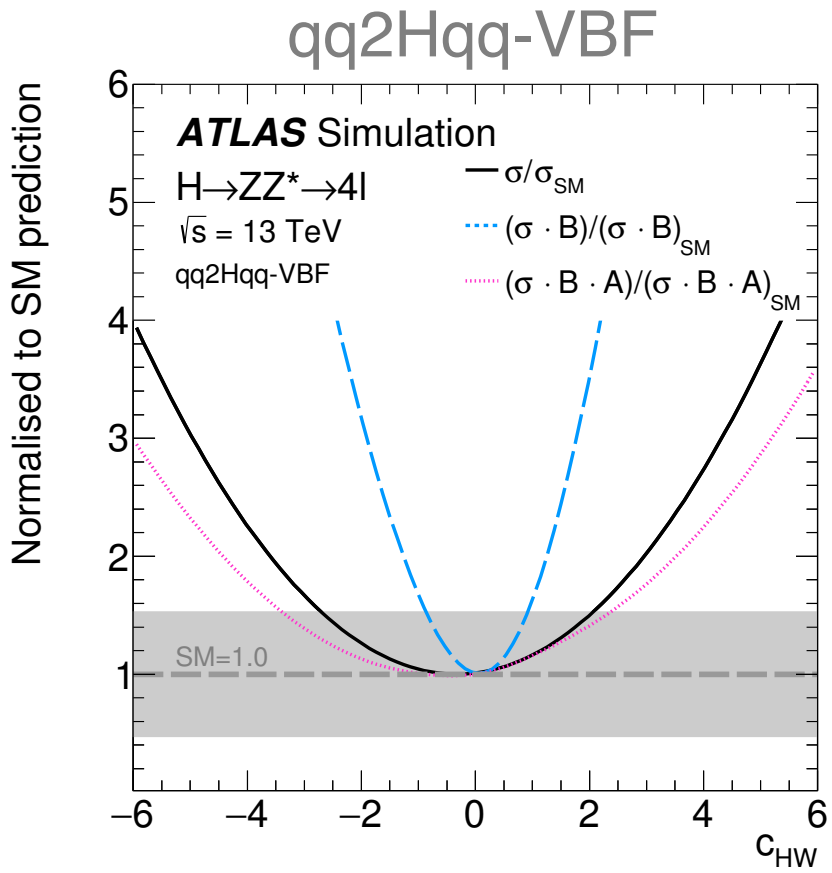

EFT: Acceptance Parametrisation

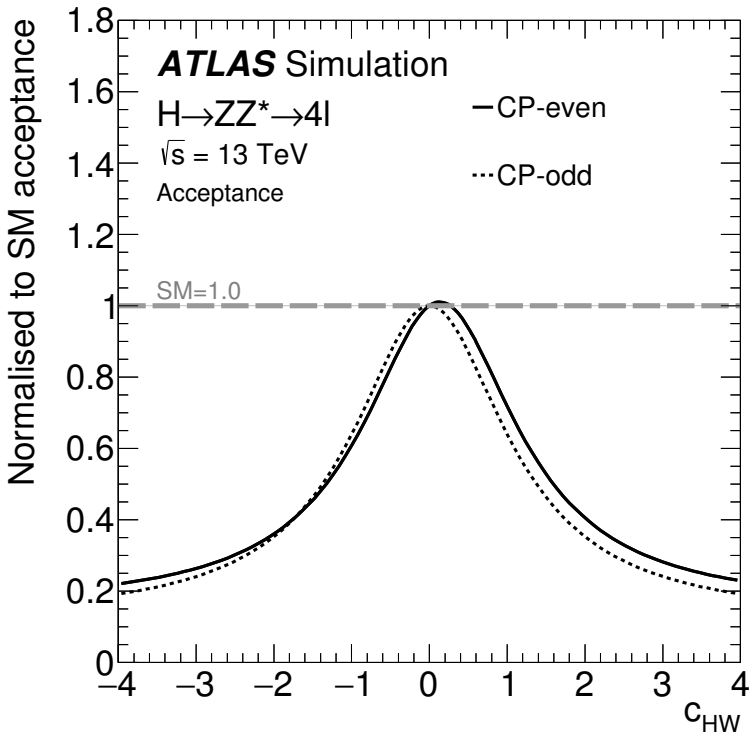

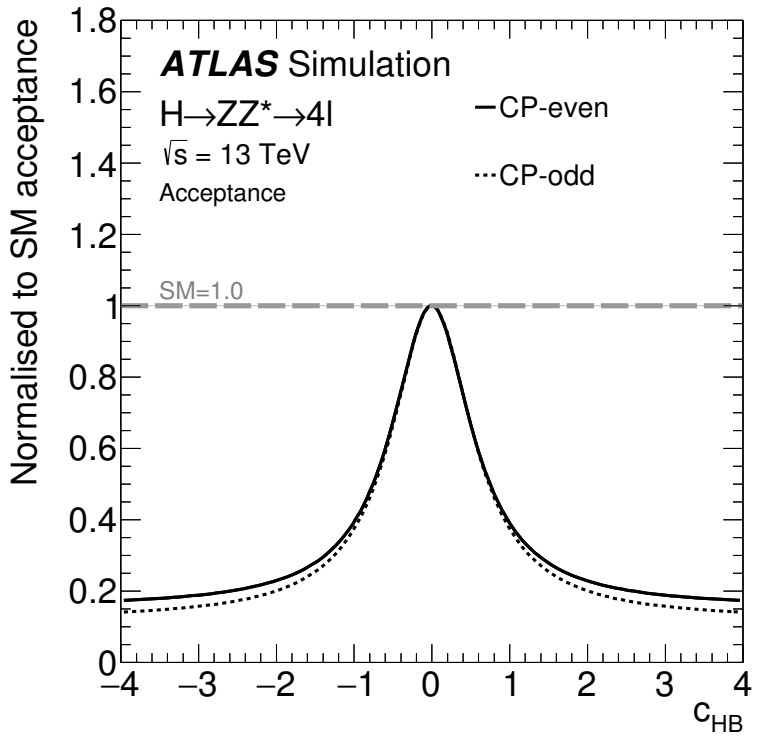

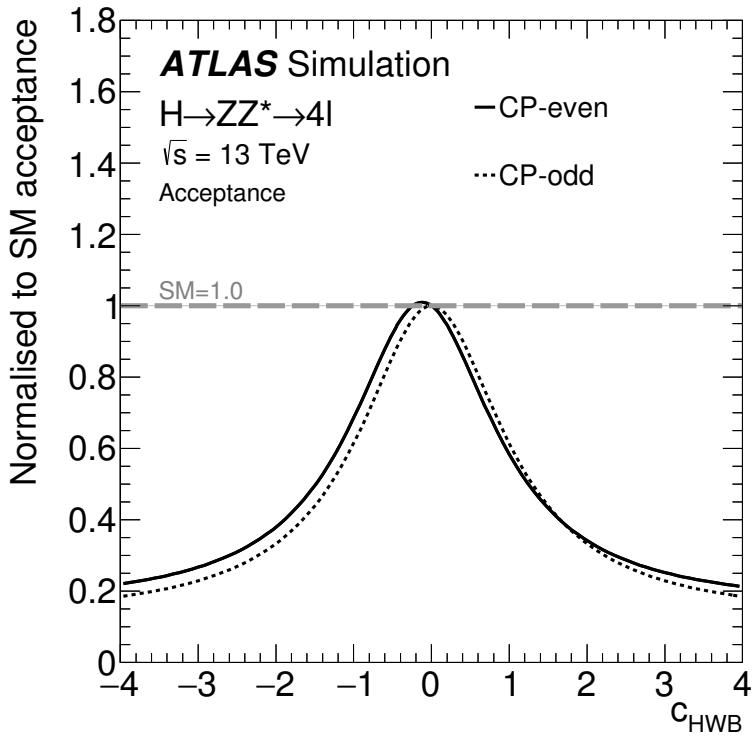

EFT: BSM Parametrisation

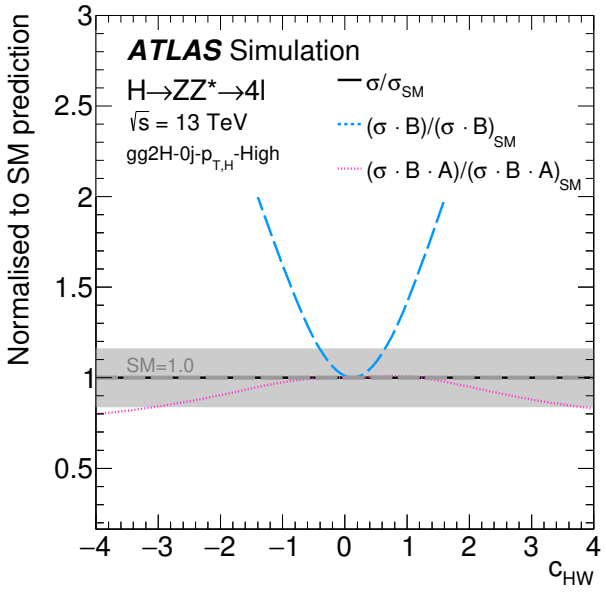

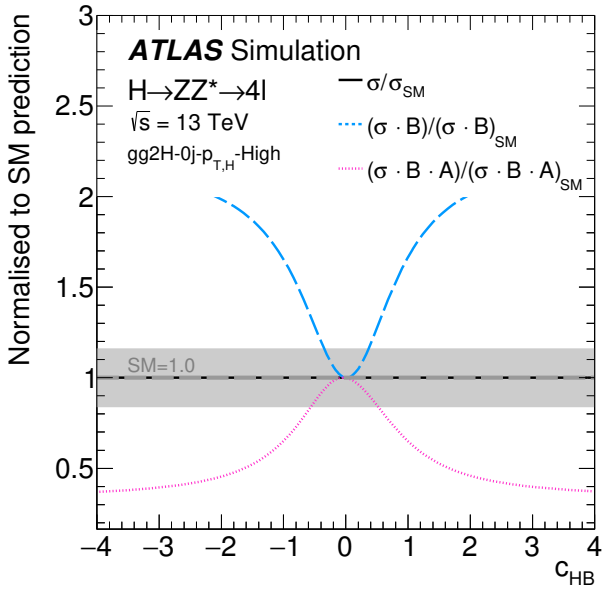

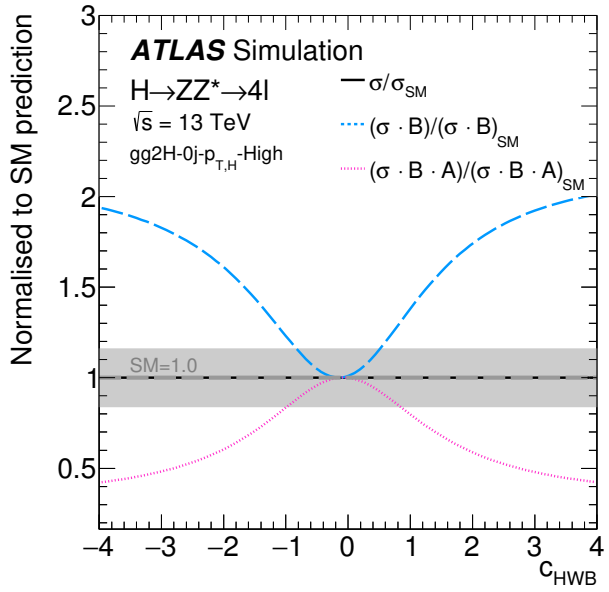

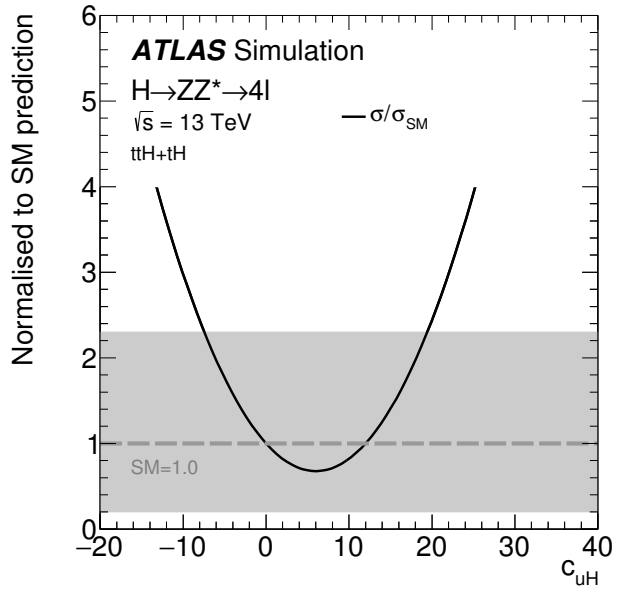

BSM Parametrisation

Table 13: EFT parameterisation of the cross-section ratio $\sigma/\sigma_{\mathrm{SM}}$ for each of the Reduced Stage-1.1 production bins and of the ratio of decay widths $\Gamma/\Gamma_{\mathrm{SM}}$ as a function of the CP-even Wilson coefficients.

STXS bin	Cross-section parameterisation, $\sigma/\sigma_{\mathrm{SM}}$
gg2H-0j-p_{T}^{H}-Low	$1 + 35.80c_{HG} + 326.23c_{HG}^2$
gg2H-0j-p_{T}^{H}-High	$1 + 35.33c_{HG} + 319.05c_{HG}^2$
gg2H-1j-p_{T}^{H}-Low	$1 + 31.27c_{HG} + 264.44c_{HG}^2$
gg2H-1j-p_{T}^{H}-Med	$1 + 29.55c_{HG} + 236.09c_{HG}^2$
gg2H-1j-p_{T}^{H}-High	$1 + 28.00c_{HG} + 225.53c_{HG}^2$
gg2H-2j	$1 + 17.62c_{HG} + 118.92c_{HG}^2$
gg2H-p_{T}^{H}-High	$1 + 17.77c_{HG} + 162.65c_{HG}^2$
qq2Hqq-VH	$1+0.593c_{HW}+0.258c_{HW}^2+0.019c_{HB}+0.014c_{HB}^2+0.088c_{HWB}+0.023c_{HWB}^2+0.005c_{HW}c_{HB}+0.034c_{HW}c_{HWB}+0.005c_{HB}c_{HWB}$
qq2Hqq-BSM	$1+0.190c_{HW}+0.506c_{HW}^2-0.002c_{HB}+0.057c_{HB}^2+0.042c_{HWB}+0.048c_{HWB}^2+0.012c_{HW}c_{HB}-0.059c_{HW}c_{HWB}-0.028c_{HB}c_{HWB}$
qq2Hqq-VBF	$1+0.059c_{HW}+0.092c_{HW}^2+0.002c_{HB}+0.027c_{HB}^2+0.037c_{HWB}+0.018c_{HWB}^2+0.015c_{HW}c_{HB}-0.016c_{HW}c_{HWB}-0.024c_{HB}c_{HWB}$
VH-Lep	$1+0.828c_{HW}+0.321c_{HW}^2+0.035c_{HB}+0.013c_{HB}^2+0.127c_{HWB}+0.026c_{HWB}^2-0.218c_{HW}c_{HB}-0.155c_{HW}c_{HWB}+0.020c_{HB}c_{HWB}$
ttH	$1 + 0.483c_{HG} + 0.590c_{HG}^2 - 0.108c_{uH} + 0.009c_{uH}^2 - 0.015c_{HG}c_{uH}$
Decay process	Decay width parameterisation, $\Gamma/\Gamma_{\mathrm{SM}}$
$\frac{\Gamma(H\to 4\ell)}{\Gamma_{\mathrm{SM}}(H\to 4\ell)}$	$1-0.199c_{HW}+0.753c_{HW}^2-0.112c_{HB}+2.665c_{HB}^2+0.181c_{HWB}+0.760c_{HWB}^2-0.043c_{HW}c_{HB}-1.288c_{HW}c_{HWB}-1.397c_{HB}c_{HWB}$
$\frac{\Gamma(H\to all)}{\Gamma_{\mathrm{SM}}(H\to all)}$	$1-0.054c_{HW}+0.162c_{HW}^2-0.076c_{HB}+1.209c_{HB}^2+0.062c_{HWB}+0.357c_{HWB}^2+1.519c_{HG}+14.922c_{HG}^2+0.518c_{HW}c_{HB}-0.441c_{HW}c_{HWB}-1.132c_{HB}c_{HWB}$

Table 14: Values of acceptance parameters obtained from the fit to the three-dimensional Lorentzian function in Eq. 4 for CP-even coupling parameters.

Acceptance parameter	Fit result	Acceptance parameter	Fit result
α_0	0.153 ± 0.003	δ_{HW}	0.614 ± 0.027
α_1	0.874 ± 0.010	δ_{HB}	2.294 ± 0.033
α_2	0.881 ± 0.019	δ_{HWB}	0.703 ± 0.029
β_{HW}	-0.133 ± 0.012	$\delta_{(HW,HWB)}$	-1.21 ± 0.04
β_{HB}	0.005 ± 0.005	$\delta_{(HB,HWB)}$	-1.22 ± 0.06
β_{HWB}	0.120 ± 0.011	$\delta_{(HW,HB)}$	0.08 ± 0.07
		δ	0.05 ± 0.06

$$\frac{A(\vec{c})}{A_{\mathrm{SM}}} = \alpha_0 + (\alpha_1)^2 \cdot \left[\alpha_2 + \sum_i \delta_i \cdot (c_i + \beta_i)^2 + \sum_{\substack{ij \\ i\neq j}} \delta_{(i,j)} \cdot c_i c_j + \sum_{i\neq j\neq k} \delta_{(i,j,k)} \cdot c_i c_j c_k\right]^{-1},$$

BSM Parametrisation

Table 15: EFT parameterisation of the cross-section ratio $\sigma/\sigma_{\mathrm{SM}}$ for each of the Reduced Stage-1.1 production bins and of the ratio of decay widths $\Gamma/\Gamma_{\mathrm{SM}}$ as a function of the CP-odd Wilson coefficients.

STXS bin	Cross-section parameterisation, $\sigma/\sigma_{\mathrm{SM}}$
gg2H-0j-p_{T}^{H}-Low	$1 + 317.69c^2_{H\widetilde{G}}$
gg2H-0j-p_{T}^{H}-High	$1 + 319.85c^2_{H\widetilde{G}}$
gg2H-1j-p_{T}^{H}-Low	$1 + 272.23c^2_{H\widetilde{G}}$
gg2H-1j-p_{T}^{H}-Med	$1 + 238.29c^2_{H\widetilde{G}}$
gg2H-1j-p_{T}^{H}-High	$1 + 233.95c^2_{H\widetilde{G}}$
gg2H-2j	$1 + 113.95c^2_{H\widetilde{G}}$
gg2H-p_{T}^{H}-High	$1 + 162.11c^2_{H\widetilde{G}}$
qq2Hqq-VH	$1 + 0.1912c^2_{H\widetilde{W}} + 0.0125c^2_{H\widetilde{B}} + 0.0124c^2_{H\widetilde{W}B} + 0.0022c_{H\widetilde{W}}c_{H\widetilde{B}} + 0.0101c_{H\widetilde{W}}c_{H\widetilde{W}B} - 0.0002c_{H\widetilde{B}}c_{H\widetilde{W}B}$
qq2Hqq-BSM	$1 + 0.5138c^2_{H\widetilde{W}} + 0.0585c^2_{H\widetilde{B}} + 0.0523c^2_{H\widetilde{W}B} + 0.0105c_{H\widetilde{W}}c_{H\widetilde{B}} - 0.0665c_{H\widetilde{W}}c_{H\widetilde{W}B} - 0.0334c_{H\widetilde{B}}c_{H\widetilde{W}B}$
qq2Hqq-VBF	$1 + 0.0617c^2_{H\widetilde{W}} + 0.0253c^2_{H\widetilde{B}} + 0.0148c^2_{H\widetilde{W}B} + 0.0148c_{H\widetilde{W}}c_{H\widetilde{B}} - 0.0190c_{H\widetilde{W}}c_{H\widetilde{W}B} - 0.0256c_{H\widetilde{B}}c_{H\widetilde{W}B}$
VH-Lep	$1 + 0.2075c^2_{H\widetilde{W}} + 0.0141c^2_{H\widetilde{B}} + 0.0158c^2_{H\widetilde{W}B} - 0.0009c_{H\widetilde{W}}c_{H\widetilde{B}} + 0.0203c_{H\widetilde{W}}c_{H\widetilde{W}B} + 0.0083c_{H\widetilde{B}}c_{H\widetilde{W}B}$
ttH	$1 + 0.599c^2_{H\widetilde{G}} + 0.0020c^2_{\widetilde{u}H} + 0.043c_{H\widetilde{G}}c_{\widetilde{u}H}$
Decay process	Decay width parameterisation, $\Gamma/\Gamma_{\mathrm{SM}}$
$\frac{\Gamma(H\to 4\ell)}{\Gamma_{\mathrm{SM}}(H\to 4\ell)}$	$1 + 0.702c^2_{H\widetilde{W}} + 2.586c^2_{H\widetilde{B}} + 0.811c^2_{H\widetilde{W}B} + 0.050c_{H\widetilde{W}}c_{H\widetilde{B}} - 1.325c_{H\widetilde{W}}c_{H\widetilde{W}B} - 1.434c_{H\widetilde{B}}c_{H\widetilde{W}B}$
$\frac{\Gamma(H\to all)}{\Gamma_{\mathrm{SM}}(H\to all)}$	$1 + 0.161c^2_{H\widetilde{W}} + 1.206c^2_{H\widetilde{B}} + 0.357c^2_{H\widetilde{W}B} 14.888c^2_{H\widetilde{G}} + 0.518c_{H\widetilde{W}}c_{H\widetilde{B}} - 0.440c_{H\widetilde{W}}c_{H\widetilde{W}B} - 1.129c_{H\widetilde{B}}c_{H\widetilde{W}B}$

Table 16: Values of acceptance parameters obtained from the fit to the three-dimensional Lorentzian function in Eq. 4 for CP-odd coupling parameters.

Acceptance parameter	Fit result	Acceptance parameter	Fit result
α_0	0.118 ± 0.001	$\delta_{H\widetilde{W}}$	0.572 ± 0.003
α_1	0.853 ± 0.001	$\delta_{H\widetilde{B}}$	2.022 ± 0.004
α_2	0.826 ± 0.002	$\delta_{H\widetilde{W}B}$	0.644 ± 0.001
$\beta_{H\widetilde{W}}$	-0.001 ± 0.001	$\delta_{(H\widetilde{W},H\widetilde{W}B)}$	-1.070 ± 0.004
$\beta_{H\widetilde{B}}$	-0.001 ± 0.001	$\delta_{(H\widetilde{B},H\widetilde{W}B)}$	-1.085 ± 0.006
$\beta_{H\widetilde{W}B}$	0.001 ± 0.001	$\delta_{(H\widetilde{W},H\widetilde{B})}$	-0.010 ± 0.008
		δ	-0.060 ± 0.088

$$\frac{A(\vec{c})}{A_{\mathrm{SM}}} = \alpha_0 + (\alpha_1)^2 \cdot \left[\alpha_2 + \sum_i \delta_i \cdot (c_i + \beta_i)^2 + \sum_{\substack{ij \\ i\neq j}} \delta_{(i,j)} \cdot c_i c_j + \delta_{(i,j,k)} \cdot c_i c_j c_k \right]^{-1},$$

Results: per STXS bin

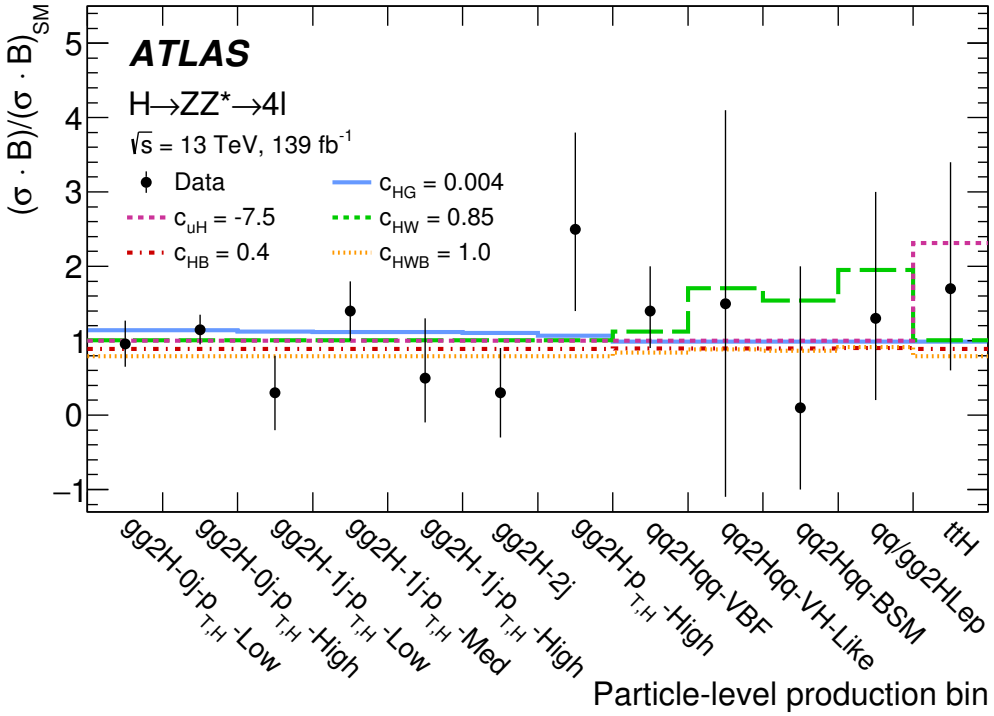

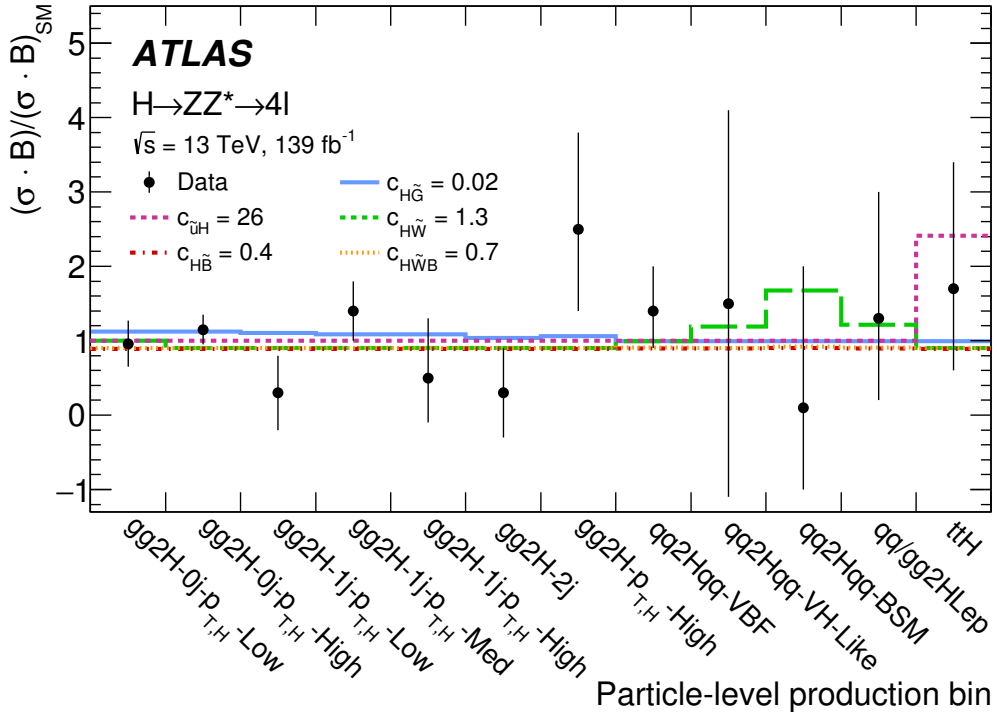

Results: 1D

- Only one parameter is fitted, the rest is set to zero

CP-even:

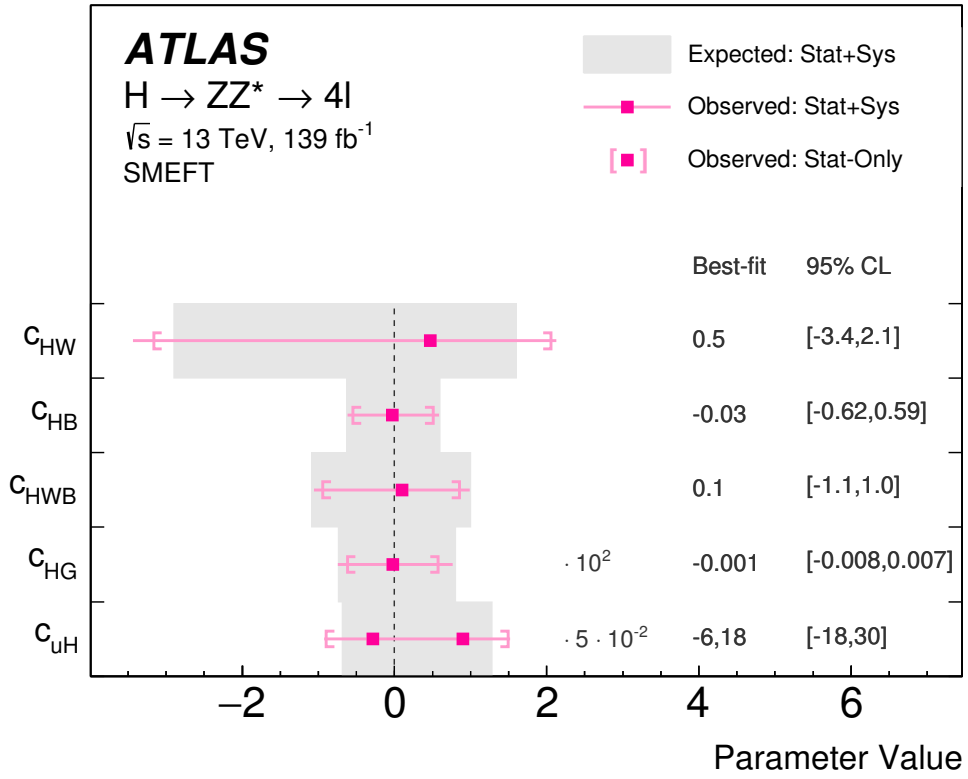

CP-odd:

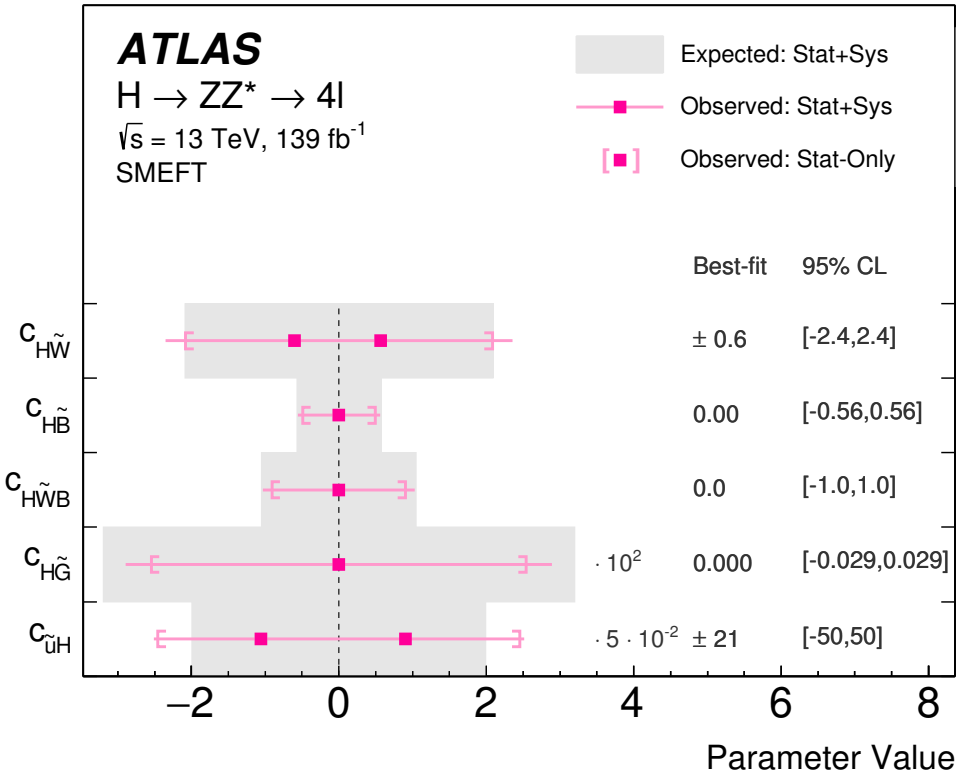

In good agreement with the SM prediction

Results: 2D

c_{HW} vs. c_{HB}

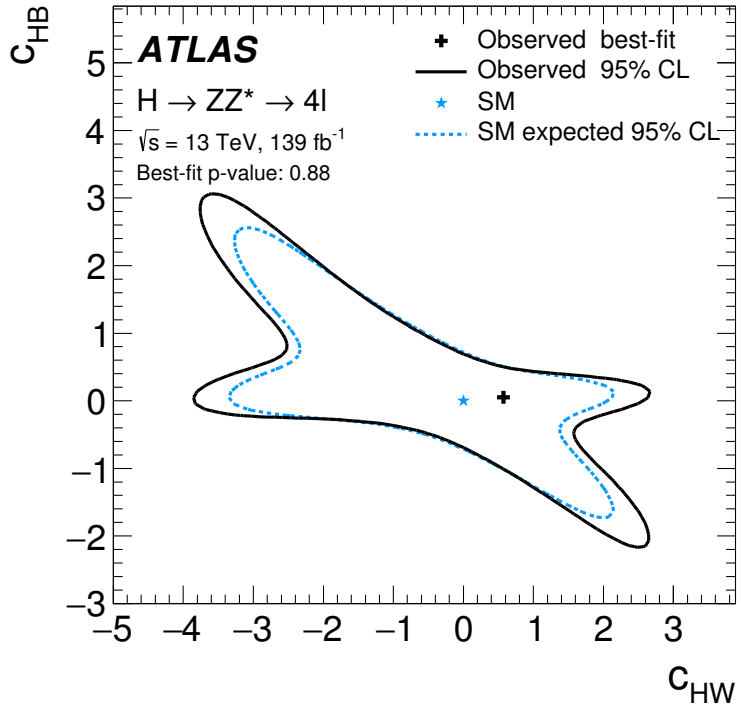

$c_{H\tilde{W}}$ vs. $c_{H\tilde{B}}$

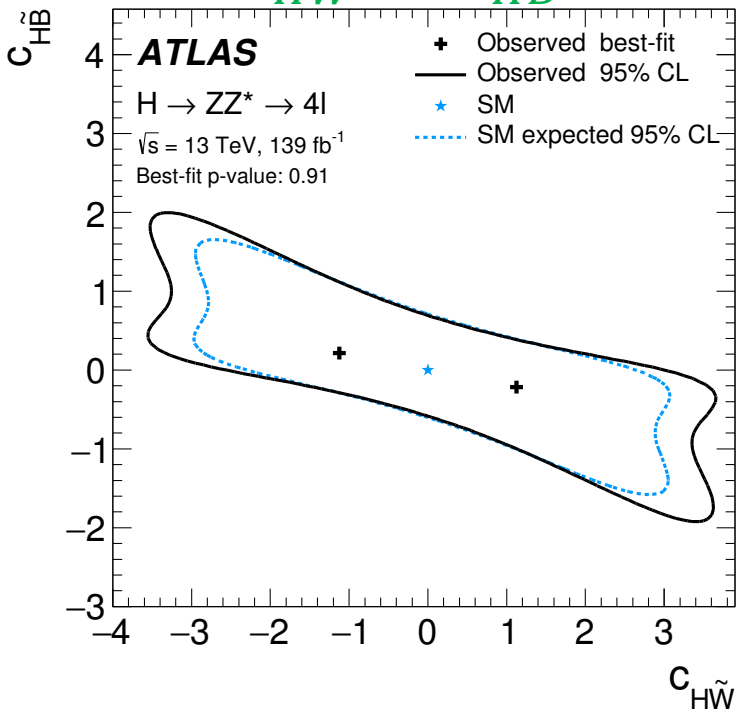

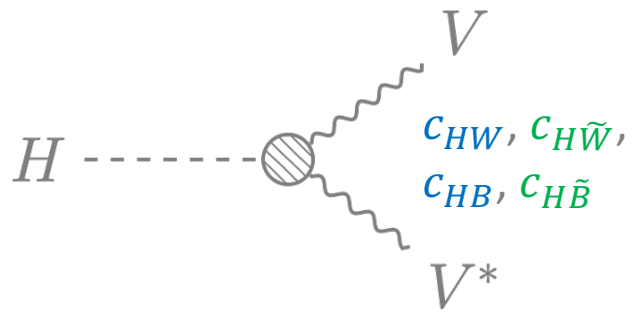

In good agreement with the SM prediction

Remaining → BACKUP

Results: 2D

c_{uH} vs. c_{HG}

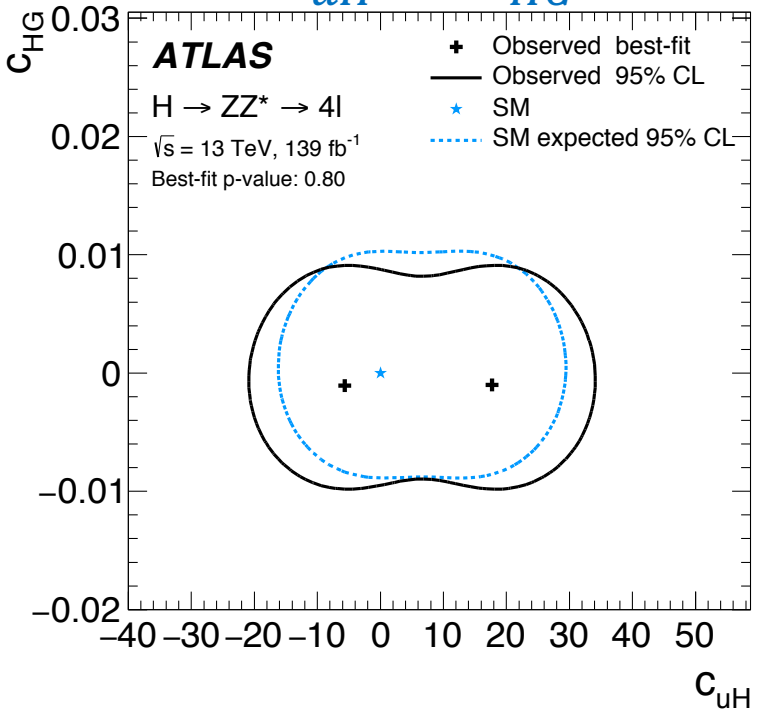

$c_{\tilde{u}H}$ vs. $c_{H\tilde{G}}$

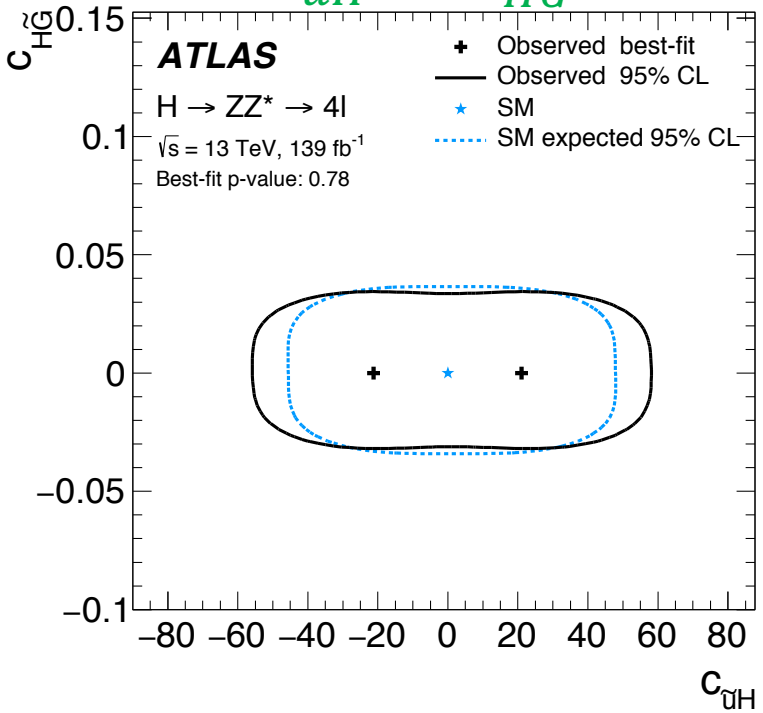

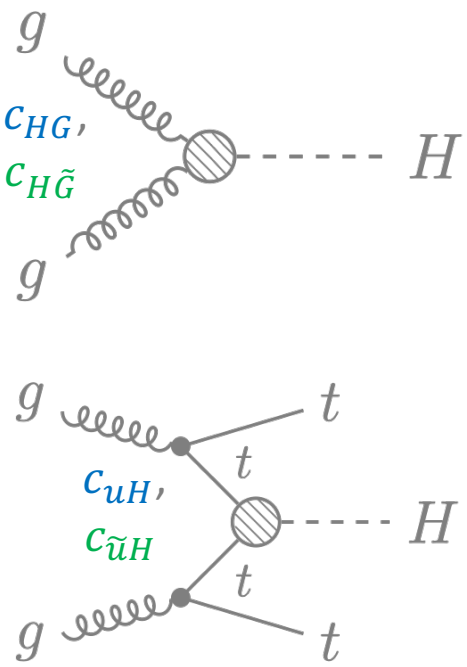

In good agreement with the SM prediction

Remaining → BACKUP

1D NLL scans

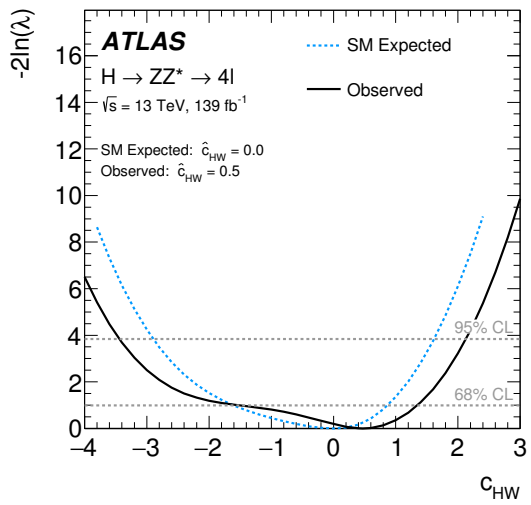
ATLAS
SM Expected
Observed
H → ZZ* → 4l
√s = 13 TeV, 139 fb-1
SM Expected: ĉHW = 0.0
Observed: ĉHW = 0.5
95% CL
68% CL
-2ln(λ)
cHW

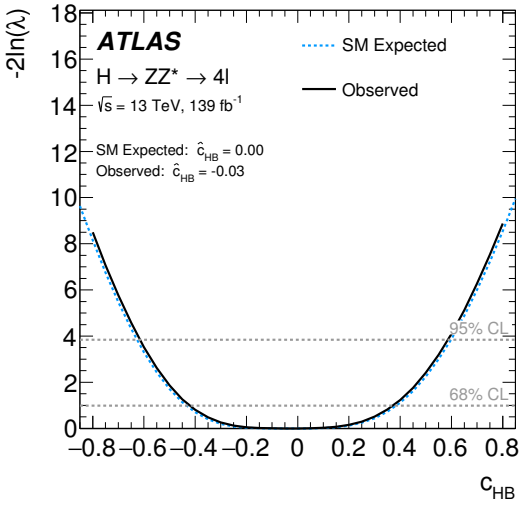
ATLAS
SM Expected
Observed
H → ZZ* → 4l
√s = 13 TeV, 139 fb-1
SM Expected: ĉHB = 0.00
Observed: ĉHB = -0.03
95% CL
68% CL
-2ln(λ)
cHB

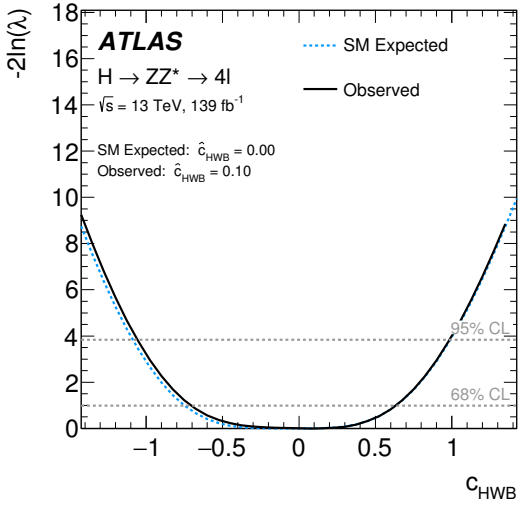
ATLAS
SM Expected
Observed
H → ZZ* → 4l
√s = 13 TeV, 139 fb-1
SM Expected: ĉHWB = 0.00
Observed: ĉHWB = 0.10
95% CL
68% CL
-2ln(λ)
cHWB

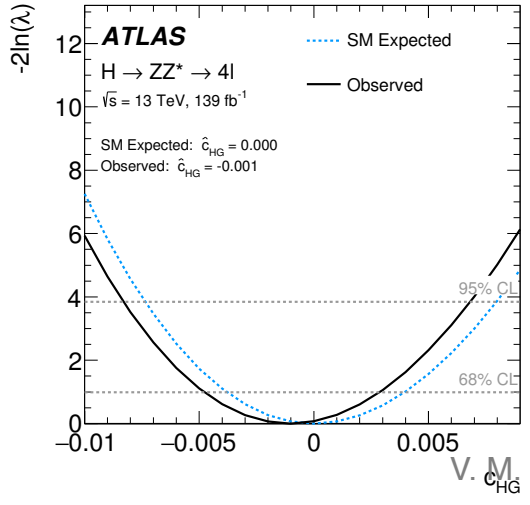
ATLAS
SM Expected
Observed
H → ZZ* → 4l
√s = 13 TeV, 139 fb-1
SM Expected: ĉHG = 0.000
Observed: ĉHG = -0.001
95% CL
68% CL
-2ln(λ)
cHG

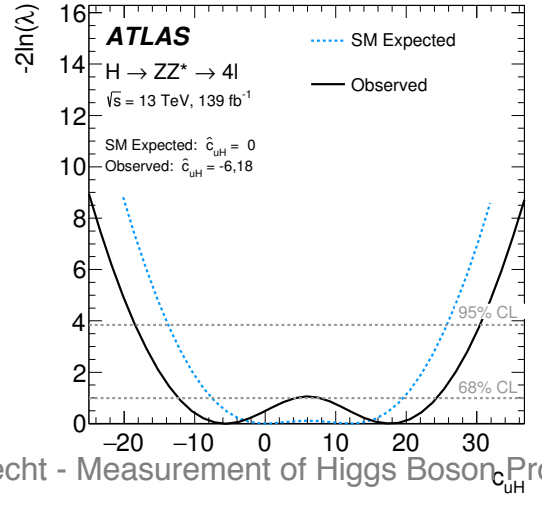
ATLAS
SM Expected
Observed
H → ZZ* → 4l
√s = 13 TeV, 139 fb-1
SM Expected: ĉuH = 0
Observed: ĉuH = -6,18
95% CL
68% CL
-2ln(λ)
cuH

1D NLL scans

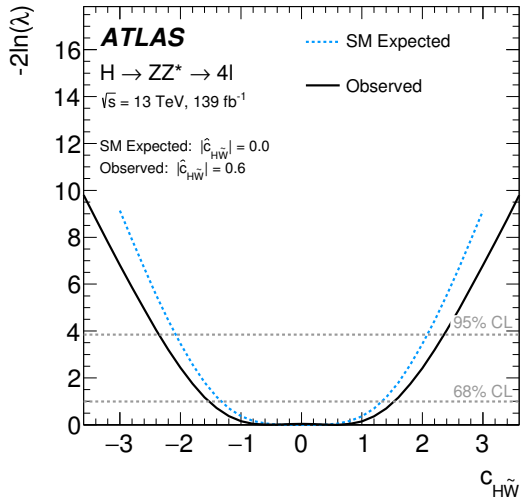
ATLAS
H → ZZ* → 4l
√s = 13 TeV, 139 fb-1
SM Expected
Observed
SM Expected: |ĉHW̃| = 0.0
Observed: |ĉHW̃| = 0.6
95% CL
68% CL
-2ln(λ)
cHW̃

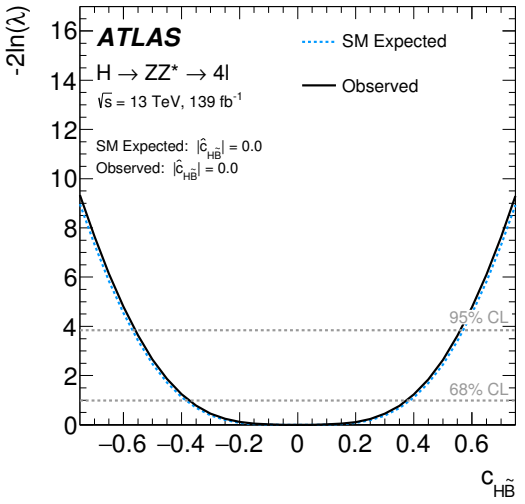
ATLAS
H → ZZ* → 4l
√s = 13 TeV, 139 fb-1
SM Expected
Observed
SM Expected: |ĉHB̃| = 0.0
Observed: |ĉHB̃| = 0.0
95% CL
68% CL
-2ln(λ)
cHB̃

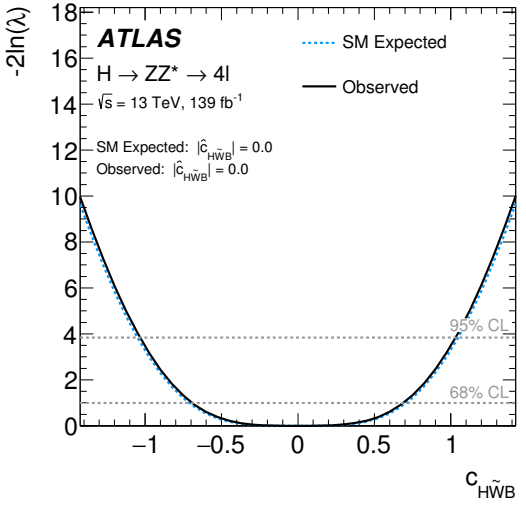
ATLAS
H → ZZ* → 4l
√s = 13 TeV, 139 fb-1
SM Expected
Observed
SM Expected: |ĉHW̃B| = 0.0
Observed: |ĉHW̃B| = 0.0
95% CL
68% CL
-2ln(λ)
cHW̃B

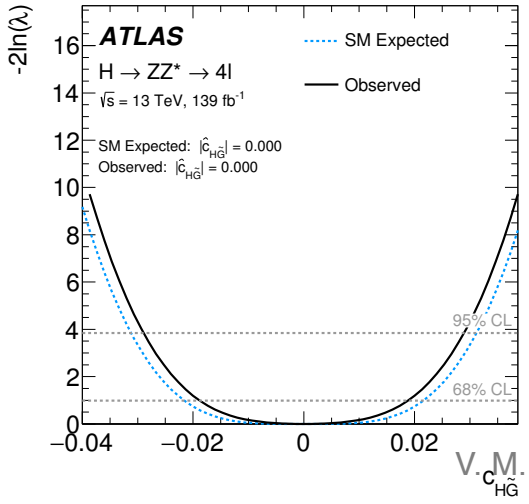
ATLAS
H → ZZ* → 4l
√s = 13 TeV, 139 fb-1
SM Expected
Observed
SM Expected: |ĉHG̃| = 0.000
Observed: |ĉHG̃| = 0.000
95% CL
68% CL
-2ln(λ)
cHG̃

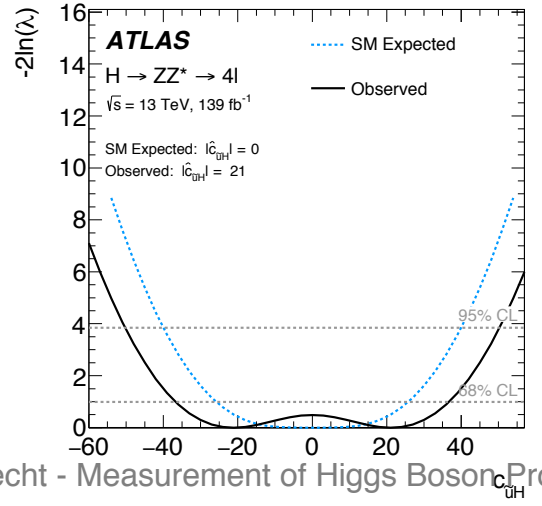
ATLAS
H → ZZ* → 4l
√s = 13 TeV, 139 fb-1
SM Expected
Observed
SM Expected: |ĉũH| = 0
Observed: |ĉũH| = 21
95% CL
68% CL
-2ln(λ)
cũH

Impact of Acceptance

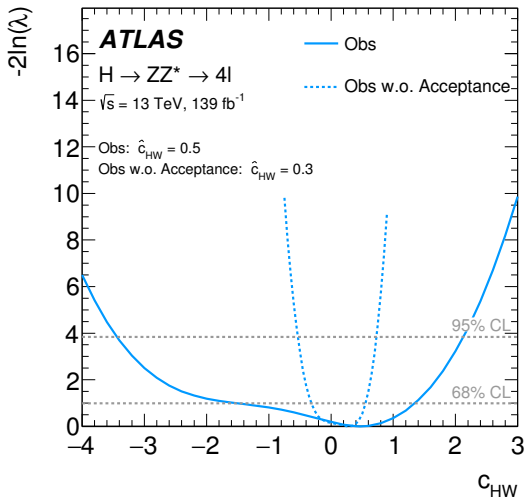

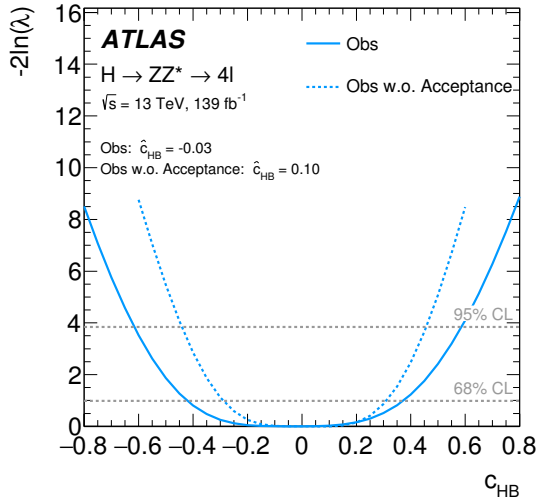

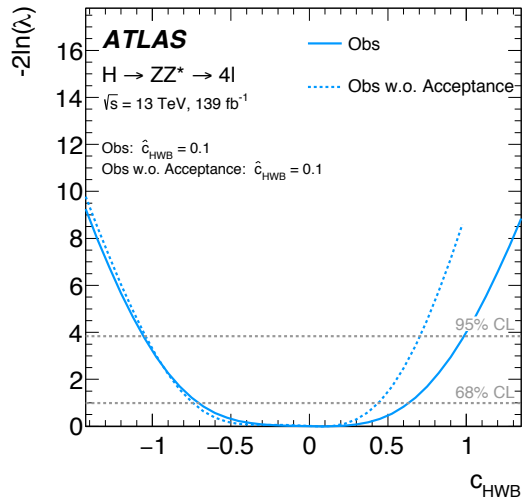

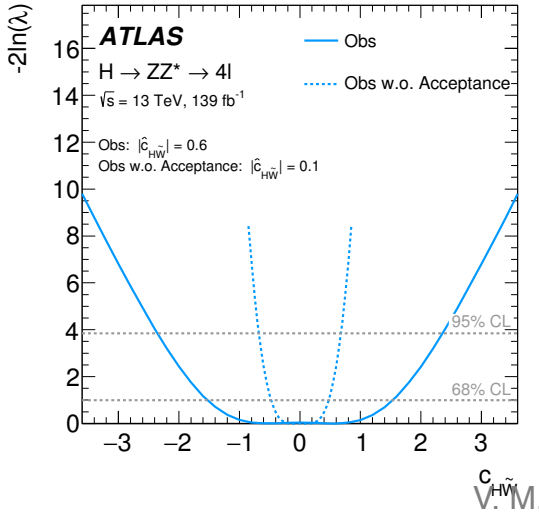

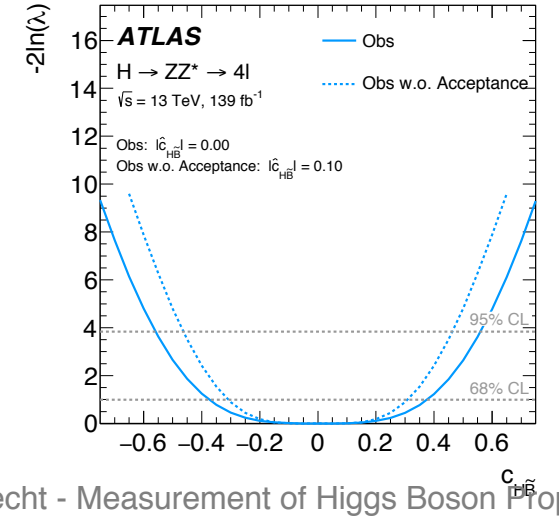

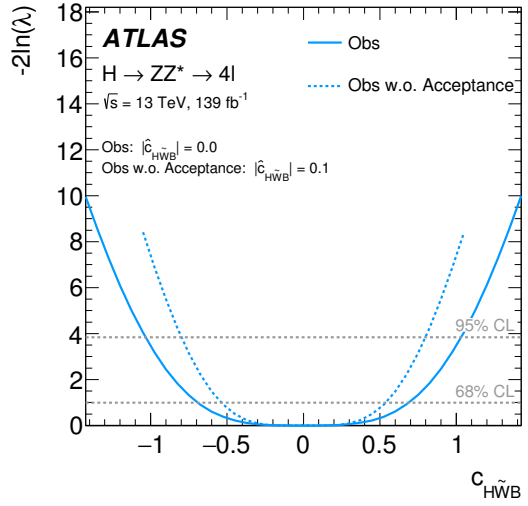

Results: 2D

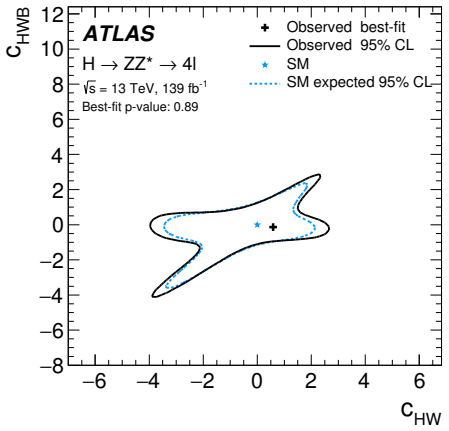
ATLAS
H → ZZ* → 4l
√s = 13 TeV, 139 fb-1
Best-fit p-value: 0.89
Observed best-fit
Observed 95% CL
SM
SM expected 95% CL
cHWB
cHW

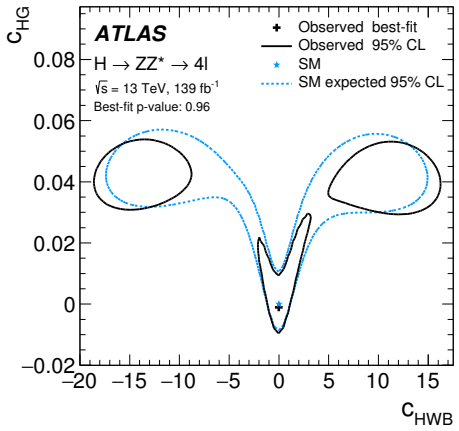
ATLAS
H → ZZ* → 4l
√s = 13 TeV, 139 fb-1
Best-fit p-value: 0.96
Observed best-fit
Observed 95% CL
SM
SM expected 95% CL
cHG
cHWB

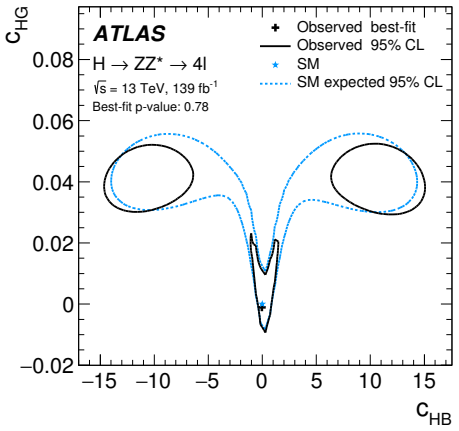
ATLAS
H → ZZ* → 4l
√s = 13 TeV, 139 fb-1
Best-fit p-value: 0.78
Observed best-fit
Observed 95% CL
SM
SM expected 95% CL
cHG
cHB

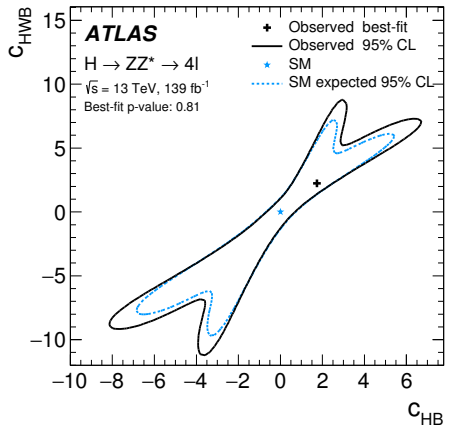
ATLAS
H → ZZ* → 4l
√s = 13 TeV, 139 fb-1
Best-fit p-value: 0.81
Observed best-fit
Observed 95% CL
SM
SM expected 95% CL
cHWB
cHB

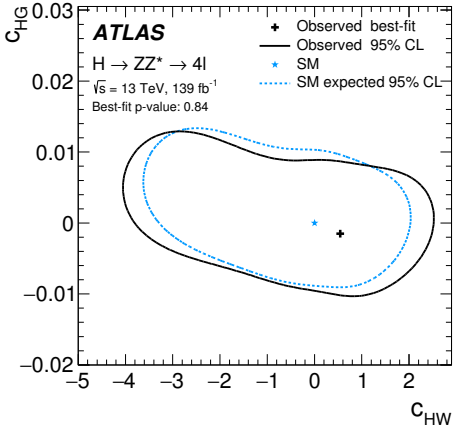
ATLAS
H → ZZ* → 4l
√s = 13 TeV, 139 fb-1
Best-fit p-value: 0.84
Observed best-fit
Observed 95% CL
SM
SM expected 95% CL
cHG
cHW

Results: 2D

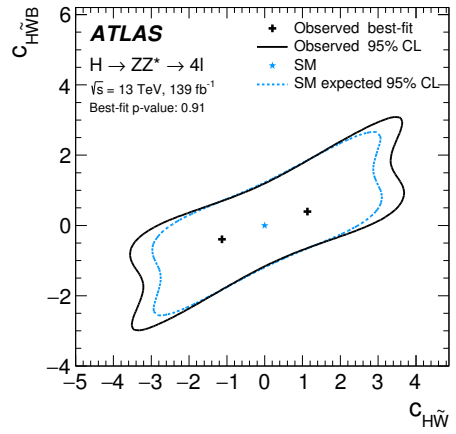
ATLAS
H → ZZ* → 4l
√s = 13 TeV, 139 fb-1
Best-fit p-value: 0.91
Observed best-fit
Observed 95% CL
SM
SM expected 95% CL
c_HW̃B
c_HW̃

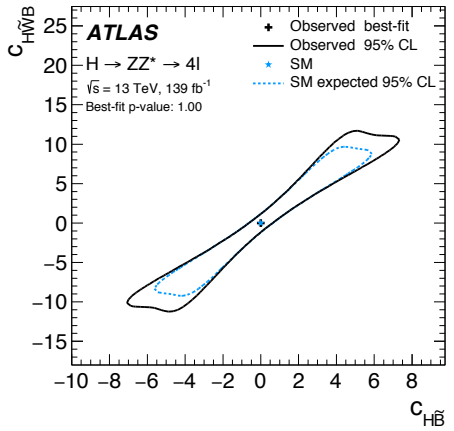
ATLAS
H → ZZ* → 4l
√s = 13 TeV, 139 fb-1
Best-fit p-value: 1.00
Observed best-fit
Observed 95% CL
SM
SM expected 95% CL
c_HW̃B
c_HB̃

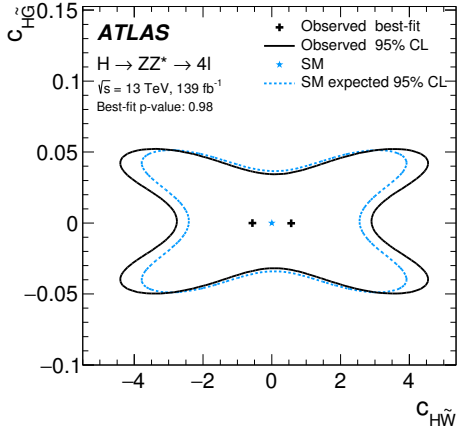
ATLAS
H → ZZ* → 4l
√s = 13 TeV, 139 fb-1
Best-fit p-value: 0.98
Observed best-fit
Observed 95% CL
SM
SM expected 95% CL
c_HG̃
c_HW̃

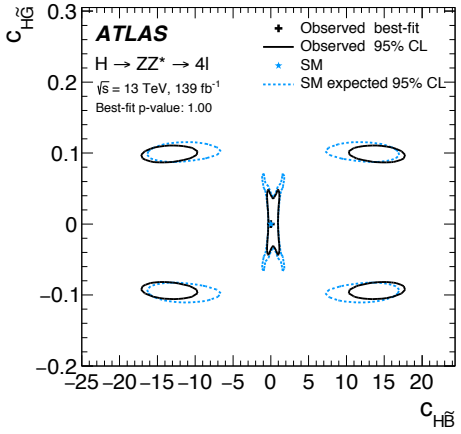
ATLAS
H → ZZ* → 4l
√s = 13 TeV, 139 fb-1
Best-fit p-value: 1.00
Observed best-fit
Observed 95% CL
SM
SM expected 95% CL
c_HG̃
c_HB̃

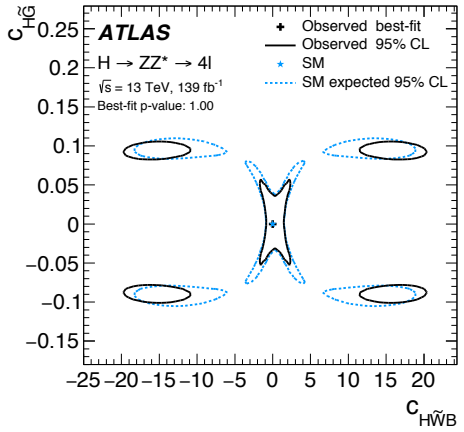
ATLAS
H → ZZ* → 4l
√s = 13 TeV, 139 fb-1
Best-fit p-value: 1.00
Observed best-fit
Observed 95% CL
SM
SM expected 95% CL
c_HG̃
c_HW̃B

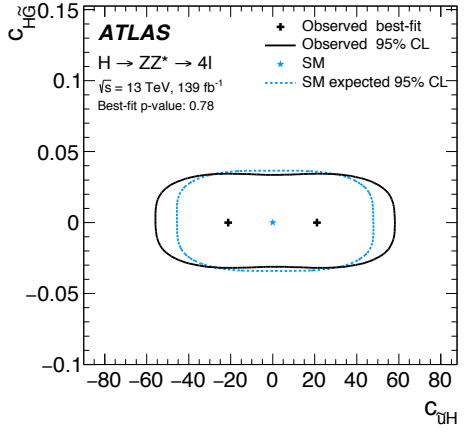
ATLAS
H → ZZ* → 4l
√s = 13 TeV, 139 fb-1
Best-fit p-value: 0.78
Observed best-fit
Observed 95% CL
SM
SM expected 95% CL
c_HG̃
c_ũH